Mechanistic Investigations of Receptor Signaling via Canonical and Non-canonical Amino Acid Mutagenesis

Thesis by

Richard Albert Mosesso

In Partial Fulfillment of the Requirements

for the degree of

Doctor of Philosophy

CALIFORNIA INSTITUTE OF TECHNOLOGY

Pasadena, California

2019

(Defended May 31, 2019)

Richard Albert Mosesso
ORCID: 0000-0003-0927-0843

For all those who have doubted themselves

Acknowledgements

I would like to start by saying that I was afraid of graduate school. Caltech is an intimidating place. I had imposter syndrome from the first day I arrived. But now that my time in graduate school is ending, I can say that I actually enjoyed it, thanks to the support I had from friends and family and all the new people I met along the way. So a big thank you to everyone who helped me through it and helped me feel like I belonged.

I would first like to thank my adviser, Prof. Dennis Dougherty. Dennis is not only a truly brilliant physical organic chemist, but also a thoughtful and sincere mentor. Dennis's combination of being hands-off while also being available and approachable was just what I needed in an adviser. By being very hands-off, Dennis actually asks a lot of his graduate students, not by telling them what to do but by *not* telling them what to do, which is simultaneously liberating and challenging. All the while, however, Dennis is there and he is ready to listen. It's a unique approach, and it has greatly helped me develop as a scientist. Dennis is also just a genuinely good person, and I am happy to have had him as my adviser. I would also like to thank Ellen Dougherty for welcoming me and the Dougherty lab as a whole into her and Dennis's home.

I would like to recognize the members of my thesis committee, Prof. David Tirrell, Prof. Mikhail Shapiro, and Prof. Douglas Rees, for all that they have done for me. Thank you all for taking the time to meet with me over the years, and for your expert feedback. It has been a privilege to work with you all.

I also owe a great deal of my development as a scientist to our lab's collaborators, Prof. Sarah Lummis and Prof. Henry Lester. It has been a pleasure working with Prof. Lummis on two projects related to proline residues – I will never underestimate the power

(and mysteries) of proline. I've very much appreciated Henry's input on my projects, and his expert neuroscience/biology wisdom. I'll always remember that "a month in the lab could save you a day in the library." I would also like to thank the Lester lab as a whole, in particular the work of Jonathan Wang, who has graciously and expertly prepared oocytes for the Dougherty lab throughout the years, and Purnima Deshpande, who manages the whole operation.

It is important to acknowledge the wonderful administrators and technical staff that make the everyday possible. I would like to thank Linda Syme, our lab's administrative assistant, for keeping everything up and running, Joseph Drew, for managing the chemistry stockroom and facilities, and Dr. Mona Shahgholi, Dr. Scott Virgil, Dr. David VanderVelde, Dr. Sonja Hess, Dr. Annie Moradian, and Dr. Michael Sweredoski, for providing invaluable technical expertise in a variety of areas.

In earning my undergraduate degree at Brown University, I worked with many people who shaped me as a scientist. First and foremost, I would like to thank my undergraduate research adviser Prof. Wesley Bernskoetter for teaching me the foundational scientific values I would use in my future. I would also like to thank Dr. Hongwei Xu for his infinite patience mentoring me as an undergraduate student. I worked in the lab of Prof. Ramanarayanan Krishnamurthy for the summer between my junior and senior years of college, and I thank him for welcoming me into his lab. My mentor for that research experience, Dr. Alba Díez, taught me much about synthetic organic chemistry, and I had a great time working with her. Lastly, I'd like to acknowledge Prof. Sarah Delaney for being an inspiring instructor and getting me interested in chemical biology.

I would also like to acknowledge my high school science teachers, Mrs. Joyce Voorhis, Mr. Philip Previte, Mrs. Jennifer Morgan, and Mr. Neil McCarthy. I was already interested in science going into high school, but I was lucky to have four wonderful science teachers who nurtured my curiosity and encouraged me to always ask questions and keep learning.

Next I would like to acknowledge all of the people with whom I have become acquainted through association with Dougherty lab. There are many, many wonderful people who have come through here. I'll start with Dr. Christopher Marotta, who more or less taught me all of the molecular biology I initially needed to get started in the lab. Chris stayed in the area after graduating, and I've been glad to get to know him outside of lab. Dr. Michael Post taught me how to use our nearly-one-of-a-kind electrophysiology rig, the OPUS Xpress, and was a focal point of our lab's social culture. Dr. Matthew Rienzo is a very adaptable scientist, and a lovely person to be around. I thank Matt for getting the estrogen receptor project started, and hopefully we will see more of one another in northern California! Dr. Matthew Davis was our lab's computational expert, and I admire his passion and appreciate his warm and welcoming personality. I also thank him for being the Dungeon Master of our Dungeons & Dragons campaign – perhaps one day I can learn what he had in store for my dragonborn paladin SHAMASH and his sword the Delian Oath. Dr. Betty Wong gave me a fresh perspective on the many different roads one can take in life. Dr. Clinton Reagan and Dr. Oliver Shafaat are both highly capable scientists and wonderful people to have worked alongside. I never overlapped with Dr. Noah Duffy, but we became good friends outside of lab, and I appreciate his chill demeanor and real-world wisdom. I always appreciated Gabrielle Tender, our lab's token undergraduate student, for her cheery

positive attitude and enthusiasm for science. I'd also like the acknowledge the three students I mentored, Malaney Young, Rachel Banks, and Juner Zhang. You were all very different and all fun to be around, and each of you taught me something about science, mentoring, and myself. I thank Dr. Catriona Blunt for her friendship and lively conversation over the years. I thank Stephen Grant for taking me under his wing on the estrogen receptor project, and just generally being an awesome person. I admire Steve's dedication to everything he does, and thank him for pushing me out of my musical comfort zone and getting me to listen to T. Swift. Annet Blom and I have been bay-mates since the day I joined the Dougherty lab, and I couldn't be happier with who I've been sitting behind the last four years. Annet is a brilliant, hard-working scientist but more importantly, she can somehow make fixing the OPUS fun. Throughout the years, from bragging about gifts we got from cats on Neko Atsume, to our famous Pokéwalks, to going to yoga together ("this is work!"), or just talking about life, Annet has brought a little bit of happiness into every day. Dr. David Paul Walton is truly a mad scientist, and has that rare combination of creativity and ability that will take him very far in life. I am so very glad to have met Paul, and I am looking forward to more adventures with him in the future. I got off on the wrong foot when I first met Paul by saying that orange juice is better without pulp, but it is and no one can change that. John Bryce Jarman's genuine zeal for science and level of scientific scrutiny are unmatched, and I'm excited to see where that brings him. I thank Bryce for being a great friend and an O.G. member of Swole Patrol, and I'm grateful that I will be able to see him in northern California as well!

I've made a lot of friends along the way, but I'd like to give special recognition to my childhood friend, Keith Kennedy. Keith and I caught grasshoppers together on a field

trip about 22 years ago, and our friendship has endured ever since, despite me trying to steal his holographic Charizard at one point in time.

It is impossible for me to imagine the last six years of my life without my wonderful girlfriend, Lena Parker-Duncan. Our lives first became entwined a year before I would even know that I was going to pursue a PhD at Caltech, and I almost decided not to, but I am glad that I did, and I am so very thankful that Lena has shared this journey with me. Nobody has known me closer over this time, and Lena's love and support have given me the stability, the levity, and the faith in myself that I needed. I would also like to thank Lena's parents, Gwendolyn Parker and Joan Duncan, for raising such a lovely young woman and welcoming me into their lives throughout the years.

Finally, I would like to thank my family for being there every step of the way: my dad, Albert Mosesso, my mom, Sonya Mosesso, my big bro, Nicholas Mosesso, and my big sis, Laura Eklund. It goes without saying, but I wouldn't be complete without you all. You have all contributed to making me who I am, and I love you all so very much.

Abstract

This dissertation primarily describes investigations of the mechanisms by which pentameric ligand-gated ion channels (pLGICs) activate ("gating") using canonical and non-canonical amino acid mutagenesis. Chapter 1 provides an introduction to the systems being studied, their physiological roles, and the techniques that we have used to study them. Chapter 2 describes a series of experiments comparing the roles of amino acid residues proximal to the neurotransmitter binding site in the type 3 serotonin receptor (5-HT_3R) to the aligning residues of the muscle-type nicotinic acetylcholine receptor (nAChR). The findings presented in Chapter 3 assess the functional roles of proline residues in the prokaryotic pLGIC, *Erwinia* ligand-gated ion channel (ELIC). Chapter 4 describes an extensive investigation of salient details of 5-HT_3R gating using canonical and non-canonical amino acid mutagenesis of amino acid residues at the interface of the extracellular domain and transmembrane domain of this receptor. Chapter 5 applies a photocrosslinking strategy employing the non-canonical amino acid *p*-azidophenylalanine to study dimerization and cofactor interactions of the estrogen receptor α.

Published Content and Contributions

1. Mosesso, R.; Dougherty, D. A.; Lummis, S. C. R. Probing Proline Residues in the Prokaryotic Ligand-Gated Ion Channel, ELIC. Biochemistry 2018, 57 (27), 4036–4043. https://doi.org/10.1021/acs.biochem.8b00379.

R.M. and S.C.R.L. performed experiments and R.M., S.C.R.L., and D.A.D. contributed to writing and editing the manuscript.

2. Mosesso, R.; Dougherty, D. A. A Triad of Residues Is Functionally Transferrable between 5-HT3 Serotonin Receptors and Nicotinic Acetylcholine Receptors. J. Biol. Chem. 2018, 293 (8), 2903–2914. https://doi.org/10.1074/jbc.M117.810432.

R.M. conducted all experimental work. R.M. and D.A.D. worked together in directing the research and in writing and editing the manuscript.

Table of Contents

List of Figures and Tables

Chapter 1: Introduction

1.1 Neurotransmission

1.1.1 Ion channels

The brain is the central hub of the nervous system, housing approximately 100 billion neurons by some estimates, each of which may have on the order of 10,000 points of connection with others neurons.[1] At these points of connection, known as synapses, presynaptic cells communicate via electrochemical signals to postsynaptic cells. This process of neurotransmission proceeds by means of action potentials, in which a wave of cell membrane depolarization propagates down the length of an axon connecting two neurons via the action of voltage-gated ion channels (**Figure 1.1A**).[2,3] These proteins span the cell membrane and allow selective passage of ions across the membrane in response to changes in cell potential, thus carrying the signal along. This electrochemical signal ultimately reaches the synapse, at which point a signal is conveyed to the postsynaptic cell via the release of neurotransmitters across the synaptic cleft (**Figure 1.1B**).[4,5]

A key role of neurotransmitters is the activation of ligand-gated ion channels (LGICs) on the postsynaptic cell surface (**Figure 1.1C**).[6–8] Like voltage-gated ion channels, LGICs are transmembrane proteins that permit the passage of select ions across the cell membrane in response to an external stimulus, only LGICs respond to small molecule neurotransmitters rather than changes in cell potential. The activation of LGICs on postsynaptic cells generates postsynaptic potentials that can be excitatory (causing depolarization of the cell) or inhibitory (causing hyperpolarization of the cell) depending on the nature of the neurotransmitters released at the synapse and the expression levels of different LGICs on the postsynaptic cell surface. In turn, the resultant postsynaptic

potentials make the postsynaptic cell more or less likely to fire an action potential, respectively. LGICs thus play a crucial role in the process of neurotransmission.

Given their important role in neurotransmission, LGICs are implicated in a wide range of conditions.[9–20] Members of the nicotinic acetylcholine receptor (nAChR) family, for example, are involved in nicotine addiction,[21,22] while another member of the family is implicated in myasthenia gravis.[23] Inhibitors of type 3 serotonin receptors (5-HT_3Rs) are prescribed to treat nausea and vomiting, yet these receptors have also been implicated in a number of mood disorders.[10] Our collective understanding of LGICs – their functions, regulation, pharmacologies, and mechanisms of action – is therefore critical to the treatment of a broad array of disorders.

1.1.2 Pentameric ligand-gated ion channels

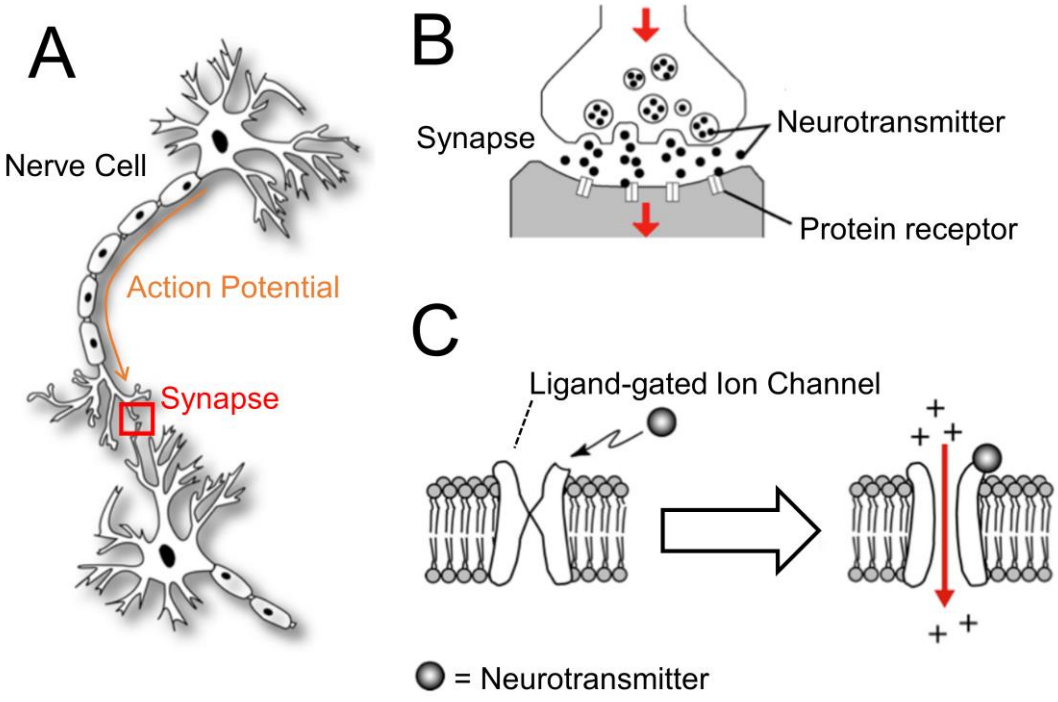

Figure 1.1. The process of neurotransmission. (*A*) Signals travel between neurons by means of action potentials. (*B*) Neurotransmitters carry forth a signal at the synapses where neurons meet. (*C*) Ligand-gated ion channels respond to neurotransmitters to conduct ions across the postsynaptic cell membrane.

A subset of LGICs, sharing a highly-conserved overall structure, is the pentameric ligand-gated ion channel (pLGIC) family.[7,8,24,25] The pLGICs that are found in vertebrates are also known as Cys-loop receptors, due to the presence of a conserved disulfide-bonded loop that is closely involved in receptor function. Members of the Cys-loop receptor family include the excitatory nAChRs[26] and 5-HT_3Rs[27] as well as the inhibitory type A γ-aminobutyric acid receptors ($GABA_A$Rs)[28] and glycine receptors (GlyRs).[29] There are also two pLGICs that are found in prokaryotes, namely *Gleobacter* ligand-gated ion channel (GLIC)[30] and *Erwinia* ligand-gated ion channel (ELIC).[32,33] These pLGICs have proven to be much more amenable to crystallization than Cys-loop receptors,

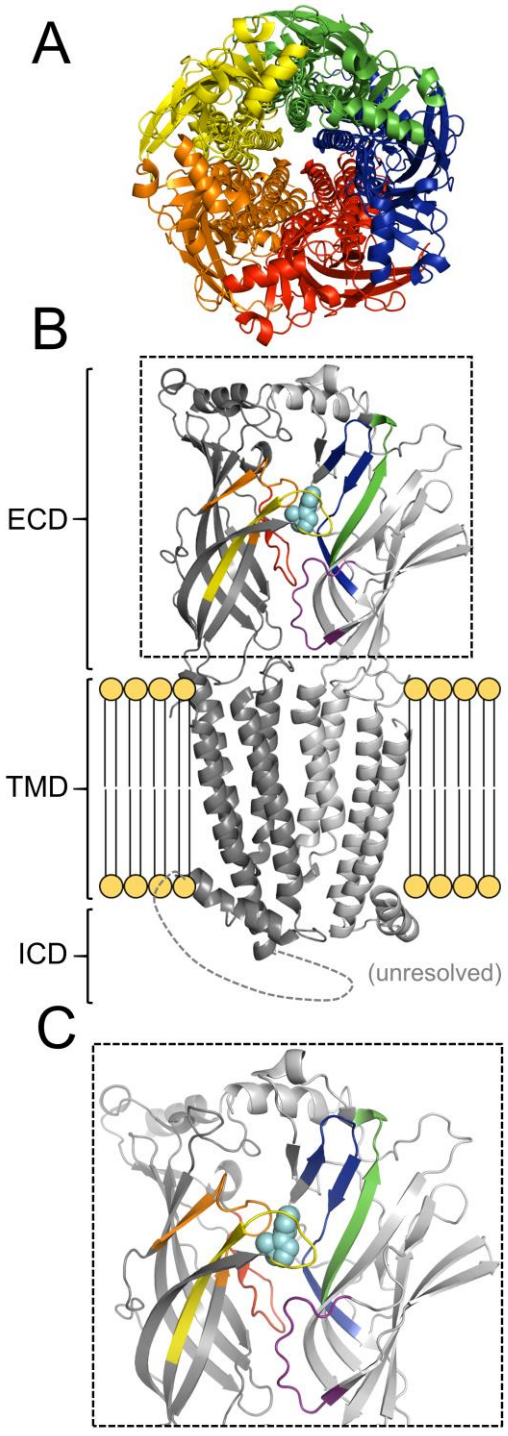

Figure 1.2. General structure of Cys-loop receptors and other pLGICS. (*A*) Overall topology of a single pentameric channel, illustrating the concentric arrangement around a central pore. (*B*) View of two adjacent receptor subunits, highlighting the multidomain architecture. (*C*) Neurotransmitter binding site between adjacent subunits. Binding loops A-E are colored red, orange, yellow, green, blue, purple, respectively. The bound ligand, nicotine, is shown in cyan. PDB ID 5KXI.[31]

which has made them a valuable model system for studying the structure and mechanics of pLGICs.[7,25]

A single Cys-loop receptor consists of five subunits assembled in a concentric fashion about an axis that passes through the channel pore (**Figure 1.2A**). Each individual subunit is composed of three domains: 1) an extracellular domain (ECD), consisting primarily of ten ß-strands which together assemble into a ß-sandwich, 2) a transmembrane domain (TMD) contributed by four α-helices, numbered M1-M4, and 3) an intracellular domain (ICD) between the M3 and M4 helices that varies considerably between different receptors and receptor subtypes (**Figure 1.2B**). Note that the prokaryotic pLGICS GLIC and ELIC are highly structurally homologous to Cys-loop receptors, but lack the disulfide of the signature Cys-loop and likewise lack the intracellular M3-M4 loop.[25]

Over the last 20+ years of structural, functional, and computational studies of pLGICs, many of the general details of receptor activation have become relatively clear.[7,8,24,34,35] Endogenous neurotransmitter agonists bind in the ECDs of these receptors at interfaces between adjacent subunits, known as the orthosteric binding sites. Noncovalent interactions are formed between ligands six canonical binding site "loops" of the receptors, designated loops A-E (**Figure 1.2C**). These are referred to as loops mainly for historical reasons, as several contain substantial ß-sheet structure. Binding of agonist causes a series of structural rearrangements collectively referred to as "gating," starting with residues immediately in and around the binding site, perhaps most notably a "clamping" of the otherwise flexible loop C around the ligand. This ligand binding event causes a quaternary twisting of the ECD relative to the TMD as well as rearrangements of several loop structures at the ECD-TMD interface. These rearrangements ultimately result

in displacement of the pore-lining M2 helices in such a way that enables the conduction of ions through the pore, which is otherwise occluded by a hydrophobic constriction.

While the global changes underlying pLGIC activation are relatively well-characterized, intimate molecular details are lacking in many areas. Over the years, our lab has contributed greatly to understanding and characterizing noncovalent interactions between pLGICs and the ligands they bind via structure-function studies, most notably by means of non-canonical amino acid mutagenesis (*section 1.3*).[36,37] Much of the research presented in this dissertation, however, has sought to derive insights into the more nebulous process of receptor gating.

1.2 Transcriptional Regulation by Estrogen Receptor α

Another means of cellular signaling is achieved by small molecule messengers that regulate the transcription of target genes. One large class of proteins responsible for carrying out this regulation is the nuclear receptor family of transcription factors.[38] These receptors bind hormones and affect transcription via recruitment of transcriptional machinery to hormone response elements within the promoters of target genes.

One important member of the nuclear receptor family is the estrogen receptor α (ERα).[39,40] As one can tell from its name, the function of ERα is to control the transcription of target genes in response to endogenous estrogens, although a structurally diverse array of exogenous compounds also has activity at ERα.[41–43] Oncogenic activation of the estrogen receptor signaling pathway occurs in many different cancers, perhaps most notably in breast cancer.[44–49] The ERα-targeting drug tamoxifen is widely prescribed in the treatment of breast cancer, with millions of people taking tamoxifen across the world every year.[50]

As with all members of the nuclear receptor family, ERα is a soluble multidomain protein, with each domain contributing to receptor function.[40,51–54] In order of primary sequence, the domains of ERα (**Figure 1.3A**) are the N-terminal domain (NTD), which contains a transcriptional "activation function" (AF-1) and is highly intrinsically disordered, the DNA-binding domain (DBD), which is mainly responsible for recognizing estrogen response elements (EREs), the hinge domain (H), which connects the DBD to the ligand-binding domain (LBD), and finally the LDB itself, which binds estrogen and is

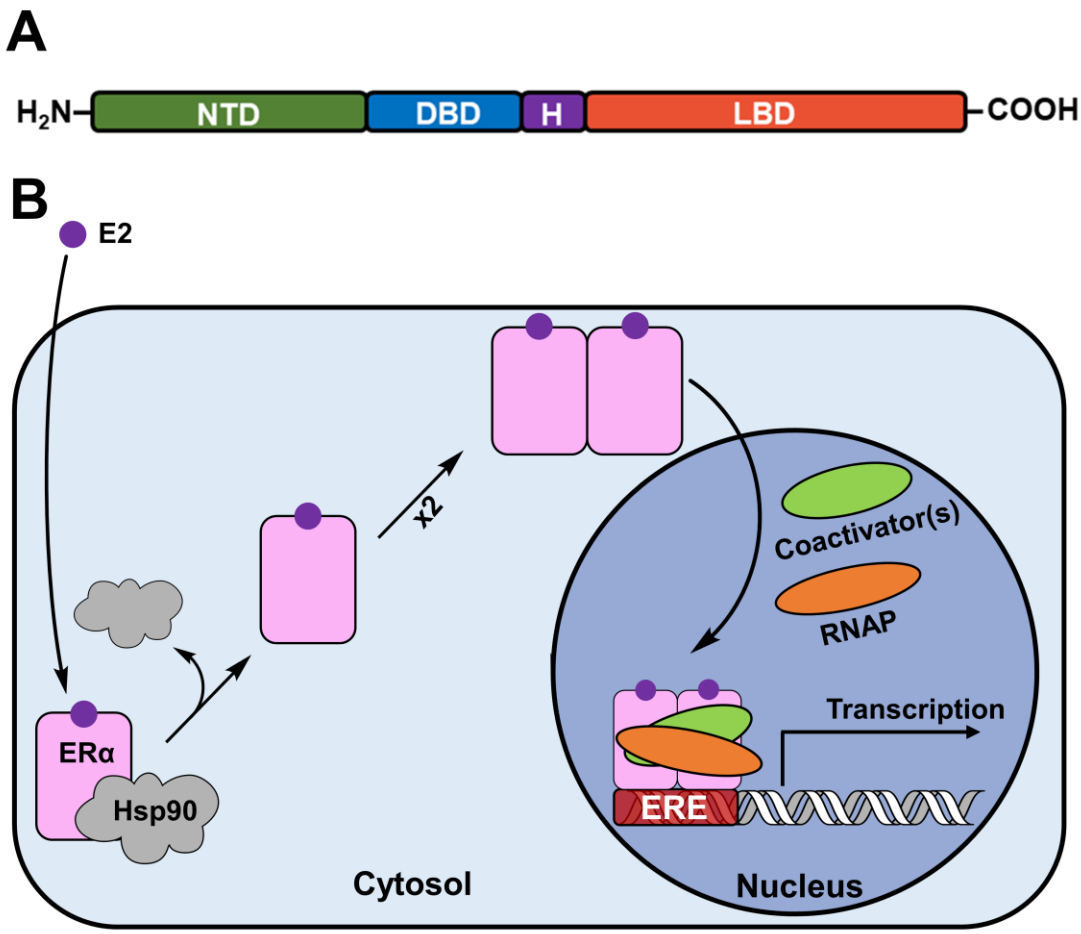

Figure 1.3. Signaling via ERα. (*A*) Domain organization of ERα. (*B*) General mechanism of action of ERα in response to E2.

mostly responsible for the estrogen-dependent transcriptional activity ("activation function 2", or AF-2).

The general mechanism of action of ERα in response to estrogens such as ß-estradiol (E2) is depicted in **Figure 1.3B**.[39,43,53] In the absence of activating estrogens, ERα resides in the cytosol as a complex with Hsp90, among other chaperones. Upon binding of an activating estrogen such as E2, ERα dissociates from Hsp90, dimerizes, and translocates to the nucleus, where it binds EREs as well as coactivators and, ultimately, RNA polymerase (RNAP) to transcribe target genes. In this simple scenario, ERα responds to E2 to upregulate target genes, however the activity of ERα is tightly regulated.[55–60] There are numerous sites of post-translational modification within ERα that affect function, and the relative abundances of coactivator and corepressor proteins can completely change the response of ERα to different estrogens in different cellular environments. In this dissertation, we have built upon previous work in the Dougherty lab to develop tools to study dimerization and sites of interaction between cofactors and the NTD of ERα.

1.3 Non-canonical Amino Acid Mutagenesis

Conventional site-directed mutagenesis is an invaluable technique for conducting biochemical investigations of proteins. There are, however, only 20 canonical naturally-occurring amino acids that together make up most of the proteins we know. We are thus limited in the range of side-chain functionalities we can easily and site-specifically introduce into proteins using endogenous translational machinery.

When different chemistries are needed, there are two methods of hijacking protein translation to site-specifically introduce non-canonical amino acids (NCAAs) into proteins.[61] Both of these methods rely on the use of tRNAs originally identified in

microorganisms that incorporate their cognate amino acids in response to sequences corresponding to nonsense codons in most other organisms; thus these methods are known generally as "nonsense suppression."

In one approach to nonsense suppression used extensively by our lab (**Figure 1.4**), the chemical aminoacylation method,[62] a circular plasmid is first mutated at the site of interest to a nonsense codon (most commonly TAG) using PCR-based methods, and the DNA is linearized and transcribed *in vitro* to yield mRNA. Separately, nearly-full-length suppressor tRNA that recognizes the stop codon is produced by *in vitro* runoff transcription, and is subsequently enzymatically ligated to the final deoxynucleic acid two-mer of the tRNA that has been chemically aminoacylated to a NCAA. Directly introducing the mRNA and the charged tRNA into cells thus gives them everything they need to incorporate a NCAA at the site of interest. A convenient expression system for this

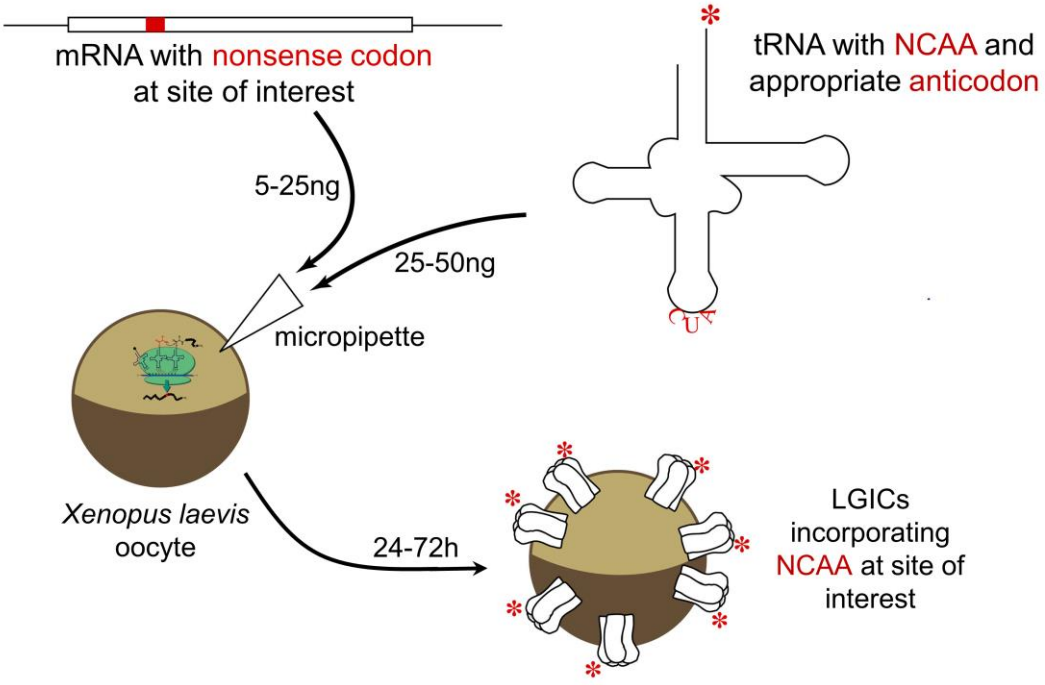

Figure 1.4. Nonsense suppression via the chemical aminoacylation method, using a *Xenopus laevis* oocyte expression system.

approach to NCAA mutagenesis is the *Xenopus laevis* oocyte, which is large enough (~1mm in diameter) that microinjection can be used to introduce the mRNA and aminoacyl tRNA.[63] This method of NCAA mutagenesis is able to introduce an impressively broad range of amino acids and amino acid analogues, limited only by the permissiveness of the ribosome. Still, it suffers from a number of other limitations, foremost of which are the limited amount of protein that can be produced, the labor-intensive process of preparing aminoacylated tRNA *in vitro*, and the complications of working with RNA *in vitro* that come with its instability relative to DNA.

Another method (**Figure 1.5**) of nonsense suppression circumvents many of the drawbacks of the above-described method, but comes with its own limitations. Originally

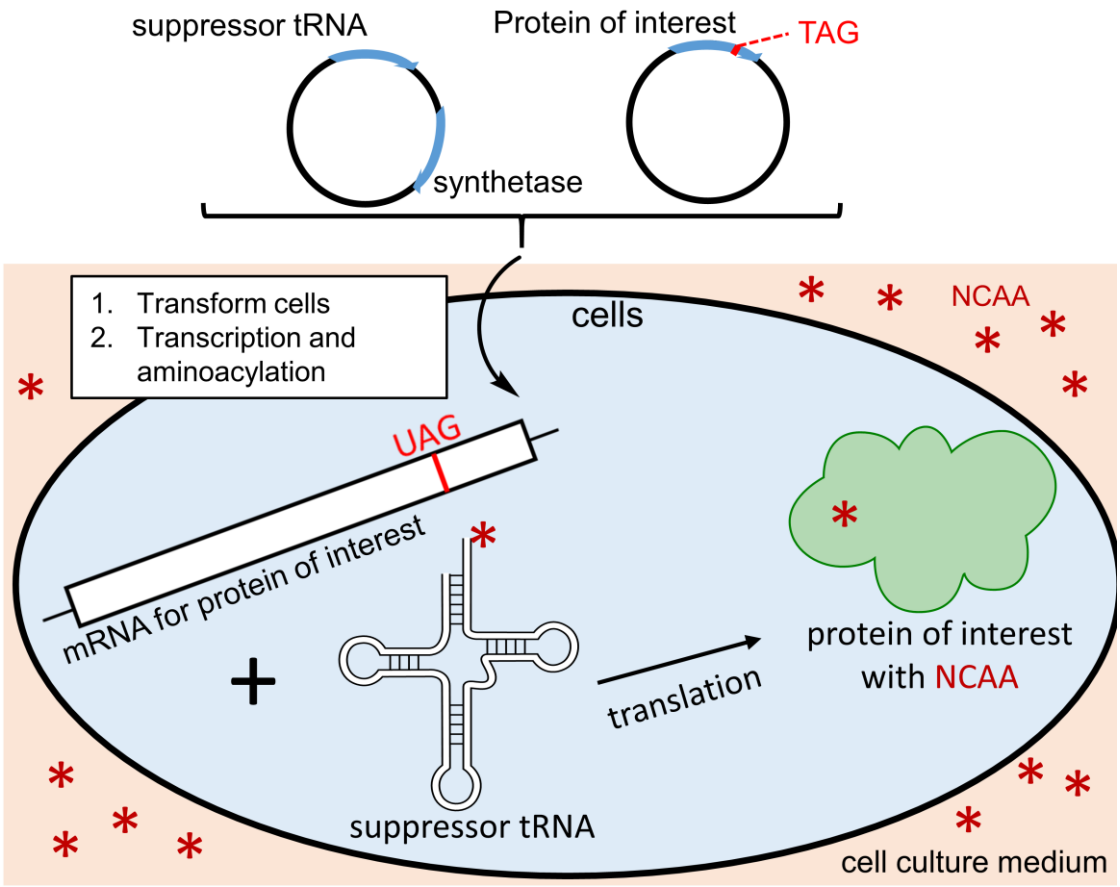

Figure 1.5. Nonsense suppression via the "synthetase method."

developed in the lab of Prof. Peter Schultz,[64,65] this method requires only DNA to be introduced into the heterologous expression system. Two expression vectors are introduced: one for the protein of interest, again with a nonsense mutation (most commonly TAG) at the specified site for incorporation of a NCAA, and another encoding the suppressor tRNA alongside an engineered aminoacyl tRNA synthetase that is able to charge the suppressor tRNA with a free NCAA that is included in the growth medium. Given that this method relies on the action of a synthetase to aminoacylate the suppressor tRNA, we colloquially refer to this technique as the "synthetase method." This method yields greater amounts of protein than the aforementioned approach, but suffers from the need to engineer a new orthogonal tRNA/synthetase pair for any new NCAA that one would like to incorporate. Thus both are useful methods, but excel at different applications.

1.4 Structure-function Analysis of pLGICs

1.4.1 Two-electrode voltage clamp electrophysiology

Electrophysiology is a very powerful method for characterizing ion channel function.[66] While several electrophysiological methods exist, our lab has primarily used two-electrode voltage clamp (TEVC) electrophysiology to characterize ion channel function (**Figure 1.6A**). In this setup, cells (in our case, *Xenopus laevis* oocytes) are impaled with two electrodes: a voltage electrode for monitoring cell potential over the course of the experiment, and a current electrode for injecting current into cells to "clamp" them at a constant membrane potential. Throughout the course of the experiment, the amount of injected current needed to maintain the clamped membrane potential is recorded, and serves as a readout of ion flux across the membrane. This technique can be used to

record currents as small as tens of nanoamps, and thus can be used to measure responses from very small numbers of ion channels.

We use TEVC to generate dose-response curves in the characterization of ion channels in structure-function studies.[36,67] Starting with a low concentration of agonist and applying successively larger concentrations, we measure the current flux across the cell membrane up to some maximum value, I_{max}, at which point a maximal number of ion channels are active (**Figure 1.6B**). The value for I_{max} varies between experiments, however in the analysis of the data, each response is normalized to the I_{max}, which is set to one. Averaging these dose-response relationships for individual cells yields a composite dose-response curve. We then fit these data to the Hill equation,

$$I_{norm} = \frac{1}{\left[1 + \left(\frac{EC_{50}}{[agonist]}\right)^{n_H}\right]}$$

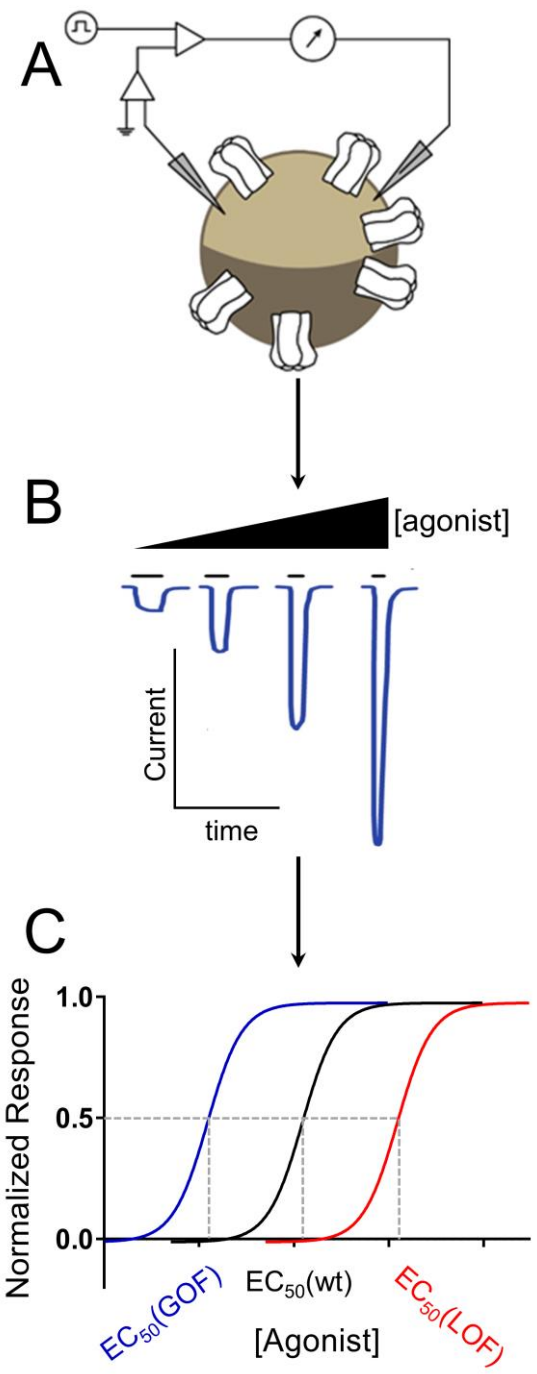

Figure 1.6. Functional characterization of pLGICs via TEVC. (*A*) TEVC setup, using a *Xenopus laevis* oocyte. (*B*) Raw data; current traces in response to agonist. (*C*) Dose-response curves illustrating wild-type, gain of function (GOF), and loss of function (LOF) variants.

where I_{norm} is the normalized current at a given concentration of agonist, n_H is the Hill coefficient (a measure of cooperativity), and EC_{50} is the effective concentration for a half-maximal response (a measure of agonist sensitivity). The metric we mainly compare is EC_{50}. Mutations that make receptors more sensitive to agonist, deemed "gain-of-function", shift the curve to lower EC_{50} values, while those that shift the EC_{50} to higher values are called "loss-of-function" mutants (**Figure 1.6C**). We consider differences in EC_{50} greater than two-fold to be meaningfully different. Notably, changes in EC_{50} may reflect changes in both the binding of ligand and changes in receptor gating.

1.4.2 Mutant cycle analysis

Beyond interpreting changes in EC_{50}, one can perform double-mutant cycle analysis in order to quantify interactions between mutations.[68,69] In a double-mutant cycle analysis (**Figure 1.7A**) of two residues in a pLGIC, dose-response data are collected and EC_{50} values are determined and compared between wild-type receptors, the two single-mutant receptors, and the double-mutant receptor. These EC_{50} values are then used to define a "coupling parameter," Ω:

$$\Omega = \frac{\mathrm{EC}_{50}(wt) * EC_{50}(AB)}{\mathrm{EC}_{50}(A) * EC_{50}(B)}$$

where A and B denote single-mutant receptors and AB designates the double-mutant receptor. This coupling parameter quantifies the extent to which the effects of two mutations deviate from additivity. The extent of this deviation is further reflected in a ΔΔG value, the difference in the free energy of activation between the expected (additive) value versus the observed value for the double mutant, given by the equation

$$\Delta\Delta G = R * T * \ln(\Omega)$$

where R is the gas constant and T is the temperature in kelvins. We consider deviations from additivity ≥ 2-fold ($\Omega \geq 2$ or $\Omega \leq 0.5$) to constitute "meaningful" functional coupling of the mutations. This corresponds to $|\Delta\Delta G| \geq 0.40$ kcal•mol^{-1}. The sign of $\Delta\Delta G$ has to do with the directionality of the deviation from additivity (ie, whether the EC_{50} is higher or lower than expected), however we report $|\Delta\Delta G|$ values throughout, as the magnitude of the coupling energy can be used as a general readout of the functional cooperativity between pairs of mutations, with higher values indicating stronger cooperation.

Mutant cycle analysis can be further used to quantify the cooperativity between three mutations as a unit in a so-called triple mutant cycle analysis.[70] In this type of analysis, depicted pictorially as a cube (**Figure 1.7B**), EC_{50} values are determined for wild-type receptors, three single-mutant and double-mutant receptors, and a triple mutant receptor with all three mutations. In the case when the three mutations of interest do function as a unit, each double-mutant cycle between two mutations on a wild-type

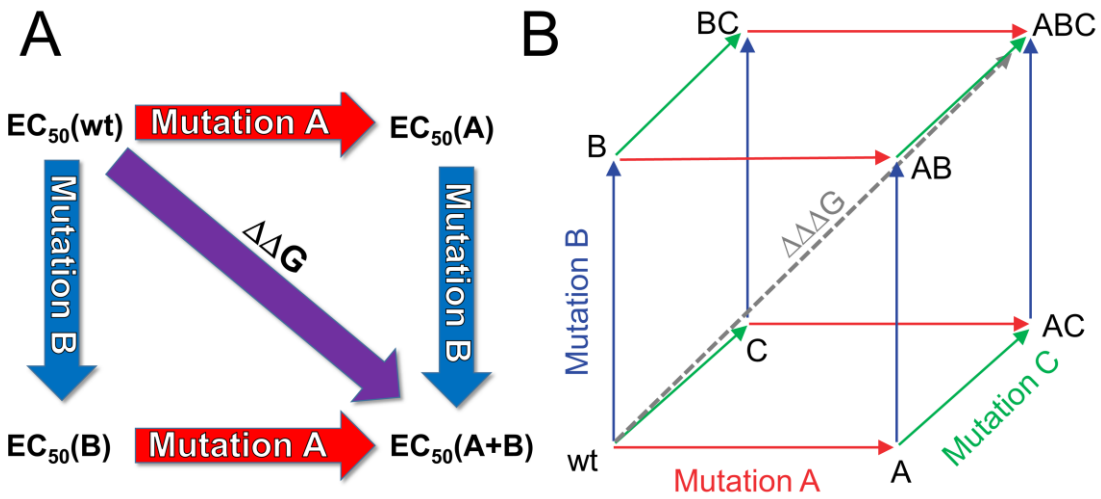

Figure 1.7. Cartoon representations of (*A*) double-mutant cycle analysis and (*B*) triple-mutant cycle analysis. ΔΔG and ΔΔΔG values are determined as described in the text.

background will yield a meaningful ΔΔG value, while the ΔΔG values of the mutant cycles

on the opposite faces of the cube will drop to nearly 0 kcal•mol^{-1}. These opposing faces of the cube represent the equivalent mutant cycle in the background of the third mutation, the presence of which should remove energetic coupling between the other two mutations if the three do indeed function as a co-dependent unit. We then define a coupling energy for the triad as a whole, a ΔΔΔG value, calculated by taking the difference between any two opposite faces of the cube. The ΔΔΔG thus describes the difference between ΔΔG values for double mutant cycles between two mutations in the presence and absence of the third mutation, and greater values of ΔΔΔG reflect a greater energetic dependence among residues of the triad.

1.5 Probing Protein-Protein Interactions using Photocrosslinking Non-canonical Amino Acids

Protein-protein interactions are ubiquitous in biological systems, serving many different functions, including many of clinical relevance.[71–73] Understanding the nature of particular protein-protein interactions and developing tools to better study them is thus invaluable to our ability to address issues of human health and disease.

The use of non-canonical amino acids bearing photoreactive side-chain groups can be very useful for the mapping of protein-protein interaction interfaces and for the identification of novel interacting partners of a protein of interest.[74,75] Using the synthetase method (*section 1.3*), one can introduce a NCAA such as 4-benzoylphenylalanine, *p*-azidophenylalanine (N_3Phe), or any of a number of amino acids containing a diazirine group site-specifically into a protein and irradiate with UV light to generate a radical species that can react with a nearby interactor to form a chemical crosslink. The reaction mechanism for crosslinking using N_3Phe is shown in **Figure 1.8**. Crosslinked complexes

can be purified for downstream analysis using antibodies against the protein of interest or affinity tags**.** Photocrosslinking can then be combined with low-resolution methods like western blotting or higher-resolution methods like mass spectrometry to characterize and/or identify the crosslinked products.[76,77]

There are several advantages to using photocrosslinking NCAAs over other methods of isolating interacting proteins.[74,78] First off, methods such as co-immunoprecipitation that rely on noncovalent interactions between the protein of interest and interacting partners may miss weaker interactions that may nonetheless be functionally relevant. This can be circumvented by using chemical crosslinking methods to create covalent complexes between the target and the protein of interest. However, this approach suffers from the lack of generality of the crosslinking reaction: chemical crosslinkers depend on the presence of certain functional groups, most notably the primary amines of lysine side-chains and the thiols of cysteine side-chains, that may not be present in the protein-protein interface, which itself may not be accessible to the crosslinker. On the other hand, the radical species generated via irradiation of photoreactive NCAAs insert into a

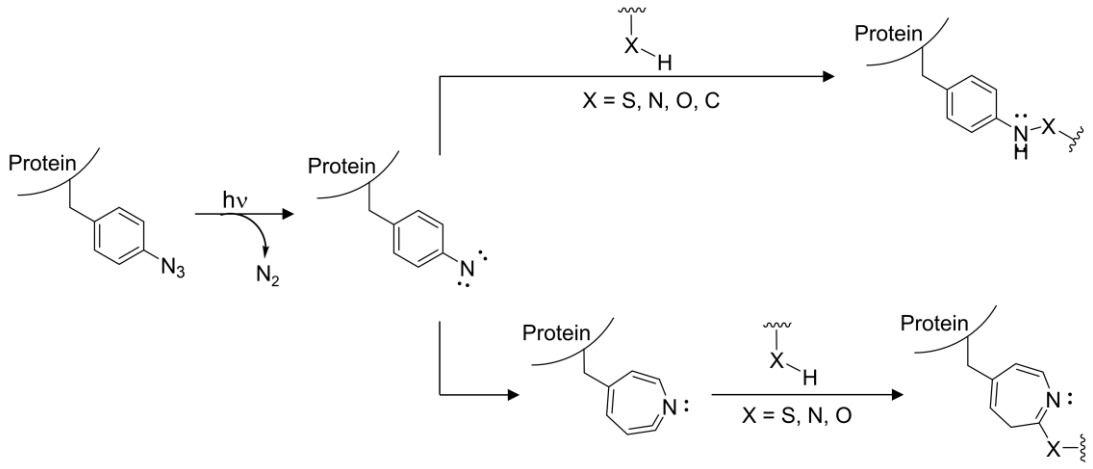

Figure 1.8. Site-specific crosslinking using the NCAA, N_3Phe. Expulsion of N_2 generates a reactive nitrene that can react directly with X-H bonds or rearrange to the ketenimine, whereupon crosslinking can occur via nucleophilic attack.

broad range of bonds, including relatively inert C-H bonds that cannot otherwise be chemically crosslinked. Finally, photocrosslinking NCAAs can be used to detect protein-protein interactions in live cells with high spatiotemporal control while introducing minimal perturbations to the protein of interest. This exquisite combination of control and specificity cannot be found with any other method.

1.6 Summary of Dissertation Work

In this dissertation, canonical and non-canonical amino acid mutagenesis have been used alongside other techniques to perform structure-function studies of pLGICs and probe protein-protein interactions of ERα. The results described herein constitute basic science investigations of protein function, and contribute to our collective knowledge of pLGICs and nuclear receptors, which we hope will have lasting impact on the field.

Chapter 2 describes an investigation of amino acid residues involved in the early steps of gating in the 5-HT_{3A}R and the muscle-type nAChR. Using canonical site-directed mutagenesis to perform an extensive series of double mutant cycle analyses and a triple mutant cycle analysis, we compare the contributions of a triad of residues immediately adjacent to the orthosteric agonist binding site in these two receptors. We further analyze how this triad of residues affects ligand selectivity in the 5-HT_{3A}R, and extend the study to other residues previously implicated in receptor gating.

Chapter 3 presents an investigation of the roles of proline residues in the prokaryotic pLGIC, ELIC. Proline is unique among the naturally-occurring amino acids, being the only amino acid with a side chain that is cyclized onto the peptide backbone, which imbues proline with properties unseen in the other amino acids. By conducting an initial alanine scan of the proline residues in ELIC, we identify those that are most critical

for receptor function. An extensive investigation of the one proline found to be critical for ELIC function via non-canonical amino acid mutagenesis provides insights into the salient chemical features of this residue.

Chapter 4 combines canonical and non-canonical amino acid mutagenesis in a structure-function study of the region at the interface of the ECD and TMD of the 5-HT_{3A}R. This region has been previously implicated in receptor gating of various pLGICs. We add upon what was previously known about the workings of this key gating region by characterizing function of various 5-HT_{3A}R single-mutants, and further combining these mutations in double-mutant cycle analyses to quantify energetic cooperativity between residues in the ECD-TMD interface.

Chapter 5 builds off of previous work in our group to use site-specific incorporation of a photocrosslinking NCAA in ERα overexpressed in mammalian cells in order to quantify receptor homodimerization in response to different drugs, as well as to identify novel interactions between cofactors and the ERα NTD. Using this method, we successfully demonstrate dose-dependent ERα dimerization in response to ß-estradiol (E2), 4-hydroxytamoxifen (4-OHT), the active metabolite of the anticancer drug tamoxifen, and ICI-182780 (fulvestrant), another anticancer drug. We also use photocrosslinking and visualization by western blotting to identify several potential sites within the ERα NTD for cofactor interactions.

1.7 References

1. von Bartheld, C. S., Bahney, J. & Herculano-Houzel, S. The Search for True Numbers of Neurons and Glial Cells in the Human Brain: A Review of 150 Years of Cell Counting. *J. Comp. Neurol.* **524**, 3865–3895 (2016).
2. Lodish, H. *et al.* The Action Potential and Conduction of Electric Impulses. *Mol. Cell Biol. 4th Ed.* (2000).

3. Kress, G. J. & Mennerick, S. Action potential initiation and propagation: upstream influences on neurotransmission. *Neuroscience* **158**, 211–222 (2009).
4. Katz, B. Neural transmitter release: from quantal secretion to exocytosis and beyond. *J. Neurocytol.* **32**, 437–446 (2003).
5. Rangel-Gomez, M. & Meeter, M. Neurotransmitters and Novelty: A Systematic Review. *J. Psychopharmacol. (Oxf.)* **30**, 3–12 (2016).
6. Nemecz, Á., Prevost, M. S., Menny, A. & Corringer, P.-J. Emerging Molecular Mechanisms of Signal Transduction in Pentameric Ligand-Gated Ion Channels. *Neuron* **90**, 452–470 (2016).
7. daCosta, C. J. B. & Baenziger, J. E. Gating of Pentameric Ligand-Gated Ion Channels: Structural Insights and Ambiguities. *Structure* **21**, 1271–1283 (2013).
8. Andrew J Thompson, H. A. L. The structural basis of function in Cys-loop receptors. *Q. Rev. Biophys.* **43**, 449–99 (2010).
9. Dineley, K. T., Pandya, A. A. & Yakel, J. L. Nicotinic ACh Receptors as Therapeutic Targets in CNS Disorders. *Trends Pharmacol. Sci.* **36**, 96–108 (2015).
10. Thompson, A. J. & Lummis, S. C. The 5-HT3 receptor as a therapeutic target. *Expert Opin. Ther. Targets* **11**, 527–540 (2007).
11. Lynch, J. W. Molecular Structure and Function of the Glycine Receptor Chloride Channel. *Physiol. Rev.* **84**, 1051–1095 (2004).
12. Schaefer, N., Roemer, V., Janzen, D. & Villmann, C. Impaired Glycine Receptor Trafficking in Neurological Diseases. *Front. Mol. Neurosci.* **11**, (2018).
13. Greenfield, L. J. Molecular Mechanisms of Antiseizure Drug Activity at GABAA Receptors. *Seizure J. Br. Epilepsy Assoc.* **22**, 589–600 (2013).
14. Nuss, P. Anxiety disorders and GABA neurotransmission: a disturbance of modulation. *Neuropsychiatr. Dis. Treat.* **11**, 165–175 (2015).
15. Palma, E. *et al.* Modulation of GABAA Receptors in the Treatment of Epilepsy. *Curr. Pharm. Des.* **23**, 5563–5568 (2017).
16. Tomek, S. E., LaCrosse, A. L., Nemirovsky, N. E. & Olive, M. F. NMDA Receptor Modulators in the Treatment of Drug Addiction. *Pharmaceuticals* **6**, 251–268 (2013).
17. Ghasemi, M., Phillips, C., Fahimi, A., McNerney, M. W. & Salehi, A. Mechanisms of action and clinical efficacy of NMDA receptor modulators in mood disorders. *Neurosci. Biobehav. Rev.* **80**, 555–572 (2017).
18. Bowie, D. Ionotropic Glutamate Receptors & CNS Disorders. *CNS Neurol. Disord. Drug Targets* **7**, 129–143 (2008).
19. Burnstock, G., Nistri, A., Khakh, B. S. & Giniatullin, R. ATP-gated P2X receptors in health and disease. *Front. Cell. Neurosci.* **8**, (2014).
20. Lee, K. *et al.* Chapter Six - AMPA Receptors as Therapeutic Targets for Neurological Disorders. in *Advances in Protein Chemistry and Structural Biology* (ed. Donev, R.) **103**, 203–261 (Academic Press, 2016).
21. Sharma, G. & Vijayaraghavan, S. Nicotinic Receptors: Role in Addiction and Other Disorders of the Brain. *Subst. Abuse Res. Treat.* **1**, 81–95 (2008).
22. Brunzell, D. H., Stafford, A. M. & Dixon, C. I. Nicotinic receptor contributions to smoking: insights from human studies and animal models. *Curr. Addict. Rep.* **2**, 33–46 (2015).
23. Vincent, A., Palace, J. & Hilton-Jones, D. Myasthenia gravis. *The Lancet* **357**, 2122–2128 (2001).

24. Nys, M., Kesters, D. & Ulens, C. Structural insights into Cys-loop receptor function and ligand recognition. *Biochem. Pharmacol.* **86**, 1042–1053 (2013).
25. Corringer, P.-J. *et al.* Structure and Pharmacology of Pentameric Receptor Channels: From Bacteria to Brain. *Structure* **20**, 941–956 (2012).
26. Albuquerque, E. X., Pereira, E. F. R., Alkondon, M. & Rogers, S. W. Mammalian Nicotinic Acetylcholine Receptors: From Structure to Function. *Physiol. Rev.* **89**, 73–120 (2009).
27. Lummis, S. C. R. 5-HT3 Receptors. *J. Biol. Chem.* **287**, 40239–40245 (2012).
28. Sigel, E. & Steinmann, M. E. Structure, Function, and Modulation of GABAA Receptors. *J. Biol. Chem.* **287**, 40224–40231 (2012).
29. Betz, H. & Laube, B. Glycine receptors: recent insights into their structural organization and functional diversity. *J. Neurochem.* **97**, 1600–1610 (2006).
30. Bocquet, N. *et al.* A prokaryotic proton-gated ion channel from the nicotinic acetylcholine receptor family. *Nature* **445**, 116–119 (2007).
31. Morales-Perez, C. L., Noviello, C. M. & Hibbs, R. E. X-ray structure of the human α4β2 nicotinic receptor. *Nature* **538**, 411–415 (2016).
32. Tasneem, A., Iyer, L. M., Jakobsson, E. & Aravind, L. Identification of the prokaryotic ligand-gated ion channels and their implications for the mechanisms and origins of animal Cys-loop ion channels. *Genome Biol.* **6**, R4 (2005).
33. Hilf, R. J. C. & Dutzler, R. X-ray structure of a prokaryotic pentameric ligand-gated ion channel. *Nature* **452**, 375–379 (2008).
34. Jennie M E Cederholm, P. R. S. Gating mechanisms in Cys-loop receptors. *Eur. Biophys. J. EBJ* **39**, 37–49 (2009).
35. Lynagh, T. & Pless, S. A. Principles of agonist recognition in Cys-loop receptors. *Membr. Physiol. Membr. Biophys.* **5**, 160 (2014).
36. Van Arnam, E. B. & Dougherty, D. A. Functional Probes of Drug–Receptor Interactions Implicated by Structural Studies: Cys-Loop Receptors Provide a Fertile Testing Ground. *J. Med. Chem.* **57**, 6289–6300 (2014).
37. Xiu, X., Puskar, N. L., Shanata, J. A. P., Lester, H. A. & Dougherty, D. A. Nicotine binding to brain receptors requires a strong cation–π interaction. *Nature* **458**, 534–537 (2009).
38. Sever, R. & Glass, C. K. Signaling by Nuclear Receptors. *Cold Spring Harb. Perspect. Biol.* **5**, (2013).
39. Yaşar, P., Ayaz, G., User, S. D., Güpür, G. & Muyan, M. Molecular mechanism of estrogen–estrogen receptor signaling. *Reprod. Med. Biol.* **16**, 4–20 (2017).
40. Arnal, J.-F. *et al.* Membrane and Nuclear Estrogen Receptor Alpha Actions: From Tissue Specificity to Medical Implications. *Physiol. Rev.* **97**, 1045–1087 (2017).
41. Farooq, A. Structural and Functional Diversity of Estrogen Receptor Ligands. *Curr. Top. Med. Chem.* **15**, 1372–1384 (2015).
42. McDonnell, D. P. The molecular determinants of estrogen receptor pharmacology. *Maturitas* **48**, 7–12 (2004).
43. Cheskis, B. J., Greger, J. G., Nagpal, S. & Freedman, L. P. Signaling by estrogens. *J. Cell. Physiol.* **213**, 610–617 (2007).
44. Deroo, B. J. & Korach, K. S. Estrogen receptors and human disease. *J. Clin. Invest.* **116**, 561–570 (2006).

45. Lim, E. *et al.* Pushing estrogen receptor around in breast cancer. *Endocr. Relat. Cancer* **23**, T227–T241 (2016).
46. Hua, H., Zhang, H., Kong, Q. & Jiang, Y. Mechanisms for estrogen receptor expression in human cancer. *Exp. Hematol. Oncol.* **7**, 24 (2018).
47. Rothenberger, N. J., Somasundaram, A. & Stabile, L. P. The Role of the Estrogen Pathway in the Tumor Microenvironment. *Int. J. Mol. Sci.* **19**, (2018).
48. Jameera Begam, A., Jubie, S. & Nanjan, M. J. Estrogen receptor agonists/antagonists in breast cancer therapy: A critical review. *Bioorganic Chem.* **71**, 257–274 (2017).
49. Patel, H. K. & Bihani, T. Selective estrogen receptor modulators (SERMs) and selective estrogen receptor degraders (SERDs) in cancer treatment. *Pharmacol. Ther.* **186**, 1–24 (2018).
50. Heery, M., Corbett, P. & Zelkowitz, R. Precautions for Patients Taking Tamoxifen. *J. Adv. Pract. Oncol.* **9**, 78–83 (2018).
51. Robinson-Rechavi, M., Garcia, H. E. & Laudet, V. The nuclear receptor superfamily. *J. Cell Sci.* **116**, 585–586 (2003).
52. Heldring, N. *et al.* Estrogen Receptors: How Do They Signal and What Are Their Targets. *Physiol. Rev.* **87**, 905–931 (2007).
53. Parker, M. G. Structure and Function of Estrogen Receptors. in *Vitamins & Hormones* (ed. Litwack, G.) **51**, 267–287 (Academic Press, 1995).
54. Kumar, R. *et al.* The Dynamic Structure of the Estrogen Receptor. *Journal of Amino Acids* (2011). doi:10.4061/2011/812540
55. Norris, J. D., Chang, C. & McDonnell, D. P. Estrogen receptor-cofactor interactions as targets for novel drug discovery. *Ernst Scher. Res. Found. Workshop* 181–201 (2001).
56. Atsriku, C. *et al.* Systematic Mapping of Posttranslational Modifications in Human Estrogen Receptor-α with Emphasis on Novel Phosphorylation Sites. *Mol. Cell. Proteomics MCP* **8**, 467–480 (2009).
57. Anbalagan, M., Huderson, B., Murphy, L. & Rowan, B. G. Post-translational modifications of nuclear receptors and human disease. *Nucl. Recept. Signal.* **10**, (2012).
58. Merrell, K. W. *et al.* Differential recruitment of nuclear receptor coregulators in ligand-dependent transcriptional repression by estrogen receptor-α. *Oncogene* **30**, 1608–1614 (2011).
59. Tremblay, G. B. & Giguère, V. Coregulators of estrogen receptor action. *Crit. Rev. Eukaryot. Gene Expr.* **12**, 1–22 (2002).
60. Manavathi, B., Samanthapudi, V. S. K. & Gajulapalli, V. N. R. Estrogen receptor coregulators and pioneer factors: the orchestrators of mammary gland cell fate and development. *Front. Cell Dev. Biol.* **2**, (2014).
61. Leisle, L., Valiyaveetil, F., Mehl, R. A. & Ahern, C. A. Incorporation of non-canonical amino acids. *Adv. Exp. Med. Biol.* **869**, 119–151 (2015).
62. Dougherty, D. A. & Van Arnam, E. B. In Vivo Incorporation of Unnatural Amino Acids Using the Chemical Aminoacylation Strategy. A Broadly Applicable Mechanistic Tool. *Chembiochem Eur. J. Chem. Biol.* **15**, 1710–1720 (2014).
63. Nowak, M. W. *et al.* [28] In vivo incorporation of unnatural amino acids into ion channels in Xenopus oocyte expression system. in (ed. Enzymology, B.-M. in) **293**, 504–529 (Academic Press, 1998).

64. Noren, C. J., Anthony-Cahill, S. J., Griffith, M. C. & Schultz, P. G. A general method for site-specific incorporation of unnatural amino acids into proteins. *Science* **244**, 182–188 (1989).
65. Liu, C. C. & Schultz, P. G. Adding New Chemistries to the Genetic Code. *Annu. Rev. Biochem.* **79**, 413–444 (2010).
66. Papke, R. L. & Smith-Maxwell, C. High-throughput electrophysiology with Xenopus oocytes. *Comb. Chem. High Throughput Screen.* **12**, 38–50 (2009).
67. Colquhoun, D. Binding, gating, affinity and efficacy: The interpretation of structure-activity relationships for agonists and of the effects of mutating receptors. *Br. J. Pharmacol.* **125**, 923–947 (1998).
68. Horovitz, A. Double-mutant cycles: a powerful tool for analyzing protein structure and function. *Fold. Des.* **1**, R121–R126 (1996).
69. Shanata, J. A. P., Frazier, S. J., Lester, H. A. & Dougherty, D. A. Using Mutant Cycle Analysis to Elucidate Long-Range Functional Coupling in Allosteric Receptors. *Methods Mol. Biol. Clifton NJ* **796**, 97–113 (2012).
70. Miles, T. F., Bower, K. S., Lester, H. A. & Dougherty, D. A. A Coupled Array of Noncovalent Interactions Impacts the Function of the 5-HT3A Serotonin Receptor in an Agonist-Specific Way. *ACS Chem. Neurosci.* **3**, 753–760 (2012).
71. Modell, A. E., Blosser, S. L. & Arora, P. S. Systematic Targeting of Protein–Protein Interactions. *Trends Pharmacol. Sci.* **37**, 702–713 (2016).
72. Jin, L., Wang, W. & Fang, G. Targeting Protein-Protein Interaction by Small Molecules. *Annu. Rev. Pharmacol. Toxicol.* **54**, 435–456 (2014).
73. Scott, D. E., Bayly, A. R., Abell, C. & Skidmore, J. Small molecules, big targets: drug discovery faces the protein–protein interaction challenge. *Nat. Rev. Drug Discov.* **15**, 533–550 (2016).
74. Coin, I. Application of non-canonical crosslinking amino acids to study protein–protein interactions in live cells. *Curr. Opin. Chem. Biol.* **46**, 156–163 (2018).
75. Tanaka, Y., Bond, M. R. & Kohler, J. J. Photocrosslinkers illuminate interactions in living cells. *Mol. Biosyst.* **4**, 473–480 (2008).
76. O'Reilly, F. J. & Rappsilber, J. Cross-linking mass spectrometry: methods and applications in structural, molecular and systems biology. *Nat. Struct. Mol. Biol.* **25**, 1000 (2018).
77. Sinz, A. Cross-Linking/Mass Spectrometry for Studying Protein Structures and Protein–Protein Interactions: Where Are We Now and Where Should We Go from Here? *Angew. Chem. Int. Ed.* **57**, 6390–6396 (2018).
78. Chin, J. W. & Schultz, P. G. In Vivo Photocrosslinking with Unnatural Amino Acid Mutagenesis. *ChemBioChem* **3**, 1135–1137 (2002).

Chapter 2: A triad of residues is functionally transferrable between 5-HT_3 serotonin receptors and nicotinic acetylcholine receptors*

2.1 Abstract

Cys-loop receptors are pentameric ligand-gated ion channels that facilitate communication within the nervous system. Upon ligand binding, these receptors undergo an allosteric activation mechanism connecting the binding event to the membrane-spanning channel pore, which expands to conduct ions. Some of the earliest steps in this activation mechanism are carried out by residues proximal to the binding site, the relative positioning of which may reflect functional differences among the receptors. Herein, we investigated key side-chain interactions near the binding site via mutagenesis and two-electrode voltage-clamp electrophysiology in serotonin-gated 5-HT_{3A} receptors (5-HT_{3A}Rs) and nicotinic acetylcholine receptors (nAChRs) expressed in *Xenopus laevis* oocytes. We found that a triad of residues aligning to Thr-152, Glu-209, and Lys-211 in the 5-HT_{3A}R can be exchanged between the homomeric 5-HT_{3A}R and the muscle-type nAChR α-subunit with small functional consequences. Via triple mutant cycle analysis, we demonstrated that this triad forms an interdependent network in the muscle-type nAChR. Further, nAChR-type mutations of the 5-HT_{3A}R affect the affinity of nicotine, a competitive antagonist of 5-HT_{3A}Rs, in a cooperative manner. Using mutant cycle analyses between the 5-HT_{3A} triad,

---

* *This chapter is adapted with permission from: Mosesso, R. & Dougherty, D. A. A triad of residues is functionally transferrable between 5-HT3 serotonin receptors and nicotinic acetylcholine receptors. J. Biol. Chem.* ***293****, 2903–2914 (2018).*

loop A residues Asn-101 and Glu-102, ß9 residue Lys-197, and the channel gate at Thr-257, we observed that residues in this region are energetically linked to the channel gate and are particularly sensitive to mutations that introduce a net positive charge. This study expands our understanding of the differences and similarities in the activation mechanisms of Cys-loop receptors.

2.2 Introduction

Cys-loop receptors are the subset of pentameric ligand-gated ion channels found in vertebrates, and include excitatory nicotinic acetylcholine receptors (nAChRs) and serotonin-activated 5-HT_3 receptors (5-HT_3Rs), as well as inhibitory type A γ-aminobutyric acid receptors ($GABA_A$Rs), and glycine receptors (GlyRs).[1–4] The pharmacology of these receptors is quite broad, and targeted therapeutics may lead to novel treatments for a variety of conditions.[5–7]

The overall structure of Cys-loop receptors is highly conserved.[8] Each subunit is composed of an extracellular domain (ECD) beta sandwich, a transmembrane domain (TMD) formed by four α-helices (numbered M1-M4), and a variable intracellular domain defined primarily by the loop between the M3 and M4 helices. Five subunits assemble in a concentric manner to form a single receptor. Ligand binding sites are formed at subunit interfaces in the ECD by three primary (+) face "loops" A-C, and three complementary (-) face "loops" D-F. An overall picture of the 5-HT_3R and the interface between two subunits, as exemplified in a cryo-EM structure of the homopentameric 5-HT_{3A}R, is shown in **Figure 2.1A** (PDB ID: 6HIO).[9]

The advent of complete structures of eukaryotic Cys-loop receptors, while generally at fairly low resolution, has provided valuable guidance for comparing members of the Cys-loop receptor family. The present work was motivated by the recognition of a

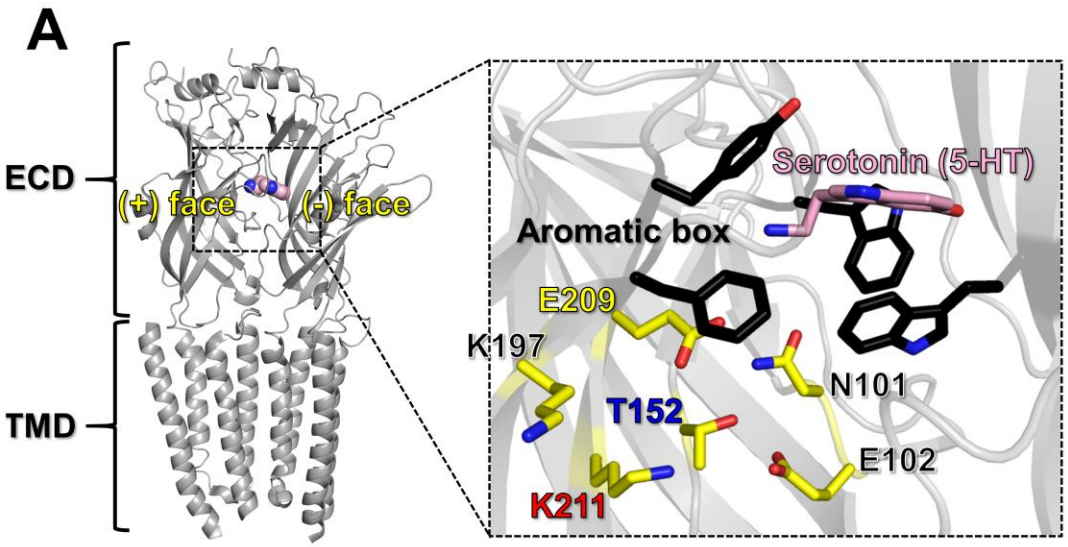

B

Residue number*:	...	152	...	209	210	211	...
human 5-HT$_{3A}$	...	T	...	E	M	K	...
human α1 nAChR	...	K	...	D	I	T	...
human α2 nAChR	...	K	...	D	V	T	...
human α3 nAChR	...	K	...	D	I	T	...
human α4 nAChR	...	K	...	D	I	T	...
human α5 nAChR	...	K	...	Y	I	T	...
human α6 nAChR	...	K	...	D	I	T	...
human α7 nAChR	...	K	...	D	V	T	...
human α9 nAChR	...	T	...	D	V	T	...
human α10 nAChR	...	T	...	D	V	T	...
human ß1 GABAA	...	E	...	R	L	S	...
human ß2 GABAA	...	E	...	R	L	S	...
human ß3 GABAA	...	E	...	R	L	S	...

Figure 2.1. Region of interest in this study. *A*, View of two adjacent receptor subunits from the 5-HT$_{3A}$R cryo-EM (PDB 6HIO), with 5-HT shown as spheres (left). Yellow, carbon atoms of residues mutated in this study; pink, serotonin carbon atoms; black, aromatic box carbon atoms; blue, nitrogen atoms; red, oxygen atoms. *B*, Sequence alignment of subunits contributing to the primary binding face of human-type 5-HT$_{3A}$Rs, nAChRs, and GABA$_A$Rs. Cells are colored according to side-chain chemistry. Unfilled cells indicate non-conservation with regard to the triad in that receptor subtype. ECD, extracellular domain; TMD, transmembrane domain; ICD, intracellular domain, was excluded from this figure. *Residue numbers corresponding to the 5-HT$_{3A}$R cryo-EM structure (PDB: 6HIO).

triad of residues that are, in a global sense, conserved across several members of the family. Our primary focus has been on the homopentameric 5-HT_{3A}R, for which the residues of interest are T152, E209, and K211 (numbering as in the crystal structure[10] and cryo-EM structures;[9,11,12] these have been referred to elsewhere at T179, E236, and K238). The aligning residues in the nAChR α-subunits are typically K, D, and T, respectively, while those in the $GABA_A$R ß-subunits are E, R, and S, respectively. Thus, in each triad, there is a cationic residue (K/R), an anionic residue (D/E), and a residue with an alcohol side chain (S/T), however the relative positioning of these functionalities varies among these receptors. This curious observation led us to ask whether the arrangement reflects differences among receptors. A sequence alignment (**Figure 2.1B**) illustrates the conservation of these arrangements within individual receptor subfamilies in humans. Note that there are exceptions in the α5 and α10 nAChR subunits, however these particular α-subunits do not contribute to the primary binding face of nAChRs.[1] The α8 nAChR subunit was excluded because it is not found in mammals.[1]

Herein we evaluate the functional role of this triad in two excitatory Cys-loop receptors – the 5-HT_{3A}R and the muscle-type ($(\alpha_1)_2ß_1\gamma\delta$) nAChR – using two-electrode voltage clamp electrophysiology of mutant receptors expressed in *Xenopus laevis* oocytes. We find that the 5-HT_{3A}R and nAChR triads can be swapped between these two receptors with only small losses of function. Additionally, substituting the nAChR triad into the 5-HT_{3A}R increases the affinity of nicotine, demonstrating that this triad influences ligand binding. In contrast, swapping the triad from the inhibitory $GABA_A$R into the 5-HT_{3A}R does not result in a functional receptor.

We note from the start that several of the residues considered here have been evaluated by other investigators, and we have built off that work. In muscle-type nAChRs, state-dependent interactions have been proposed between K145, D200, and Y190.[13–18] The former two residues are part of the above-described "triad," and Y190 sits on loop C and is part of the aromatic box that contributes to the agonist binding site.[19,20] The key hydrogen bonding role proposed for Y190, however, is not possible in the 5-HT_{3A}R, as the aligning residue is F199. As described below, a more general interaction between the 5-HT_3R triad and loop A of the agonist binding site is seen. Overall, these results highlight similarities and variations across members of the Cys-loop family.

2.3 Results and Discussion

2.3.1 Effects of exchanging triads between the 5-HT_{3A}R and the muscle-type nAChR

To evaluate the role of the triad of residues, we used site-directed mutagenesis to introduce mutations into receptors expressed in *Xenopus laevis* oocytes and measured functional responses via dose-response relationships using two-electrode voltage clamp electrophysiology, as described in *Experimental Procedures*. We generated the 5-HT_{3A}R single mutants T152K, E209D and K211T, (corresponding to the aligning nAChR residues) as well at the double mutants T152K/K211T, E209D/K211T, and T152K/K211T and the triple mutant T152K/E209D/K211T. The average dose-response curves measured for these mutant receptors are compared in **Figure 2.2A**, and **t**he full pharmacological characterization in response to the native agonist serotonin (5-hydroxytryptamine, or 5-HT) is provided in **Table 2.1**. Relative to the wild-type 5-HT_{3A}R, the single mutant receptors had EC_{50} values for serotonin that were 39-, 10-, and 1.2-fold greater than wild-type for T152K, E209D, and K211T, respectively. While the losses of function for T152K

and E209D are clearly meaningful, the consequence K211T is not. Note that structurally, however, the E209D mutation would be expected to be the least perturbing.

Next, double mutants incorporating each of the above three mutations in pairs were generated in order to evaluate energetic coupling between the mutations via mutant cycle analyses. The extent of energetic coupling in a mutant cycle analysis is defined as the ΔΔG° value for the double mutant, and quantifies the extent to which the individual mutations cooperate in the activation mechanism of the receptor.[21] If residues are close enough in space that a direct interaction is

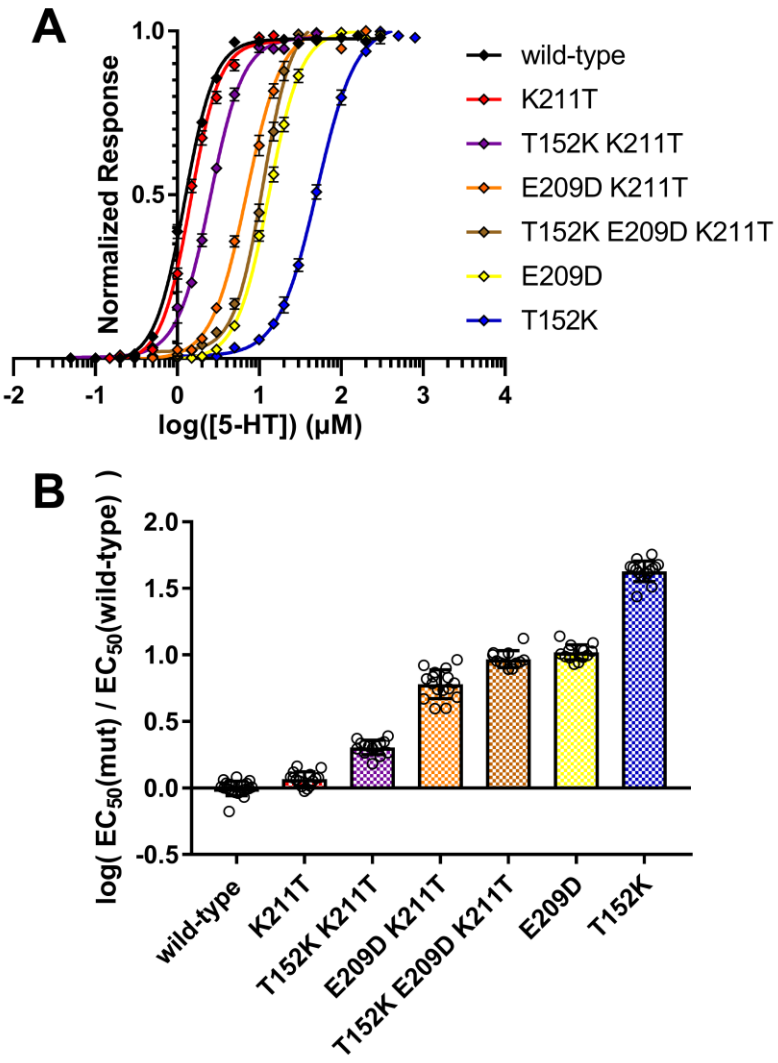

Figure 2.2. Mutating residues T152, E209, and K211 in 5-HT$_{3A}$Rs to their equivalents in nAChRs has non-additive effects on receptor function. *A*, Dose-response curves of wild-type and mutant receptors to 5-HT. Variants are ordered from top to bottom in order of increasing EC_{50}. *B*, Scatterplots illustrating losses of function (±S.D.) of mutants on a logarithmic scale. The double mutants and triple mutant display considerable deviations from additivity.

possible, the ΔΔG° value can also be used as a readout of the strength of this interaction.

The results of the double mutant cycles are provided in **Table 2.1**. **Figure 2.2B** illustrates the non-additive effects of the mutations as a scatterplot. The T152K/K211T double-mutant had an EC_{50} of only 2.5 ± 0.05μM 5-HT, a mere 2-fold loss of function relative to wild-type (1.3 ± 0.03μM) and a 19-fold gain of function relative to the single mutant T152K (EC_{50} = 49 ± 1.03μM). Thus, these two mutations are strongly energetically coupled, with ΔΔG° = 1.8 kcal•mol^{-1}. This and their close orientation in space suggest a direct interaction between these two residues. The double mutant E209D/K211T showed a much lower coupling energy of ΔΔG° = 0.49 kcal•mol^{-1}. We consider a two-fold deviation from additivity (ΔΔG° ≥ 0.40 kcal•mol^{-1}) to be meaningful, suggesting that the E209D and K211T mutations do affect one another, albeit much less so than the T152K/K211T double mutant.

The double mutant T152K/E209D was nonfunctional up to 800μM 5-HT. If the effects of the two mutations were additive, one would expect an EC_{50} on the order of ~500μM 5-HT. If this were the case, we unfortunately could not measure a full dose-

Table 2.1
Response to 5-HT of 5-HT_{3A}Rs incorporating nAChR-type mutations.

Mutation(s)	EC_{50} (μM)	n_H	$\|I_{max}\|$ (μA)	Fold	N	ΔΔG†
-	1.3 ± 0.03	2.4 ± 0.11	1.1 - 78	1.0	21	-
T152K	49 ± 1.03	1.9 ± 0.06	0.14 - 11	39	15	-
E209D	13 ± 0.20	2.3 ± 0.07	0.53 - 21	10	15	-
K211T	1.5 ± 0.04	2.9 ± 0.16	1.9 - 25	1.2	15	-
T152K E209D	NR	NR	NR	NR	15	0.04*
T152K K211T	2.5 ± 0.05	2.1 ± 0.08	1.3 - 56	2.0	14	1.8
E209D K211T	6.9 ± 0.25	2.1 ± 0.11	0.18 - 12	5.5	16	0.49
T152K E209D K211T	11 ± 0.39	2.4 ± 0.18	0.15 - 19	8.4	12	-

†kcal•mol^{-1}; *Measured in the background of K211T; NR = no response; ± indicates SEM.

response relationship due to open channel block of 5-HT_{3A}Rs at high concentrations of 5-HT. In order to meet our criterion for a meaningful coupling energy of ≥ 0.40 kcal•mol^{-1}, the EC_{50} would either have to be less than ~200μM 5-HT if the mutations are meaningfully sub-additive or greater than ~800μM 5-HT if they are superadditive. The two mutations are clearly not sub-additive, as we observed no response to concentrations of 5-HT up to 800μM. It remains possible that the effects of these mutations are superadditive, i.e. the deleterious effects of the mutations are augmented when both are included together. It is also possible that combining the T152K and E209D mutations impairs proper folding or trafficking of receptors to the cell surface, as we did not control for this possibility.

Having generated the single mutants and double mutants, we next generated the 5-HT_{3A}R variant T152K/E209D/K211T, incorporating all three residues of the nicotinic triad. This receptor had only an 8.4-fold increase in 5-HT EC_{50} relative to wild type, comparable to the single-mutant E209D and much less than the single-mutant T152K. The increase in EC_{50} for the triple mutant is much less than would be expected if the effects of three mutations were additive. Thus, the full three-residue swap of nAChR residues into the 5-HT_{3A}R produces functional receptors.

Having the triple mutant enables a mutant cycle between T152K and E209D in the background of the K211T mutation. This mutant cycle has a $\Delta\Delta G° = 0.04$ kcal•mol^{-1} (**Table 2.1**), suggesting that T152K and E209D affect the receptor in distinct ways, at least in the background of K211T. The triple mutant also had somewhat different apparent activation/deactivation kinetics than wild-type receptors, and a greater extent of open channel block at concentrations of 5-HT above those that caused a maximal response.

We next tested to see how a prototypical nAChR, the muscle-type ($(\alpha1)_2\beta1\gamma\delta$) nAChR, would respond when the 5-HT_{3A}R triad was introduced. While the most recent nAChR structural data are for the α4ß2 neuronal subtype,[22,23] we were unable to perform the desired experiments in that subtype due to poor expression levels. This can be addressed by introducing mutations to the channel pore residue L9' that enhance gating of nAChRs in a general way,[24–26] however this would complicate our analysis as the residues of interest are involved in receptor gating. However, the muscle-type nAChR expresses robustly in *Xenopus* oocytes. The relevant residues are the same in the α1 (muscle-type) and α4 subunits, and they are positioned similarly in the cryo-EM structure of the highly homologous *Torpedo* receptor (PDB ID: 2BG9).[27] We generated single mutants α1 K145T, D200E, and T202K, and the pharmacological responses of these mutants to the native agonist acetylcholine (ACh) are summarized in **Table 2.2**. Dose-response relationships and scatterplots of log(fold-shift) values for individual runs are compared between the mutant receptors and wild-type in **Figure 2.3A** and **2.3B**, respectively. All single mutations caused modest losses of function: 4.9-, 2.9-, and 9.0-fold for K145T, D200E, and T202K, respectively.

Table 2.2
Response to ACh of muscle-type nAChRs incorporating 5-HT_{3A}R-type mutations.

Mutation(s)	EC_{50} (μM)	n_H	$\lvert I_{max}\rvert$ (μA)	Fold	N	$\Delta\Delta G^{\dagger}$
-	15 ± 0.08	1.5 ± 0.08	3.6 - 47	-	14	-
α1 K145T	75 ± 3.6	1.4 ± 0.05	4.0 - 62	4.9	16	-
α1 D200E	45 ± 0.20	1.2 ± 0.08	0.05 - 0.58	2.9	13	-
α1 T202K	140 ± 2.5	1.5 ± 0.03	10 - 62	9.0	10	-
α1 K145T D200E	44 ± 2.4	1.2 ± 0.09	0.08 - 23	2.8	13	0.94
α1 K145T T202K	110 ± 0.95	1.3 ± 0.04	0.35 - 5.9	7.2	12	1.0
α1 D200E T202K	82 ± 3.8	1.4 ± 0.08	0.05 - 0.14	5.3	10	0.93
α1 K145T D200E T202K	67 ± 5.3	1.1 ± 0.06	0.05 - 0.18	4.3	10	-

†kcal•mol^{-1}; ± indicates SEM.

We next generated double mutant pairs in the nAChR (**Table 2.2**) as described previously for the 5-HT_{3A}R. Interestingly, the ΔΔG° values for each of the double mutants K145T/D200E, D200E/T202K, and K145T/T202K were all near 1.0 kcal•mol^{-1}, indicating a similar degree of cooperativity between any two mutations. It is not surprising that mutations to K145 and D200 should be coupled, as previous work has proposed a salt bridge between these residues in the muscle-type nAChR.[13] Indeed, analysis via patch clamp electrophysiology of the steady-state dissociation of ACh from the double mutant K145Q D200N has been previously observed to

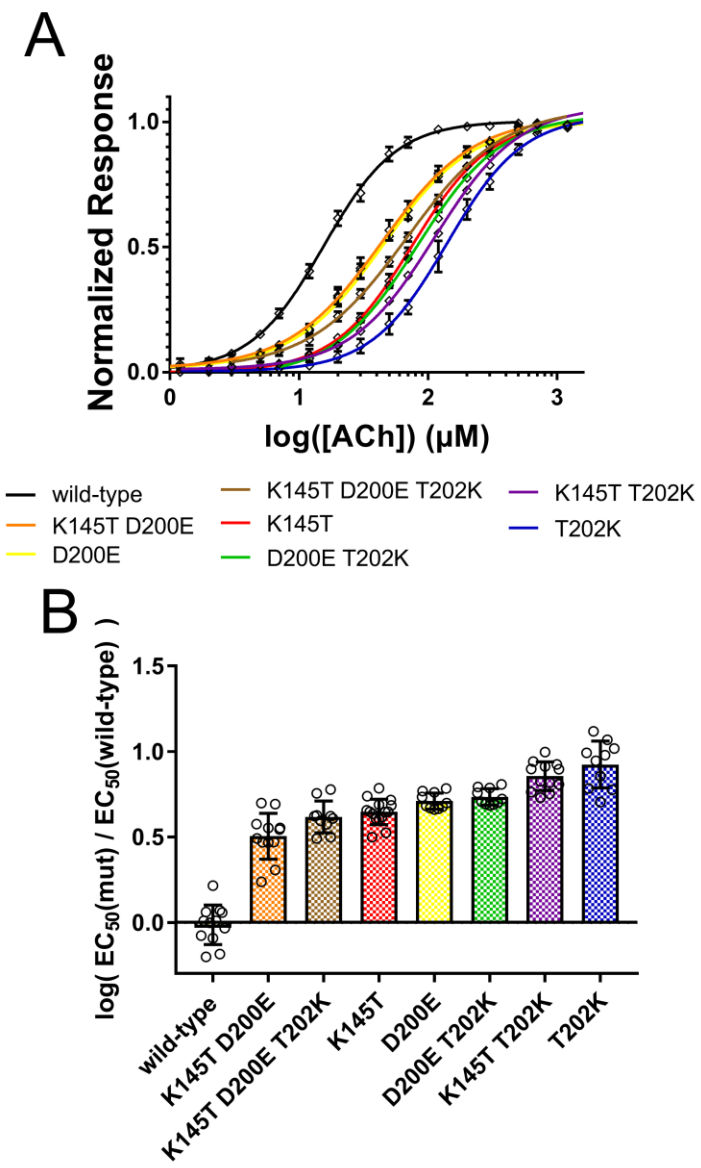

Figure 2.3. Mutating muscle-type nAChR residues K145, D200, and T202 to their equivalents in 5-HT_{3A}Rs has non-additive effects on receptor function. *A*, Dose-response curves of wild-type and mutant receptors to ACh. *B*, Scatterplots illustrating losses of function (±S.D.) of mutants on a logarithmic scale. The double mutants and triple mutant display considerable deviations from additivity.

give a very similar ΔΔG° value of 1.0 kcal•mol^{-1}, and other measures suggest a strong interaction between the two.[13] Our observation that both residues also couple to T202 suggests interactions among all three.

The next logical step was to evaluate the functional response to ACh of the triple mutant: α1 K145T/D200E/T202K. The triple mutant receptor was functional, with EC_{50} = 67 ± 5.3μM ACh, a 4.3-fold increase from wild-type (**Table 2.2**). The data from the single, double, and triple mutants enables a triple mutant cycle analysis of these three mutations. A triple mutant cycle can be represented as a cube (**Figure 2.4**), with the difference between each opposite face giving a ΔΔΔG°, which quantifies the interaction energy among all three residues as a unit.[28] We find in each case that ΔΔΔG° = 0.95 kcal•mol^{-1}. That is, any pair of mutations gives ΔΔG° ≈ 0.95 kcal•mol^{-1}, but in the background of any single mutation a double mutant cycle of the other two mutations yields ΔΔG° ≈ 0 kcal•mol^{-1}.

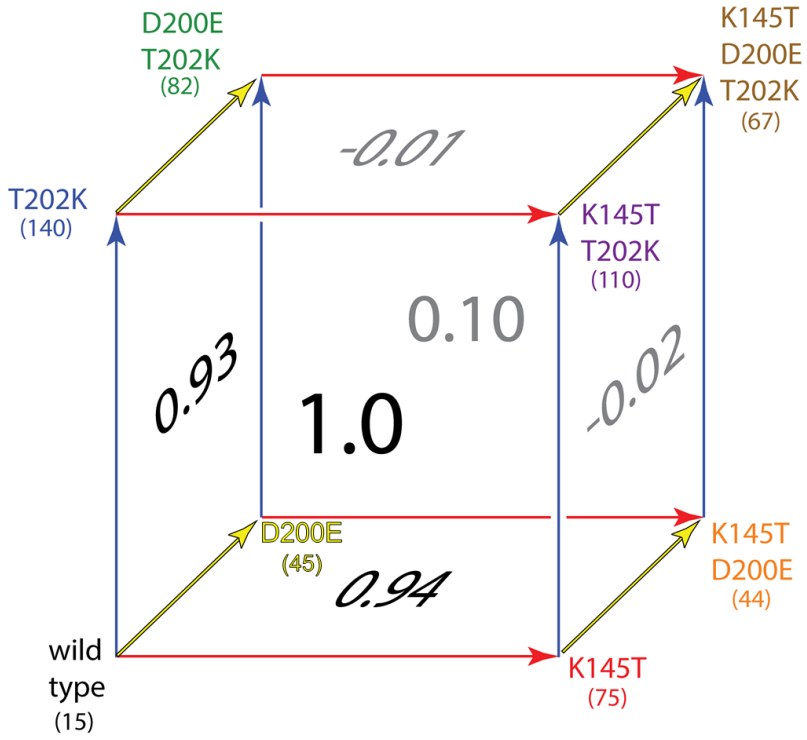

Figure 2.4. Triple mutant cycle in the muscle-type nAChR. Each face of the cube represents a double mutant cycle. Double mutant cycles from wild-type are meaningfully coupled, however any pair of mutations is uncoupled in the background of the other mutation of the triad. This analysis yields ΔΔΔG = 0.95 kcal•mol^{-1} for the three mutations.

Thus, these residues not only interact with one another in the activation mechanism, but operate as a co-dependent unit in the mouse muscle-type nAChR. Each pair of residues is energetically dependent on the third residue of the triad.

To further evaluate the role of this triad, we mutated residues in the 5-HT_{3A}R to their equivalents in $GABA_A$R ß-subunits, which form the primary binding face in $GABA_A$Rs. The results are summarized in **Table 2.3**. The single-mutant T152E showed a 10-fold loss of function, while the mutation K211S had no functional consequence. The single-mutant E209R, however, was nonfunctional up to 800µM 5-HT. Attempts to transplant the entire $GABA_A$R triad into the 5-HT_{3A}R – T152E/E209R/K211S – yielded no observable response to concentrations of 5-HT as high as 800µM. Thus, the triad of $GABA_A$Rs appears to behave differently than that of the excitatory 5-HT_{3A}R. It is also possible, however, that the receptor mutants that did not appear to respond to 5-HT were not expressing or not reaching the cell surface.

2.3.2 Mutating the 5-HT_{3A}R triad to that of the nAChR increases the binding affinity of nicotine

Table 2.3
Response to 5-HT of 5-HT3ARs incorporating GABAAR-type mutations.

Mutation(s)	EC_{50} (µM)	n_H	$\|I_{max}\|$ (µA)	Fold	N
-	1.3 ± 0.03	2.4 ± 0.11	1.0 - 78	1.0	21
T152E	13 ± 0.37	1.8 ± 0.08	0.25 - 3.6	10	15
E209R	NR	NR	NR	NR	12
K211S	1.3 ± 0.05	2.1 ± 0.14	5.0 - 47	1.1	15
T152E E209R	NR	NR	NR	NR	8
T152E K211S	NE	NE	NE	NE	0
E209R K211S	NR	NR	NR	NR	12
T152E E209R K211S	NR	NR	NR	NR	4

[†]$kcal \bullet mol^{-1}$; NR = no response; NE = not established; ± indicates SEM.

Having established that 5-HT$_{3A}$Rs incorporating the nAChR-type triad are functional, we next evaluated whether residues in the 5-HT$_{3A}$R triad contribute to the

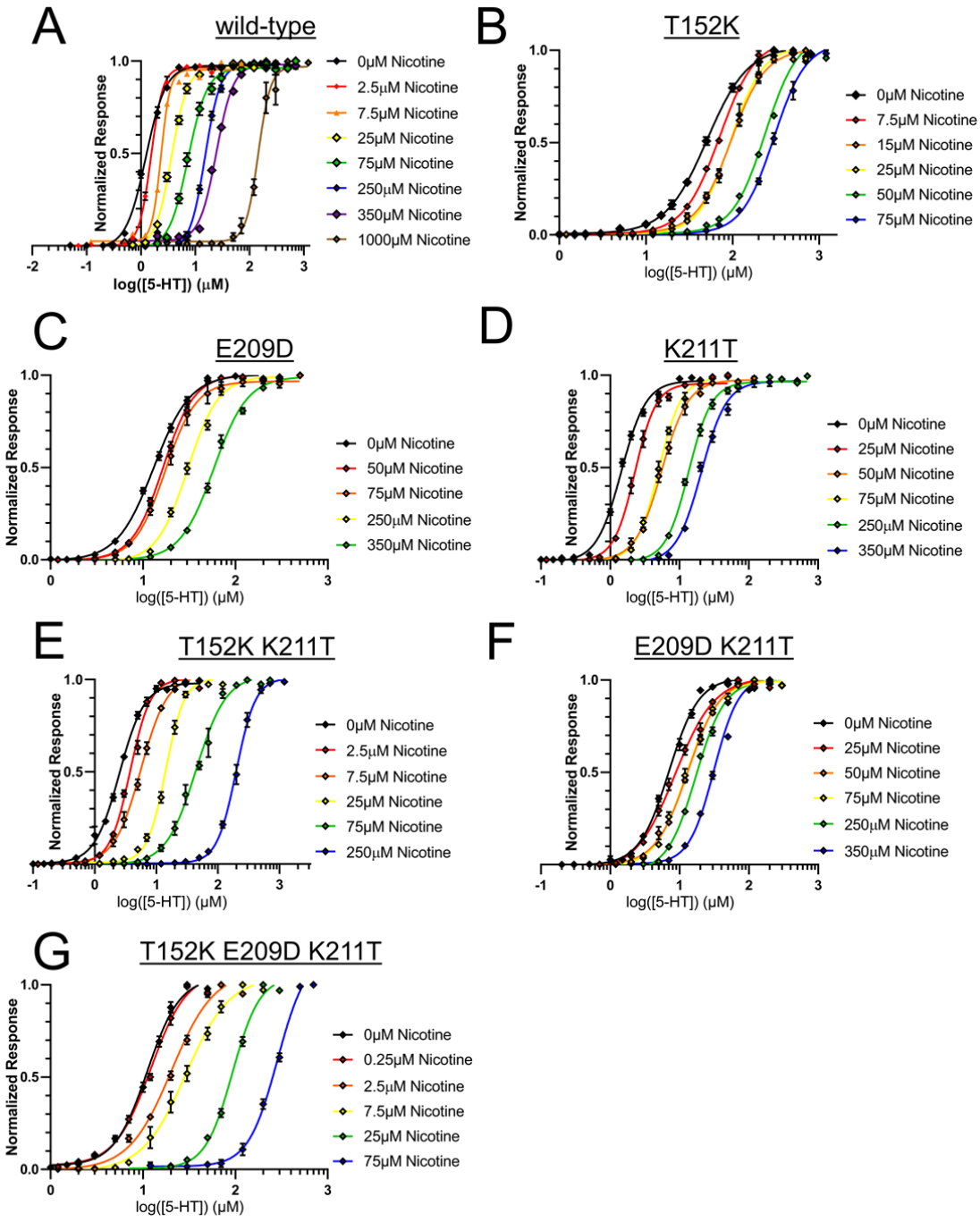

Figure 2.5. Dose-response curves of 5-HT$_{3A}$R variants in the presence of varying concentrations of nicotine. As a competitive antagonist, nicotine shifts the dose-response curve of 5-HT$_{3A}$Rs to higher EC_{50} values. Some variants are more sensitive to competitive inhibition by nicotine than others.

pharmacological properties of nicotine, an agonist of most neuronal nAChRs and a competitive antagonist of 5-HT_{3A}Rs.[1,29] To accomplish this, we again expressed mutant 5-HT_{3A}Rs incorporating the nicotinic-type mutations T152K, E209D, and K211T as single, double, and triple mutants in *Xenopus laevis* oocytes, and generated Schild plots for each receptor variant.[30,31] In this procedure, dose-response relationships of each receptor variant were measured in the presence of different concentrations of nicotine. Higher concentrations of nicotine progressively increase the EC_{50} of 5-HT as nicotine displaces 5-HT in the orthosteric binding site (**Figure 2.5**). In a Schild plot, the x-intercept gives a readout of the equilibrium dissociation constant (K_d) for the antagonist.[30,31]

The Schild plots for each variant are compared to that of the wild-type nAChR in **Figure 2.6**, the

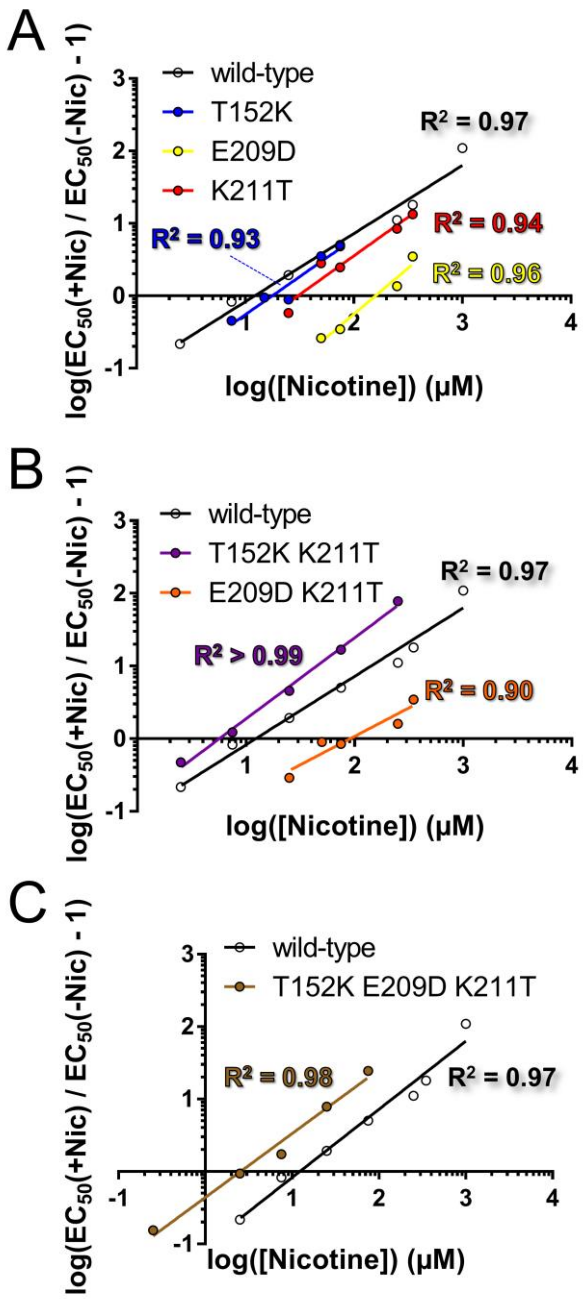

Figure 2.6. Schild analysis of inhibition of 5-HT_{3A}Rs by nicotine. Schild plots of *A*, single mutant, *B*, double mutant, and *C*, triple mutant 5-HT_{3A}Rs with nAChR-type substitutions. Meaningful changes in nicotine K_d are observed, and the mutations have non-additive effects. Error bars are shown as S.E.M., and are often smaller than the data points.

parameters of the linear fits are provided in **Table 2.4**, and the full pharmacological characterization of the nicotine inhibition experiments is provided in **Table 2.5**. The single mutants T152K, E209D, and K211T increased the K_d of nicotine by 1.5-, 13-, and 2.5-fold, respectively.

Meaningful non-additive effects are observed when the mutations are combined in the double mutants and the triple mutant. Despite T152K and K211T each producing small increases in the K_d of nicotine, the double-mutant T152K/K211T is 2.2-fold more sensitive to nicotine than wild-type. The double mutant E209D/K211T is more sensitive to inhibition by nicotine than E209D on its own, even though K211T increases the K_d of nicotine on its own. The triple mutant is the most nicotine-sensitive of all the variants, with a K_d 5-fold lower than that of wild-type. Thus these three residues influence the binding of nicotine to the 5-HT_{3A}R. In particular, rearranging the side-chain groups T152 and K211 to their respective positions in nAChRs generates variants that are more sensitive to nicotine inhibition than wild-type. The mutation E209D, while causing a sizable decrease in nicotine affinity on its own, gives further increase in nicotine sensitivity when combined with T152K and K211T in the triple mutant receptor.

Table 2.4
Schild fit parameters for 5-HT_{3A}R variants.

Mutation(s)	Slope	R^2	K_d (μM)	Fold	ΔΔG (kcal•mol^{-1})
wild-type	0.94 ± 0.07	0.97	12 ± 3.4	1.0	-
T152K	1.0 ± 0.17	0.93	18 ± 4.7	1.5	-
E209D	1.3 ± 0.18	0.96	160 ± 84	13	-
K211T	1.07 ± 0.16	0.94	31 ± 8.2	2.5	-
T152K K211T	1.1 ± 0.04	>0.99	5.7 ± 0.85	0.46	1.1
E209D K211T	0.78 ± 0.15	0.90	91 ± 49	7.4	0.60
T152K E209D K211T	0.88 ± 0.06	0.98	2.6 ± 0.78	0.21	1.2*

*measured in the background of K211T.

All this together suggests intimate cooperativity between these three residues in regard to nicotine binding. Mutant cycles of nicotine K_d values (**Table 2.4**) yield meaningful coupling energies for all pairs of mutations: 1.1kcal•mol^{-1} for T152K and K211T, 0.60kcal•mol^{-1} for E209D and K211T, and 1.2kcal•mol^{-1} for T152K and E209D in the background of K211T.

Table 2.5
Response to 5-HT of 5-HT_{3A}Rs in the presence of varying concentrations of (-)-nicotine.

Mutation(s)	[Nicotine] (μM)	EC_{50} (μM)	n_H	|Imax| (μA)	Fold	N
wt	0	1.3 ± 0.03	2.4 ± 0.11	1.0 - 78	1.0	21
wt	2.5	1.5 ± 0.02	4.0 ± 0.13	0.68 - 7.4	1.2	14
wt	7.5	2.3 ± 0.06	5.0 ± 0.61	0.99 - 4.8	1.8	8
wt	25	3.7 ± 0.06	3.0 ± 0.12	0.50 - 4.4	2.9	14
wt	75	7.6 ± 0.22	2.5 ± 0.16	1.1 - 10	6.0	15
wt	250	15 ± 0.38	3.1 ± 0.20	1.7 - 4.4	12	7
wt	350	24 ± 0.77	2.6 ± 0.20	0.20 - 3.1	19	6
wt	1000	143 ± 5.9	3.3 ± 0.38	0.41 - 2.8	110	6
T152K	0	49 ± 1.0	1.9 ± 0.06	0.14 - 11	1.0	15
T152K	7.5	71 ± 1.7	2.1 ± 0.08	1.9 - 7.0	1.5	6
T152K	15	95 ± 2.5	2.1 ± 0.09	3.0 - 17	1.9	8
T152K	25	92 ± 2.3	2.4 ± 0.11	0.59 - 5.9	1.9	7
T152K	50	219 ± 13	2.4 ± 0.28	0.81 - 5.6	4.5	8
T152K	75	284 ± 9.1	2.4 ± 0.16	0.60 - 11	5.8	10
E209D	0	13 ± 0.21	2.2 ± 0.07	0.53 - 20	1.0	15
E209D	50	16 ± 0.29	2.6 ± 0.10	0.65 - 11	1.3	8
E209D	75	29 ± 1.0	1.8 ± 0.10	2.1 - 2.9	2.2	2
E209D	250	31 ± 1.1	2.7 ± 0.21	0.41 - 3.2	2.4	7
E209D	350	58 ± 1.4	2.4 ± 0.12	1.4 - 4.2	4.5	3
K211T	0	1.5 ± 0.04	2.5 ± 0.16	1.9 - 25	1.0	15
K211T	25	2.7 ± 0.05	2.8 ± 0.14	6.0 - 17	1.8	7
K211T	50	5.6 ± 0.12	2.3 ± 0.10	1.9 - 4.7	3.8	8
K211T	75	5.1 ± 0.07	2.7 ± 0.09	3.6 - 12	3.5	5
K211T	250	14 ± 0.30	2.6 ± 0.13	0.30 - 4.1	9.4	8
K211T	350	21 ± 0.72	2.5 ± 0.18	1.7 - 6.1	14	5
T152K K211T	0	2.5 ± 0.05	2.1 ± 0.08	1.3 - 56	1.0	14
T152K K211T	2.5	3.7 ± 0.11	2.7 ± 0.18	0.84 - 4.8	1.5	8
T152K K211T	7.5	5.6 ± 0.11	2.0 ± 0.07	9.7 - 38	2.2	4
T152K K211T	25	14 ± 0.32	2.9 ± 0.15	0.15 - 58	5.6	7
T152K K211T	75	45 ± 1.9	1.8 ± 0.12	22 - 46	18	4
T152K K211T	250	198 ± 3.0	2.7 ± 0.10	8.8 - 61	79	7
E209D K211T	0	6.9 ± 0.25	2.1 ± 0.11	0.18 - 12	1.0	16
E209D K211T	25	8.9 ± 0.50	1.7 ± 0.13	5.6 - 19	1.3	6
E209D K211T	50	13 ± 0.41	1.9 ± 0.09	1.5 - 5.7	1.9	8
E209D K211T	75	13 ± 0.41	2.0 ± 0.10	4.5 - 16	1.8	6
E209D K211T	250	18 ± 0.64	2.3 ± 0.16	0.74 - 3.1	2.6	7
E209D K211T	350	31 ± 1.8	2.4 ± 0.29	0.58 - 2.52	4.5	5
T152K E209D K211T	0	11 ± 0.39	2.4 ± 0.18	0.15 - 19	1.0	12
T152K E209D K211T	0.25	12 ± 0.17	2.2 ± 0.19	4.4 - 13	1.2	6
T152K E209D K211T	2.5	20 ± 0.41	1.9 ± 0.14	1.4 - 5.3	1.9	7
T152K E209D K211T	7.5	29 ± 1.2	1.9 ± 0.12	1.6 - 16	2.7	7
T152K E209D K211T	25	93 ± 3.8	2.9 ± 0.18	0.80 - 2.9	8.9	7
T152K E209D K211T	75	267 ± 15	2.8 ± 0.31	0.33 - 2.67	25	6

We attempted to measure inhibition by 5-HT of muscle-type nAChRs containing the 5-HT_{3A}R-type triad. However, the results suggested that 5-HT inhibits both wild-type and triple-mutant muscle-type nAChRs via a noncompetitive mechanism, consistent with previous work.[32] Maximal currents in the presence of 5-HT were decreased, but EC_{50}'s of ACh were relatively unchanged (**Figure 2.7**).

2.3.3 The 5-HT_{3A}R triad is functionally coupled to nearby residues and the channel gate

Previous work[13] in the muscle-type nAChR identified state-dependent interactions critical for initiation of receptor gating between triad residues K145 and D200 and the loop C residue Y190, a completely conserved contributor to the aromatic box.[33] Structural work in related nAChRs (in which this K/D/Y triad is conserved) has supported the conclusions of this early experimental work.[22,23,27] However, the same set of interactions is clearly not present in the 5-HT_{3A}R, as the residue aligning to α1 Y190 in the muscle-type nAChR is a

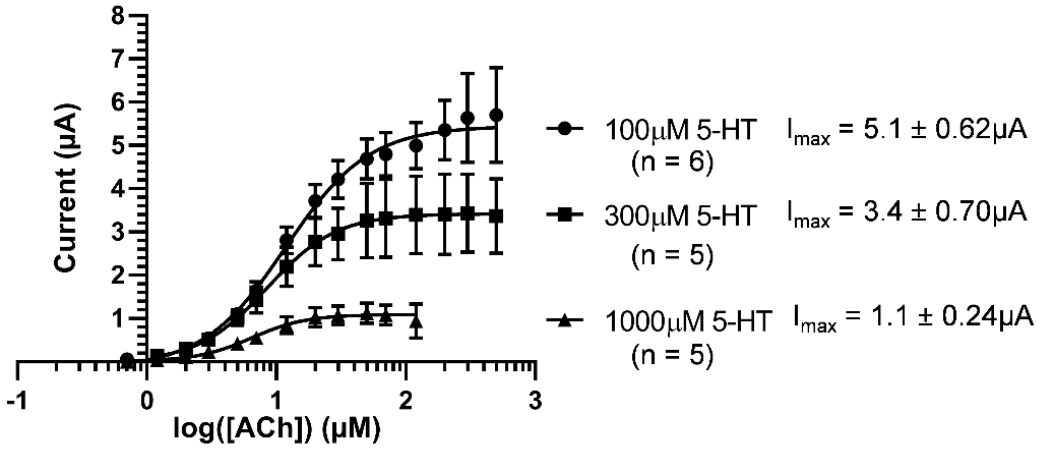

Figure 2.7. Noncompetitive inhibition by 5-HT of ACh-evoked currents in the muscle-type nAChR. Minimal changes occur in ACh EC_{50} while maximal currents are sharply reduced at high [5-HT]. Each dose-response curve was performed on different oocytes from the same batch of oocytes injected with the same amount of mRNA from the same preparation of mRNA. The first four (lowest-concentration ACh) data points on the 1000μM 5-HT curve were never actually measured, but inferred for the purpose of fitting the Hill equation. Error bars represent SEM.

phenylalanine residue in the 5-HT_{3A}R. Recent 5-HT_{3A}R structures do, however, suggest that there may be interactions between the triad residues examined herein and residues on loop A, one of the canonical binding-site loops.[9–12]

We have probed for interactions between the 5-HT_{3A}R triad and loop A residues N101 and E102 using mutagenesis. For these studies we typically used more conservative mutations than were used in the "triad swapping" experiments. For residues E102 and E209, we employ mutations to glutamine and/or aspartate; the E102D mutation was not examined as it has been observed previously that this mutation has little effect on the response of receptors to 5-HT.[28] We employ a more drastic mutation at N101, N101K. This was motivated by previous work that demonstrated a high loss of function for the N101K mutation.[34] For mutant cycles with T152, we use the conservative T152V mutation.

Table 2.6 provides the full characterization of the pharmacological response of these receptors to 5-HT. There is extensive crosstalk between the triad and the residues on loop A. All triad residues couple to N101, and K211 couples to E102. **Figure 2.8** provides a visual depiction of the largest coupling energies observed for pairs of mutations at the sites shown, including those discussed previously and those discussed hereafter. The $\Delta\Delta G°$ values for different mutant cycles in **Figure 2.8** are grouped into five categories, each representing an additional two-fold deviation from additivity.

Previous work in the 5-HT_{3A}R on loop A residues N101 and E102 showed that mutations to these residues that introduce a net positive charge (N101K and E102Q) generate very large losses of function.[28,34] This parallels our observation on the T152K mutation, which is the most disruptive of the single mutations in the triad swap. We also observed a large loss of function for E209Q, which likewise introduces a net positive

charge. In contrast, both K211T and K211M, mutations that remove a positive charge, have minimal impacts on function, but K211T rescued function of receptors with T152K.

Table 2.6

Functional cooperation between triad residues, loop A, K197 (loop C), and the channel gate in mutant 5-HT_{3A}Rs. Table is divided into four sections, from top to bottom: 1. Single mutants, 2. Mutant cycles to N101K and T152V, 3. Mutant cycles examining role of positive charge, 4. Nonresponsive variants.

Mutation(s)	EC_{50} (μM)	n_H	$\|I_{max}\|$ (μA)	Fold	N	$\Delta\Delta G^{\dagger}$
-	1.3 ± 0.03	2.4 ± 0.11	1.0 - 78	1.0	21	-
N101K	42 ± 1.1	2.4 ± 0.11	0.05 - 5.2	34	14	-
E102Q	85 ± 3.0	1.6 ± 0.07	0.53 - 5.5	68	15	-
T152V	8.5 ± 0.27	2.2 ± 0.13	0.42 - 78	6.8	11	-
T152K	49 ± 1.0	1.9 ± 0.06	0.14 - 11	39	15	-
K197M	1.5 ± 0.04	2.7 ± 0.19	2.1 - 20	1.2	10	-
E209D	13 ± 0.20	2.3 ± 0.07	0.53 - 20	10	15	-
E209Q	93 ± 4.3	2.4 ± 0.21	2.0 - 42	75	22	-
K211M	2.2 ± 0.05	2.9 ± 0.13	4.9 - 15	1.8	9	-
K211T	1.5 ± 0.04	2.5 ± 0.16	1.9 - 25	1.2	15	-
N101K T152V	84 ± 4.0	1.8 ± 0.10	7.2 - 17	67	16	0.72
N101K E209D	29 ± 0.17	2.9 ± 0.04	6.7 - 59	23	17	1.6
T152V E209D	12 ± 0.21	1.8 ± 0.05	11 - 23	9.5	13	1.1
T152V E209Q	96 ± 1.5	2.6 ± 0.09	6.1 - 87	76	16	1.0
N101K K211M	16 ± 0.31	2.0 ± 0.08	0.15 - 5.5	13	13	0.91
N101K K211T	15 ± 0.27	3.0 ± 0.16	0.09 - 4.2	12	15	0.73
E102Q K211M	8.7 ± 0.15	2.2 ± 0.06	0.28 - 18	6.9	15	1.7
E102Q K211T	3.1 ± 0.06	2.6 ± 0.10	6.6 - 51	2.5	15	2.0
T152K K211M	31 ± 0.39	2.0 ± 0.04	1.3 - 18	25	15	0.61
T152K K211T	2.5 ± 0.05	2.1 ± 0.08	1.3 - 56	2.0	14	1.8
T152V K211M	13 ± 0.19	2.3 ± 0.07	2.2 - 19	10	15	0.05
E209Q K211M	27 ± 0.28	2.6 ± 0.06	3.2 - 16	21	14	1.1
E209Q K211T	15 ± 0.37	2.7 ± 0.15	5.0 - 16	12	12	1.2
K197M E209Q	36 ± 0.24	2.8 ± 0.04	4.6 - 12	29	11	0.65
N101K K197M	24 ± 1.43	1.9 ± 0.18	0.05 - 0.74	19	12	0.43
T152K K197M	32 ± 1.30	1.5 ± 0.08	0.08 - 1.8	25	10	0.35
N101K T152K	NR	NR	NR	NR	9	NR
N101K E209Q	NR	NR	NR	NR	16	NR
E102Q T152V	NR	NR	NR	NR	10	NR
E102Q T152K	NR	NR	NR	NR	5	NR
E102Q E209Q	NR	NR	NR	NR	8	NR
T152K E209D	NR	NR	NR	NR	15	NR
T152K K211T E102Q	NR	NR	NR	NR	9	NR

$^{\dagger}kcal \bullet mol^{-1}$; NR = no response; ± indicates SEM.

In an effort to further probe this ostensible role of positive charge, the single-mutants N101K, E102Q, and E209Q, and the double mutants N101K/K211T, E102Q/K211T, and E209Q/ K211T were evaluated (**Figure 2.9A, 2.9B**, and **2.9C** respectively; **Table 2.6**). We measured $\Delta\Delta G° = 0.73$, 2.0, and 1.2 kcal•mol^{-1}, respectively for these three double mutant pairs. Thus, all three pairs of mutations are meaningfully coupled, albeit to differing degrees. Recall the large coupling ($\Delta\Delta G° = 1.8$ kcal/mol) for T152K/K211T, shown again in **Figure 2.9D**.

We also generated the double mutants around the mutation K211M, the reasoning being that the nonpolar side chain of methionine is sterically similar to the lysine side chain, and does not introduce any other functionalities as in the case of the threonine hydroxyl in K211T. The $\Delta\Delta G°$ values observed for the double mutants N101K

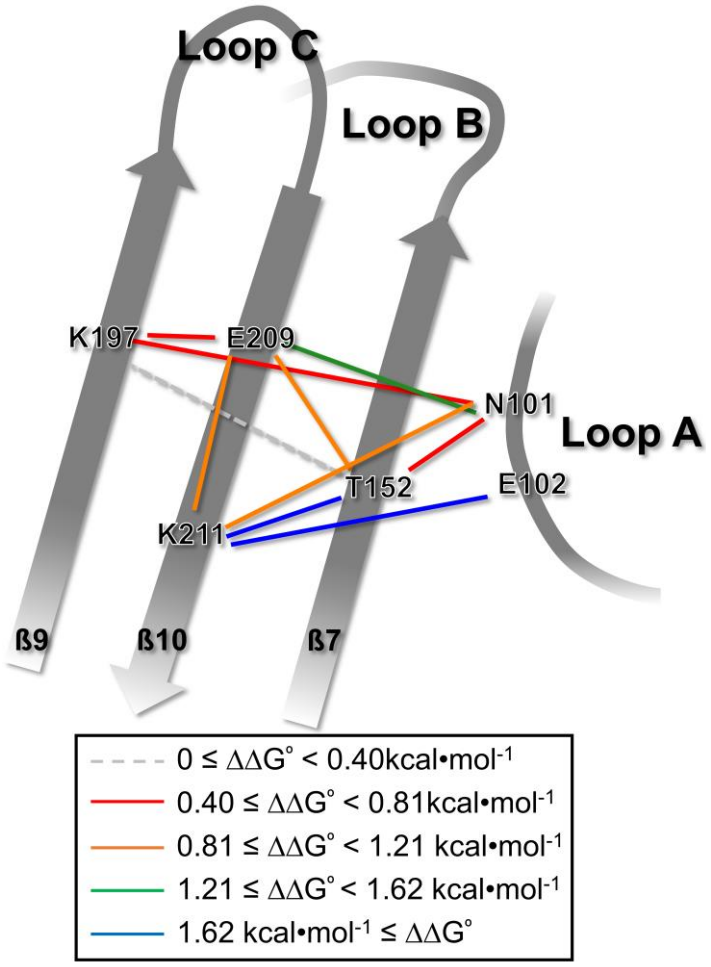

Figure 2.8. Greatest-magnitude coupling energies observed between pairs of mutations at residues in 5-HT$_{3A}$Rs. Meaningful coupling energies are depicted in color, with a different color for each additional 2-fold deviation from additivity. Full data can be found in **Tables 2.1 and 2.6.**

K211M, E102Q K211M, T152K K211M, and E209Q K211M were 0.91, 1.7, 0.61, and 1.1 kcal•mol^{-1}, respectively (**Figure 2.9**; **Table 2.6**). We also generated the double mutant T152V K211M, for which the ΔΔG° value was only 0.05kcal•mol^{-1} (**Table 2.6**), demonstrating that a positive charge must be introduced at T152 in order to couple to K211.

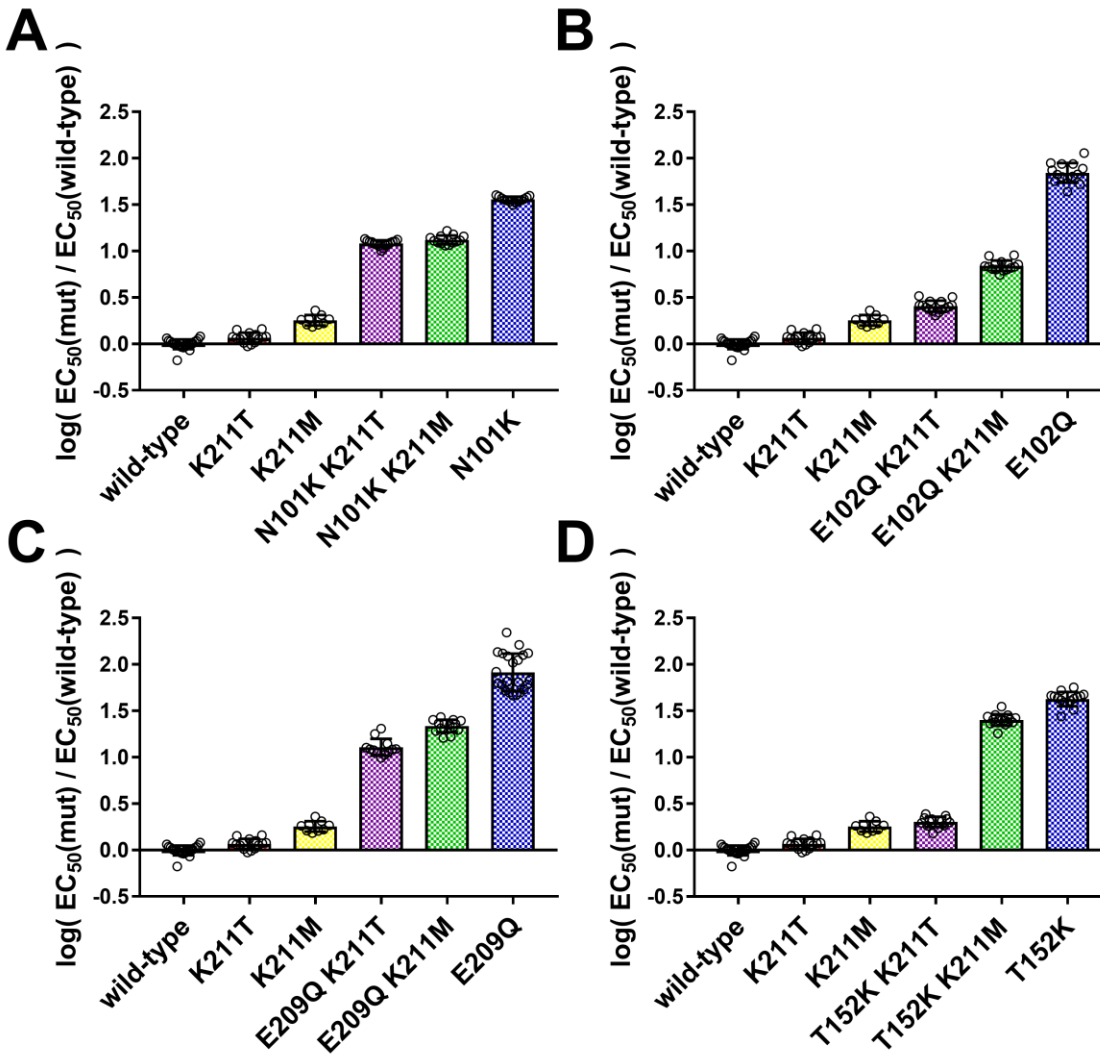

Figure 2.9. In 5-HT$_{3A}$Rs, mutations which remove the cationic amine on K211 functionally couple to nearby mutations which introduce positive charge. *A*, Mutant cycles with N101K. *B*, Mutant cycles with E102Q. *C*, Mutant cycles with E209Q. *D*, Mutant cycles with T152K. Full pharmacological data can be found in **Table 2.6**. Error bars represent S.D.

Interestingly, each of the mutations that introduce a net positive charge couple comparably to K211T and K211M, with the exception of T152K. This mutation couples strongly to K211T ($\Delta\Delta G°$ = 1.8 kcal/mol) but more weakly to K211M ($\Delta\Delta G°$ = 0.61 kcal/mol). That is to say, the K211T mutation rescues function of T152K more than eight times better than K211M does (**Figure 2.9D**). We therefore argue that there is a direct interaction between T152 and K211 in the 5-HT_{3A}R, the likes of which cannot be accounted for by merely eliminating the nearby positive charge of the K211 side chain. On the other hand, the deleterious effects of introducing a net positive charge either by introducing N101K, E102Q, or E209Q, are attenuated whenever the basic amine on K211 is removed, regardless of the ability of the residue at position 211 to hydrogen bond.

We also considered another charged residue, K197, that seemed a good candidate for coupling based on its proximity to the residues heretofore examined. In the $GABA_AR$, a functionally important salt bridge has been demonstrated between residues aligning to K197 and T152.[35] The 5-HT_{3A}R mutation K197M couples weakly to the nearby E209Q ($\Delta\Delta G°$ = 0.65 kcal•mol^{-1}) and N101K ($\Delta\Delta G°$ = 0.43 kcal/mol), but it does not couple meaningfully T152K ($\Delta\Delta G°$ = 0.35 kcal•mol^{-1}) (**Table 2.6**).

Previously, we proposed a strategy for evaluating the role of a particular residue in channel function by evaluating its coupling to a residue in the pore-lining M2 helix that is clearly involved in channel gating.[36] In the nAChR, that residue is termed Leu9' (the 9th residue from the bottom of the M2 helix). In the nAChR, our group found that D200N couples strongly to L9'S ($\Delta\Delta G$ = 1.3 kcal/mol), establishing a role in gating for D200.[37] However, K145Q and T202Tah (Tah = α-hydroxy threonine – a backbone mutation) do not show strong coupling to L9'S.[37]

In the 5-HT_{3A}R, the appropriate mutation is T6'S (T257S in our numbering scheme), which has been used extensively to modulate serotonin receptor currents.[38] We looked for coupling to T6'S at N101, E102, T152, and E209. The results are tabulated in **Table 2.7** and presented pictorially in **Figure 2.10**. We find that N101K, E102Q, T152V, and T152K are all meaningfully coupled to T6'S, suggesting a role in gating for these residues.[37] Interestingly, E209D and E209Q do not show meaningful coupling to T6'S. Thus, the nAChR and the 5-HT_{3A}R show different coupling behaviors to the pore-forming M2 helix. In the muscle-type nAChR triad, the D200N mutation couples to L9'S but K145Q does not. The opposite coupling pattern is observed at the aligning sites in the 5-HT_{3A}R: T152K couples to T6'S while E209D does not. We are unable to perform the same analysis for the 5-HT_3R mutation K211T, as none of the mutants we studied at this site lead to an interpretable loss of function relative to wild-type. However, we do note that mutations K211 couple energetically to all of the residues that couple to T6'S.

Attempted expression of the 5-HT_{3A}R double mutants E102Q/T152V, E102Q/E209Q, N101K/E209Q, and T152K/N101K yielded no measurable response to high concentrations of 5-HT (**Table 2.6**). This may result either from nonfunctional

Table 2.7
Mutant cycles between residues of interest in the 5-HT_{3A}R and the channel pore mutation T6'S. Data for wild-type type and single mutants can be found in **Table 2.6**.

Mutation(s)	EC_{50} (μM)	n_H	$\lvert I_{max}\rvert$ (μA)	Fold	N	$\Delta\Delta G^{\dagger}$
T6'S	1.3 ± 0.01	4.1 ± 0.17	0.26 - 17	1.0	22	-
N101K T6'S	11 ± 0.29	1.6 ± 0.07	0.30 - 23	8.5	11	0.83
E102Q T6'S	5.4 ± 0.28	1.4 ± 0.07	0.10 - 3.9	4.3	15	1.6
T152V T6'S	1.4 ± 0.10	1.3 ± 0.10	2.3 - 50	1.1	10	0.98
T152K T6'S	6.6 ± 0.27	2.2 ± 0.16	0.13 - 2.3	5.3	11	1.2
E209D T6'S	12 ± 0.55	1.9 ± 0.14	0.30 - 15	9.9	13	0.05
E209Q T6'S	73 ± 8.9	1.1 ± 0.09	0.11 - 15	58	15	0.17

†kcal•mol^{-1}; ± indicates SEM.

receptors or a lack of surface expression. Especially for the less-conservative mutations we employ, individual mutations likely affect multiple interactions involved in receptor function, the deleterious effects of which may sometimes add together even if other pairs of mutations at the same sites generate functional receptors.

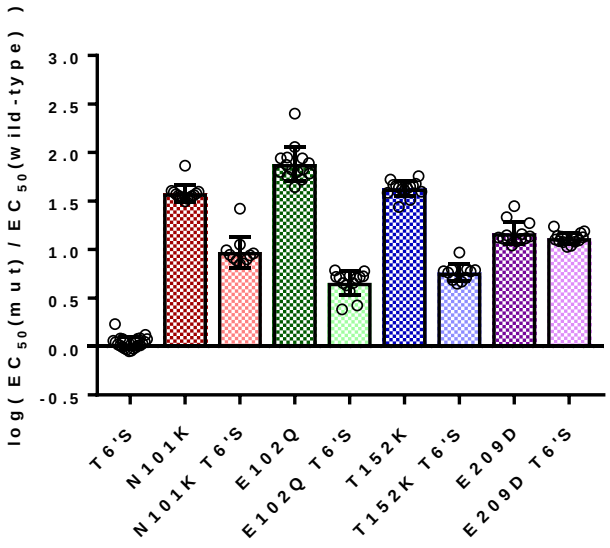

Figure 2.10. Mutant cycles between residues of interest in the 5-HT$_{3A}$R and the channel pore mutation T6'S. Receptor function is rescued upon inclusion of the T6'S mutation for all sites except E209. Full data, including that for other mutant pairs, is provided in **Table 2.7**.

2.4 Conclusions

We have identified a triad of residues with one cationic, one anionic, and one hydroxyl-containing side chain that is rearranged between the 5-HT$_{3A}$R, nAChRs, and GABA$_A$Rs, and behaves differently in different receptors. In the muscle-type nAChR, the three triad residues cooperate as a unit, as demonstrated via triple mutant cycle analysis. This corroborates previous functional and crystallographic work that suggested a salt bridge between two members of the triad is involved in receptor gating.[13,22,23,27] We show here that the salt bridge between K145 and D200 depends on T202, which may coordinate this interaction. Mutant cycles of the aligning residues in the 5-HT$_{3A}$R indicate that T152, E209, and K211 cooperate in the activation mechanism of the 5-HT$_{3A}$R, but not in a perfectly codependent manner. Interestingly, the triads of the 5-HT$_{3A}$R and the nAChR can

be swapped and still produce functional receptors with small but meaningful losses of function.

The triad of residues in the 5-HT_{3A}R affects the competitive binding of nicotine for the orthosteric site. Each mutation on its own causes a decrease in nicotine binding affinity, although the shift for T152K is very small. Interestingly however, nicotine bound more strongly to 5-HT_{3A}R variants with both the T152K and K211T mutations relative to wild-type receptors. The E209D mutation, which causes a large loss of nicotine binding affinity on its own, increases the binding affinity for the triple mutant T152K/E209D/K211T relative to double mutant T152K/K211T. These three residues thus cooperate in the binding of nicotine to the 5-HT_{3A}R, and likely represent a characteristic network of nAChRs. Worth noting is that two of the three deviations from the cationic/anion/hydroxyl triad of nAChRs are seen in the α9 and α10 nAChRs, which are *inhibited* rather than activated by nicotine.[39] In these nAChR α-subunits, the lysine residue of the triad is replaced by a threonine. It has been demonstrated elsewhere, however, that mutating the α9 Thr to a Lys does not produce receptors that are activated by nicotine,[40] so clearly there is more to nicotine's inhibitory effect on these receptors than this one residue.

The triad from the $GABA_A$R does not appear to function in the 5-HT_{3A}R, suggesting this network functions differently in $GABA_A$Rs. Other work has proposed a functionally important salt bridge between residues in the $GABA_A$R aligning to K197 and T152 in the 5-HT_{3A}R,[35] however we do not observe meaningful functional coupling between mutations at these sites in the 5-HT_{3A}R. We also note that the pattern of functionalities in the triad we have studied is not conserved in primary-face α-subunits of

inhibitory GlyRs. All this together suggests that the triad of residues behaves similarly in excitatory receptors, but is functionally distinct in inhibitory Cys-loop receptors.

Many amino acid residues we've considered in this study have been examined previously in regard to ligand binding. Based on radioligand binding studies of the 5-HT_{3A}R antagonist ^{3}H-granisetron, it has been proposed that T152 helps to shape the binding site.[41] Mutations to 5-HT_{3A}R residues E209 and K211 have been shown previously to have minimal effect on binding of ^{3}H-granisetron.[34,41] Our results show a minimal effect on nicotine binding for T152K, a modest effect for K211T, and a sizable effect for E209D. The effects of these mutations are observed to be cooperative, as single-mutants decrease the binding affinity of nicotine but have non-additive effects when the mutations are combined. Thus, these results highlight different binding modes for different competitive antagonists.

We further investigated the involvement of residues in the gating mechanism via mutant cycle analyses to the channel gate mutation T6'S. Loop A residue N101 couples to T6'S, supporting a previous proposition that this residue is involved in receptor gating.[34] The mutation E102Q couples to T6'S, in line with a previously-published result.[28] We observe that the T152K mutation affects ligand binding and also couples to the T6'S; thus we propose that this residue is involved in both binding and gating. We have not identified any single mutations to K211 that generate interpretable shifts in 5-HT EC_{50}, so we were unable to perform the same analysis on this residue. However, spatially proximal residues that couple to the channel gate (N101, E102, and T152) also couple to K211.

Quizzically, mutant cycles between E209 and T6'S do not reveal functional coupling between these residues, despite the previously published observation that E209

does not participate in the binding of ^{3}H-granisetron.[41] It is thus possible that E209 may contribute to the binding of 5-HT but not granisetron. In support of this explanation, recent cryo-EM structures of the 5-HT$_{3A}$R in the presence of tropisetron (a close structural relative of granisetron) and 5-HT demonstrate much closer interatomic distances between the E209 carbonyl and the 5-HT amine (4.3Å) versus the tropisetron amine (9.3Å; **Figure 2.11**).[9] While this is not conclusive evidence that E209 interacts directly with 5-HT, the experimental results reported herein together with structural work[9] and computational predictions[42] strongly suggest that E209 is involved in binding 5-HT.

Mutations that introduce a net positive charge in the region of the 5-HT$_{3A}$R probed here generally increase the 5-HT EC$_{50}$ by a substantial amount. Most of these large losses of function could be rescued by mutations that remove the side-chain amine of K211. An exception is the highly deleterious T152K mutation, which can be rescued by the K211T mutation – corresponding to the nAChR swap – but not by the K211M mutation. This argues for a highly specific interaction between T152 and K211 in the native receptor.

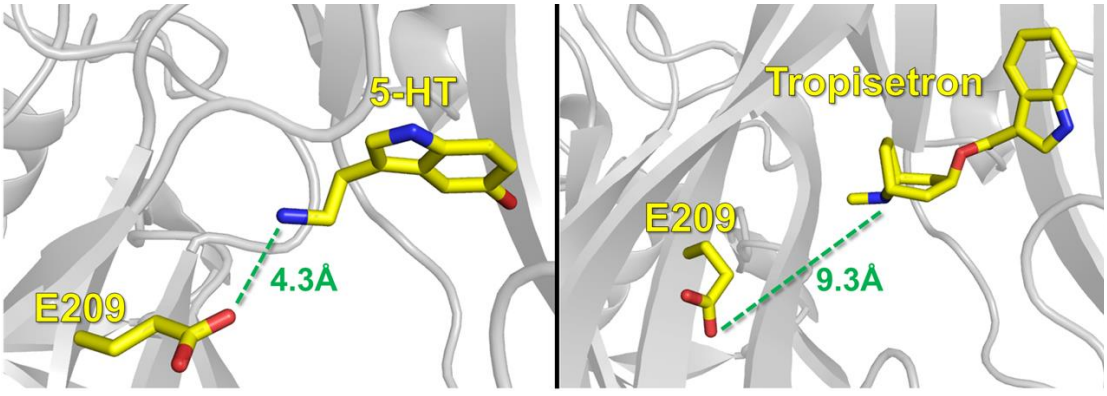

Figure 2.11. Comparison of binding poses for different ligands of the 5-HT$_{3A}$R. (Left) Cryo-EM structure in which the amine of 5-HT may engage in a weak hydrogen bond with E209; PDB ID 6HIO. (Right) Cryo-EM structure demonstrating no hydrogen bond between E209 and the amine of tropisetron; PDB ID 6HIS.

We have demonstrated via mutant cycle analyses that triad residues and loop A residues are functionally coupled in the 5-HT_{3A}R. Structural studies suggest similar interactions between the triad and loop A in nAChR. However, a previously established interaction between triad residues and loop C in nAChRs does not carry over to the 5-HT_{3A}R. These results highlight the fact that there is considerable variation in the degree to which structurally/functionally important features are or are not conserved across members of the Cys-loop family.

2.5 Experimental Procedures

2.5.1 Molecular biology

The cDNA for the mouse 5-HT_3R A subunit was in the pGEMhe vector. The cDNA for the mouse nAChR α1, ß1, γ, and δ were in the pAMV vector. The α1 subunit contains a hemagglutinin epitope tag in the M3-M4 loop, which does not alter the EC_{50} of ACh. Site-directed mutagenesis was performed using a QuikChange mutagenesis kit (Stratagene). cDNA was linearized using XhoI (New England Biolabs) for m5-HT_{3A}, XbaI (New England Biolabs) for mα1, or NotI (New England Biolabs) for mß1, mγ, and mδ subunits. Linearized DNA was purified using a Qiaquick PCR Purification Kit (Qiagen) before performing an *in vitro* runoff transcription using a T7 mMessage mMachine kit (Ambion). The mRNA was purified using an RNEasy Mini Kit (Qiagen) and concentrations were quantified via UV-Vis spectroscopy (Nanodrop 2000, ThermoFisher Scientific). cDNA was stored at -20ºC and mRNA was stored at -80ºC.

2.5.2 Protein expression in Xenopus laevis Oocytes

Stage V-VI *Xenopus laevis* oocytes were prepared as previously described.[43] Oocytes were injected with 50nL of mRNA in nuclease-free water, and expression levels of different mutants were optimized by varying mRNA concentrations and incubation times. For experiments involving 5-HT_{3A}R variants, oocytes were injected with 5-50ng mRNA once at 24h before, once at 48h before, or twice at 24h and 48h before electrophysiological recording was performed. For experiments involving muscle-type nAChRs, oocytes were injected with a mixture of α1, ß1, γ, and δ mRNAs in a 10:5:5:5ng ratio (per 50nL) once at 24h before, once at 48h before, or twice at 24h and 48h before electrophysiological recording was performed. Cells were incubated at 18ºC in ND96 (96mM NaCl, 2mM KCl, 1mM $MgCl_2$, 1.8mM $CaCl_2$, and 5mM HEPES at pH 7.5) with 0.05mg/mL gentamycin (Sigma Aldrich), 2.5mM sodium pyruvate (Acros Organics), and 0.67mM theophylline (Sigma Aldrich).

2.5.3 Whole-cell electrophysiological recording

Electrophysiology and drug perfusion were performed at ambient room temperature (20-25ºC) using the OpusXpress 6000A (Axon Instruments) in two-electrode voltage clamp (TEVC) mode. Oocytes were impaled with borosilicate glass pipettes filled with 3M KCl (R = 0.3 – 3.0MΩ) and clamped at a holding potential of -60mV. Data were sampled at 125Hz. The running buffer was Ca^{2+}-free ND96 (96mM NaCl, 2mM KCl, 1mM $MgCl_2$, and 5mM HEPES at pH 7.5). Solutions of serotonin hydrochloride (Sigma Aldrich), acetylcholine chloride (Sigma Aldrich), and (-)-nicotine tartrate (Sigma Aldrich) were prepared 0-24h before recording from stock solutions stored at -80ºC.

For dose-response experiments, cells underwent a 30s wash in Ca^{2+}-free ND96 before 1mL of each concentration of drug (dissolved in Ca^{2+}-free ND96) was applied for

15s. Cells were then washed for 116s using Ca^{2+}-free ND96 before subsequent doses. For slow-activating variants, 1mL of drug solution was applied for 15s and cells were incubated in the drug solution for an additional 15s before washout. For slow-deactivating variants, washout times were increased to 176s in between doses. The different procedure for slow activating/deactivating variants did not meaningfully change the overall dose-response relationships recorded versus the standard 15s application / 116s wash procedure.

For Schild analysis experiments, cells were continuously perfused with Ca^{2+}-free ND96 containing (-)-nicotine, and 1mL solutions of 5-HT in Ca^{2+}-free ND96 with the requisite concentration of (-)-nicotine were applied for 15s per dose, followed by 116s washes in between doses. As in the dose-response experiments, application times and wash times were adjusted for variants displaying slow activation/deactivation.

2.5.4 Data analysis

Raw TEVC traces were prepared and analyzed in Clampfit 10.3 (Axon Instruments). Raw data were first filtered using a lowpass Gaussian filter at 1Hz. A 30s baseline was established prior to each drug application during which cells were continuously perfused with Ca^{2+}-free ND96. The averaged current of the baseline was subtracted from the peak amplitude following each drug application in order to generate dose-response data.

Dose-response data for individual concentrations were averaged, plotted, and fit to the Hill equation $I / I_{max} = 1 / (1 + (EC_{50} / [agonist]^{nH})$ in Prism 7 (GraphPad), where EC_{50} is the concentration for a half-maximal response, n_H is the Hill coefficient, and I / I_{max} is the normalized response at a given drug concentration. For dose-response experiments,

data were normalized to the maximum current observed. Schild fits were determined and plots were made using Prism 7. The values for the slopes are reported in the text as slope fit ± standard error.

Coupling energies for double-mutant cycles were calculated using the formula $\Delta\Delta G = -R*T*\ln((EC_{50wt}*EC_{50AB}) / (EC_{50A}*EC_{50B}))$, where R is the gas constant, T is temperature, A and B denote individual mutations, and AB denotes double mutant receptors. The value used for T was 293.15K.

The sequence alignment in **Figure 2.1B** was performed in Clustal Omega using sequences from Uniprot corresponding to the following accession numbers: P46098 (human 5-HT_{3A}), P02708 (human α1 nAChR), Q15822 (human α2 nAChR), P32297 (human α3 nAChR), P43681 (human α4 nAChR), P30532 (human α5 nAChR), Q15825 (human α6 nAChR), P36544, (human α7 nAChR), Q9UGM1 (human α9 nAChR), Q9GZZ6 (human α10 nAChR), P18505 (human ß1 $GABA_A$), P47870 (human ß2 $GABA_A$), P28472 (human ß3 $GABA_A$).

2.6 REFERENCES

1. Albuquerque, E. X., Pereira, E. F. R., Alkondon, M. & Rogers, S. W. Mammalian Nicotinic Acetylcholine Receptors: From Structure to Function. Physiol. Rev. 89, 73–120 (2009).
2. Sigel, E. & Steinmann, M. E. Structure, Function, and Modulation of GABAA Receptors. J. Biol. Chem. 287, 40224–40231 (2012).
3. Betz, H. & Laube, B. Glycine receptors: recent insights into their structural organization and functional diversity. J. Neurochem. 97, 1600–1610 (2006).
4. Lummis, S. C. R. 5-HT3 Receptors. J. Biol. Chem. 287, 40239–40245 (2012).
5. Thompson, A. J. & Lummis, S. C. The 5-HT3 receptor as a therapeutic target. Expert Opin. Ther. Targets 11, 527–540 (2007).
6. Miller, P. S. & Smart, T. G. Binding, activation and modulation of Cys-loop receptors. Trends Pharmacol. Sci. 31, 161–174 (2010).
7. Lynagh, T. & Pless, S. A. Principles of agonist recognition in Cys-loop receptors. Front. Physiol. 5, (2014).

8. Andrew J Thompson, H. A. L. The structural basis of function in Cys-loop receptors. Q. Rev. Biophys. 43, 449–99 (2010).
9. Polovinkin, L. et al. Conformational transitions of the serotonin 5-HT 3 receptor. Nature 563, 275 (2018).
10. Hassaine, G. et al. X-ray structure of the mouse serotonin 5-HT3 receptor. Nature 512, 276–281 (2014).
11. Basak, S., Gicheru, Y., Rao, S., Sansom, M. S. P. & Chakrapani, S. Cryo-EM reveals two distinct serotonin-bound conformations of full-length 5-HT 3A receptor. Nature 563, 270 (2018).
12. Basak, S. et al. Cryo-EM structure of 5-HT3A receptor in its resting conformation. Nat. Commun. 9, (2018).
13. Mukhtasimova, N., Free, C. & Sine, S. M. Initial Coupling of Binding to Gating Mediated by Conserved Residues in the Muscle Nicotinic Receptor. J. Gen. Physiol. 126, 23–39 (2005).
14. Nasiripourdori, A., Ranjbar, B. & Naderi-Manesh, H. Binding of long-chain α-neurotoxin would stabilize the resting state of nAChR: A comparative study with α-conotoxin. Theor. Biol. Med. Model. 6, 3 (2009).
15. Horenstein, N. A., McCormack, T. J., Stokes, C., Ren, K. & Papke, R. L. Reversal of Agonist Selectivity by Mutations of Conserved Amino Acids in the Binding Site of Nicotinic Acetylcholine Receptors. J. Biol. Chem. 282, 5899–5909 (2007).
16. Dellisanti, C. D., Yao, Y., Stroud, J. C., Wang, Z.-Z. & Chen, L. Crystal structure of the extracellular domain of nAChR α1 bound to α-bungarotoxin at 1.94 Å resolution. Nat. Neurosci. 10, 953–962 (2007).
17. Mallipeddi, P. L., Pedersen, S. E. & Briggs, J. M. Interactions of acetylcholine binding site residues contributing to nicotinic acetylcholine receptor gating: Role of residues Y93, Y190, K145 and D200. J. Mol. Graph. Model. 44, 145–154 (2013).
18. Celie, P. H. N. et al. Nicotine and Carbamylcholine Binding to Nicotinic Acetylcholine Receptors as Studied in AChBP Crystal Structures. Neuron 41, 907–914 (2004).
19. Taly, A., Corringer, P.-J., Guedin, D., Lestage, P. & Changeux, J.-P. Nicotinic receptors: allosteric transitions and therapeutic targets in the nervous system. Nat. Rev. Drug Discov. 8, 733–750 (2009).
20. Dougherty, D. A. The Cation−π Interaction. Acc. Chem. Res. 46, 885–893 (2013).
21. Horovitz, A. Double-mutant cycles: a powerful tool for analyzing protein structure and function. Fold. Des. 1, R121–R126 (1996).
22. Morales-Perez, C. L., Noviello, C. M. & Hibbs, R. E. X-ray structure of the human α4β2 nicotinic receptor. Nature advance online publication, (2016).
23. Walsh, R. M. et al. Structural principles of distinct assemblies of the human α4β2 nicotinic receptor. Nature 557, 261–265 (2018).
24. Filatov, G. N. & White, M. M. The role of conserved leucines in the M2 domain of the acetylcholine receptor in channel gating. Mol. Pharmacol. 48, 379–384 (1995).
25. Labarca, C. et al. Channel gating governed symmetrically by conserved leucine residues in the M2 domain of nicotinic receptors. Nature 376, 514 (1995).
26. Xiu, X., Puskar, N. L., Shanata, J. A. P., Lester, H. A. & Dougherty, D. A. Nicotine binding to brain receptors requires a strong cation–π interaction. Nature 458, 534–537 (2009).

27. Unwin, N. Refined Structure of the Nicotinic Acetylcholine Receptor at 4 Å Resolution. J. Mol. Biol. 346, 967–989 (2005).
28. Miles, T. F., Bower, K. S., Lester, H. A. & Dougherty, D. A. A Coupled Array of Noncovalent Interactions Impacts the Function of the 5-HT3A Serotonin Receptor in an Agonist-Specific Way. ACS Chem. Neurosci. 3, 753–760 (2012).
29. Gurley, D. A. & Lanthorn, T. H. Nicotinic agonists competitively antagonize serotonin at mouse 5-HT3 receptors expressed in Xenopus oocytes. Neurosci. Lett. 247, 107–110 (1998).
30. Colquhoun, D. Why the Schild method is better than Schild realised. Trends Pharmacol. Sci. 28, 608–614 (2007).
31. Wyllie, D. J. A. & Chen, P. E. Taking The Time To Study Competitive Antagonism. Br. J. Pharmacol. 150, 541–551 (2007).
32. Cross, K. M., Foreman, R. C. & Chad, J. E. Enhancement by 5-hydroxytryptamine and analogues of desensitization of neuronal and muscle nicotinic receptors expressed in Xenopus oocytes. Br. J. Pharmacol. 114, 1636–1640 (1995).
33. Van Arnam, E. B. & Dougherty, D. A. Functional Probes of Drug–Receptor Interactions Implicated by Structural Studies: Cys-Loop Receptors Provide a Fertile Testing Ground. J. Med. Chem. 57, 6289–6300 (2014).
34. Price, K. L. et al. A Hydrogen Bond in Loop A Is Critical for the Binding and Function of the 5-HT3 Receptor. Biochemistry 47, 6370–6377 (2008).
35. Venkatachalan, S. P. & Czajkowski, C. A conserved salt bridge critical for GABAA receptor function and loop C dynamics. Proc. Natl. Acad. Sci. U. S. A. 105, 13604–13609 (2008).
36. Shanata, J. A. P., Frazier, S. J., Lester, H. A. & Dougherty, D. A. Using Mutant Cycle Analysis to Elucidate Long-Range Functional Coupling in Allosteric Receptors. Methods Mol. Biol. Clifton NJ 796, 97–113 (2012).
37. Gleitsman, K. R., Shanata, J. A. P., Frazier, S. J., Lester, H. A. & Dougherty, D. A. Long-Range Coupling in an Allosteric Receptor Revealed by Mutant Cycle Analysis. Biophys. J. 96, 3168–3178 (2009).
38. Thompson, A. J. & Lummis, S. C. R. A single channel mutation alters agonist efficacy at 5-HT3A and 5-HT3AB receptors. Br. J. Pharmacol. 170, 391–402 (2013).
39. Giastas, P., Zouridakis, M. & Tzartos, S. J. Understanding structure-function relationships of the human neuronal acetylcholine receptor: insights from the first crystal structures of neuronal subunits. Br. J. Pharmacol. n/a-n/a (2017). doi:10.1111/bph.13838
40. Zouridakis, M. et al. Crystal structures of free and antagonist-bound states of human α9 nicotinic receptor extracellular domain. Nat. Struct. Mol. Biol. 21, 976–980 (2014).
41. Thompson, A. J. et al. Locating an Antagonist in the 5-HT3 Receptor Binding Site Using Modeling and Radioligand Binding. J. Biol. Chem. 280, 20476–20482 (2005).
42. Yuan, S., Filipek, S. & Vogel, H. A Gating Mechanism of the Serotonin 5-HT3 Receptor. Structure 24, 816–825 (2016).
43. Dougherty, D. A. & Van Arnam, E. B. In Vivo Incorporation of Unnatural Amino Acids Using the Chemical Aminoacylation Strategy. A Broadly Applicable Mechanistic Tool. Chembiochem Eur. J. Chem. Biol. 15, 1710–1720 (2014).

Chapter 3: Probing proline residues in the prokaryotic ligand-gated ion channel, ELIC[*†]

3.1 Abstract

Erwinia ligand-gated ion channel (ELIC) is a bacterial homologue of vertebrate pentameric ligand-gated ion channels (pLGIC), and has proved a valuable model for understanding the structure and function of this important protein family. There is nevertheless still a question as to whether molecular details can be accurately extrapolated from this protein to those found in eukaryotes. Here we explore the role of proline residues (Pros) in ELIC by creating mutant receptors, expressing them in *Xenopus laevis* oocytes, and using whole-cell voltage-clamp electrophysiology to monitor channel activity. In contrast to eukaryotic pLGICs, proline-to-alanine (Pro-to-Ala) substitution in ELIC mostly resulted in gain of function, and even altering highly conserved Pro residues in M1 and the M2-M3 loop did not ablate function. These substitutions also mostly resulted in ablation of the modulation by Ca^{2+} observed in wild-type receptors. Substitution of the Pro in the "Cys-loop", however, did result in non-functional receptors. Probing this residue with non-canonical amino acids revealed a requirement for a substituted amine at this position, as well as a general preference for Pro analogues with greater intrinsic *cis* biases. We propose there is likely a *cis* bond at the apex of the Cys-loop in this protein, which is consistent with some, but not all, findings from other pLGIC. Overall, the data show that the roles of proline residues are less critical in ELIC than in other pLGIC, supporting other studies that suggest caution

---

[*] *This chapter is adapted with permission from: Mosesso, R., Dougherty, D. A. & Lummis, S. C. R. Probing Proline Residues in the Prokaryotic Ligand-Gated Ion Channel, ELIC. Biochemistry 57, 4036–4043 (2018).*

[†] *A substantial amount of the experimental work in this chapter was performed by Prof. Sarah C.R. Lummis. These sections are denoted with asterisks.*

must be applied in using data from this prokaryotic receptor to understand molecular details of eukaryotic pLGIC receptor function.

3.2 Introduction

The Cys-loop family of pentameric ligand-gated ion channels (pLGIC) is comprised of proteins responsible for fast excitatory and inhibitory synaptic neurotransmission in the central and peripheral nervous systems. Members of this family, which includes nicotinic acetylcholine (nACh), 5-HT_3, $GABA_A$, and glycine receptors, share a pentameric structure, with each of the subunits having extracellular, transmembrane, and intracellular domains. Neurotransmitters bind at the interface between two adjacent subunits in the extracellular domain (ECD), triggering a conformational change that opens the pore, which consists of five helices, one (M2) from each subunit.[1–3].

The mechanism of transduction of binding information to the pore remains as a significant challenge. Recent publication of high-resolution structures of the first mammalian Cys-loop receptors (nACh, $GABA_A$, 5-HT_3, and glycine)[4–8] has been enlightening, but information is still sparse compared to many other ion channels. Thus, many researchers are using prokaryotic pLGICs from *Erwinia chrysanthemi* (ELIC) and *Gloeobacter violaceus* (*Gloeobacter* ligand-gated ion channel; GLIC), as model systems.[9–13] These prokaryotic receptors share the general structure of the Cys-loop receptors, but lack the large, variable intracellular domain. In addition, the cysteines in the eponymous Cys-loop are absent in ELIC and GLIC, but the loop structure remains. GLIC has proved especially popular, with well over 70 structures in the RCSB Protein Data Bank. Nevertheless, the mechanism of ELIC is probably more similar to Cys-loop receptors, as it is activated by binding of small amines such as GABA at the orthosteric binding site,[10,14] whereas GLIC is activated by protons.[11,15,16]

We do not yet know, however, how closely ELIC models its eukaryotic relatives, and a recent report states that ELIC has atypical gating and conductance properties compared to other pLGIC.[17] In an effort to identify critical differences/similarities between ELIC and the eukaryotic Cys-loop receptors, we have chosen to focus on the proline residues of ELIC. Pro differs from other naturally occurring amino acids by its limited hydrogen bonding capability, increased steric bulk at the backbone nitrogen, and greater propensity to exist in a *cis* conformation at the peptide bond.[18,19] As such, proline residues often play critical functional roles and are frequently highly conserved in membrane receptors. Which of the unique Pro features is essential for function has previously been determined at specific locations in GLIC and some eukaryotic Cys-loop receptors.[20–22] ELIC has 15 Pro residues in each subunit **(Figure 3.1**); some of these are at locations conserved in other pLGIC, while others are not

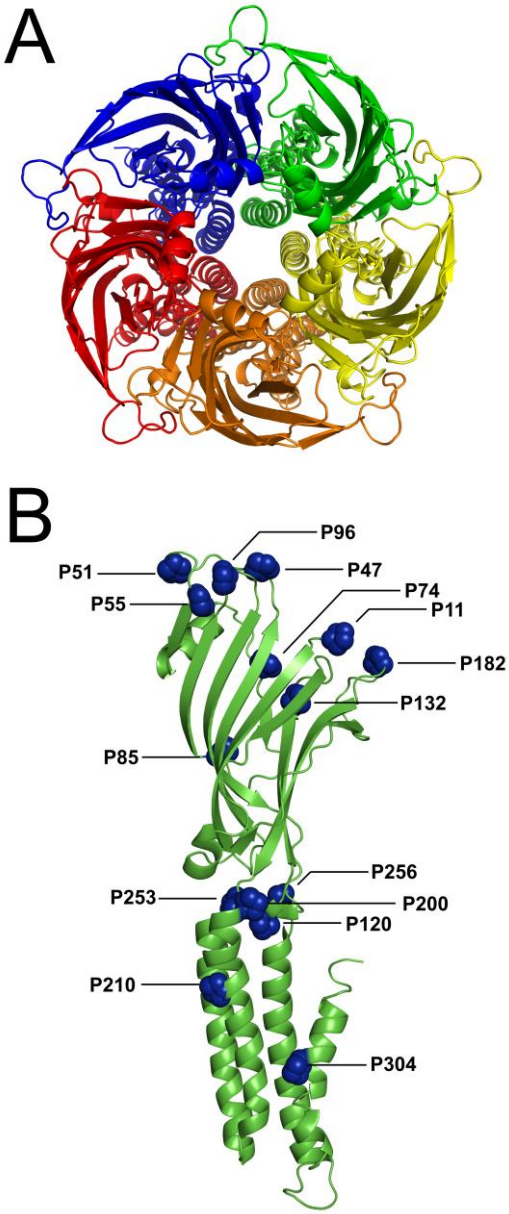

Figure 3.1. Location of Pro residues in a single ELIC subunit (PDB ID 3RQU). (A) Top-down view of ELIC, showing five subunits around the pore. (B) Single subunit of ELIC with Pro residue side-chains shown as blue spheres.

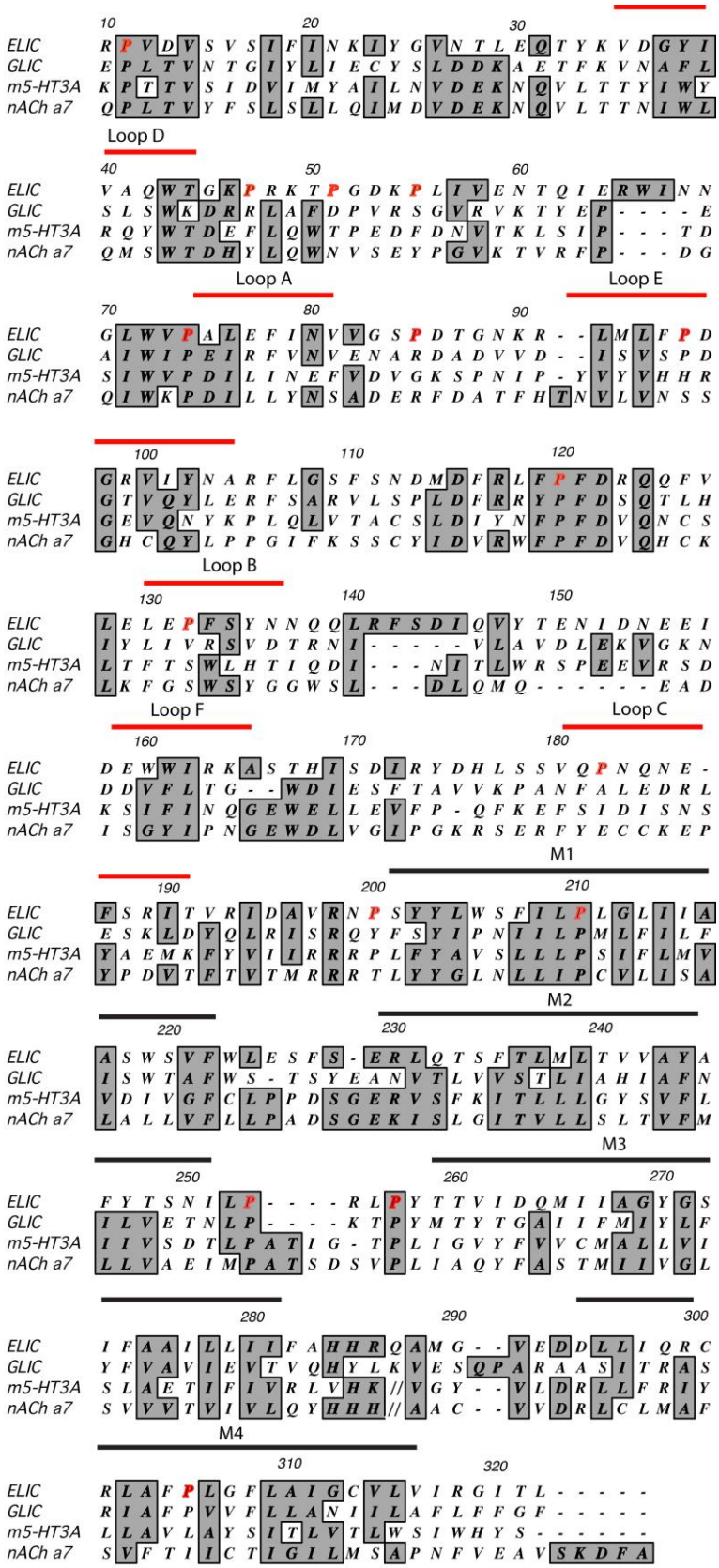

Figure 3.2. Clustal alignment of ELIC and other pLGIC subunits showing the location of the Pro residues examined in this study (red), approximate locations of the binding loops (red bars) and transmembrane α-helices (black bars), and conservation of amino acid side chain chemistry (gray boxes).

(**Figure 3.2**). Here we explore the roles of these residues using natural and non-canonical amino acid mutagenesis of Pro residues in ELIC, expressed in *Xenopus laevis* oocytes and characterized using two-electrode voltage clamp electrophysiology.

3.3 Results and Discussion

*3.3.1 Many Pro-to-Ala substitutions change functional parameters**

To probe the nature of the 15 Pro residues in each ELIC subunit, we mutated each to Ala and determined changes in functional characteristics following expression in *Xenopus* oocytes. Mutation of 14 of these to Ala resulted in functional receptors, indicating only one (P120) is critical for ELIC function.

Concentration response curves revealed EC_{50}s in the functioning mutant receptors varied between 4.4 and 92 mM, and all except one (P210A, the conserved Pro

Table 3.1
Response to GABA of Pro-to-Ala ELIC mutants in the presence and absence of Ca^{2+}. (Experiments performed by Prof. Sarah Lummis)

	+ Ca^{2+}						Ca^{2+}-free						Diff. Ca^{2+} vs Ca^{2+}-free
Variant	*p*EC_{50}			EC_{50} (mM)	n	Diff to WT	*p*EC_{50}			EC_{50} (mM)	n	Diff to WT	
WT	1.53	±	0.1	36.4	8		2.2	±	0.06	6.9	8		****
P11A	2.21	±	0.08	6.5	5	***	2.36	±	0.09	4.6	4	ns	ns
P47A	2.19	±	0.17	10.5	7	***	2.55	±	0.08	3.0	5	ns	ns
P51A	2.21	±	0.06	6.4	5	***	2.38	±	0.03	4.2	4	ns	ns
P55A	2.33	±	0.08	5.1	5	****	2.54	±	0.10	3.1	5	ns	ns
P74A	1.97	±	0.08	13.1	10	*	2.35	±	0.03	4.5	10	ns	**
P85A	1.98	±	0.09	12.4	8	*	2.06	±	0.04	8.9	8	ns	ns
P96A	2.23	±	0.09	6.5	6	****	2.31	±	0.08	5.3	6	ns	ns
P120A	NF	±			6		NF	±			6		
P132A	2.22	±	0.13	8.1	6	***	2.43	±	0.04	3.8	6	ns	ns
P182A	1.04	±	0.13	92	8	**	2.1	±	0.02	8.0	8	ns	****
P200A	2.25	±	0.14	7.7	5	***	2.41	±	0.02	3.9	5	ns	ns
P210A	1.82	±	0.03	15.3	6	ns	1.95	±	0.08	12.4	6	ns	ns
P253A	2.38	±	0.13	5.6	6	****	2.92	±	0.05	1.2	6	***	***
P256A	2.35	±	0.02	4.4	5	****	3.29	±	0.08	0.5	5	***	****
P304A	2.09	±	0.09	8.9	4	*	2.33	±	0.05	4.8	4	ns	ns

NF = non-functional; *p*EC50 data = mean ± SEM. *, **, ***, **** = significantly different ($p < 0.05, 0.01, 0.001, 0.0001$, respectively).

in the M1 helix) were significantly different to wild type ELIC (EC_{50} 36 mM) (**Table 3.1**). Most of the changes were to a lower EC_{50}, indicating GABA was more potent at these altered receptors, although one (P182A, a non-conserved Pro located in binding loop C) resulted in an increased EC_{50}.

These experiments were performed in Ca^{2+}-containing buffer. Modulation by divalent cations, and particularly Ca^{2+}, is common in pLGIC, but the effect is especially pronounced in ELIC, where it has been extensively investigated.[23,24] To probe if there were Ca^{2+}-related effects in our mutant receptors, the Ala mutagenesis experiments were repeated on all mutants in Ca^{2+}-free buffer. The presence or absence of Ca^{2+} significantly affects the functional characteristics of wild-type ELIC (as previously reported)[23] causing changes in the shape of the responses (**Figure 3.3A**) and also the EC_{50} and Hill coefficient (n_H): the EC_{50} decreased from 36 mM to 6.6 mM and n_H increased from 1.7 to 3.3 (**Tables 3.1** and **3.2**).

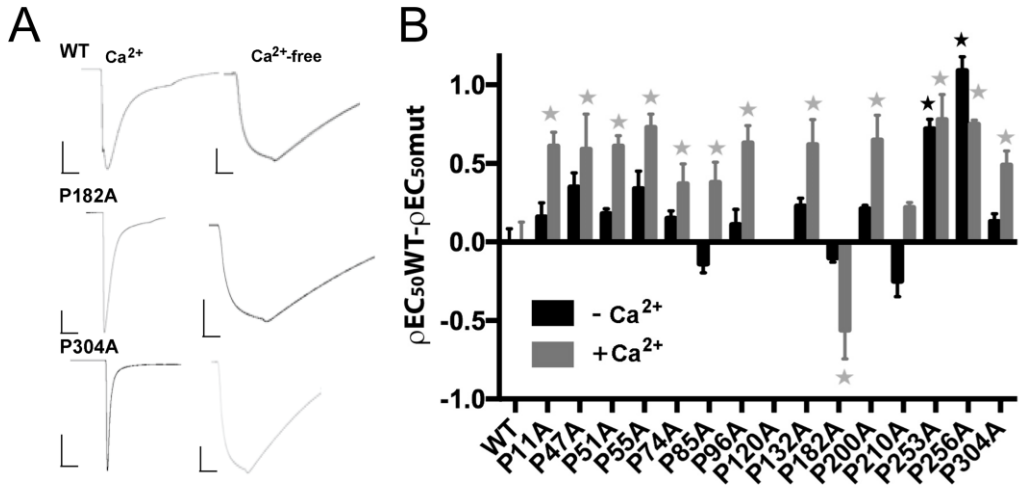

Figure 3.3. **Effects of Ca^{2+} on ELIC and ELIC Pro mutants.** (A) Effects of Ca^{2+} on typical maximal responses of wild-type and exemplar mutant ELIC to GABA. Scale bars = 5 μA and 10s. (B) Comparing effects of Ala substitutions of Pros in ELIC on GABA *p*EC_{50} values in Ca^{2+}-containing buffer versus Ca^{2+}-free buffer. Data from which these values were derived are shown in Tables 1 and 2. ★ = significantly different to WT, $p < 0.05$. (Experiments performed by Prof. Sarah Lummis.)

The use of Ca^{2+}-free buffer had a quite different effect on the mutant receptors. We observed similar effects on the shapes of the responses (**Figure 3.3A**), but, while 13 of the 14 functional Pro-to-Ala variants had pEC_{50} values that were statistically different from wild-type ELIC in buffer containing Ca^{2+}, only two variants (P253A and P256A) had statistically significant changes in pEC_{50} in Ca^{2+}-free buffer (**Figure 3.3B, Table 3.1**). Also in contrast to wild-type ELIC, 10 of the 14 functional mutants (all but P74A, P182A, P253A, and P256A) did not have statistically significant differences in pEC_{50} between Ca^{2+}-containing buffer and Ca^{2+}-free buffer (rightmost column, **Table 3.1**). Thus Ca^{2+} sensitivity is ablated in most of the Pro-to-Ala mutants, and the response to GABA of Pro-to-Ala mutants is generally more similar to wild-type ELIC in the absence of Ca^{2+}.

Table 3.2

Hill coefficients of Pro-to-Ala ELIC mutants in the presence and absence of Ca^{2+}. (Experiments performed by Prof. Sarah Lummis.)

	+ Ca^{2+}					Ca^{2+}-free					Diff Ca^{2+} vs Ca^{2+}-free
Variant	n_H			n	Diff to WT	n_H			n	Diff to WT	
WT	1.7	±	0.2	6	ns	3.3	±	0.2	6	ns	**
P27A	2.5	±	0.6	5	ns	2.1	±	0.3	4	ns	ns
P63A	2.6	±	0.5	7	ns	2.4	±	0.1	5	ns	ns
P67A	2.5	±	0.2	5	ns	3.6	±	0.2	4	ns	**
P71A	3.4	±	0.4	8	****	3.2	±	0.4	5	ns	ns
P90A	2.6	±	0.2	11	ns	3.7	±	0.3	10	ns	**
P101A	2.6	±	0.3	7	ns	3	±	0.5	7	ns	ns
P112A	2.6	±	0.4	6	ns	3	±	0.4	6	ns	ns
P136A	NF	±	NF	5	**	NF	±	NF	5	***	ns
P148A	3.1	±	0.4	8	**	3.4	±	0.2	6	ns	ns
P198A	1.7	±	0.2	8	ns	2.8	±	0.1	8	ns	**
P216A	3.1	±	0.5	7	**	3.4	±	0.4	5	ns	ns
P226A	1.8	±	0.1	6	ns	2.5	±	0.2	6	ns	ns
P269A	1.7	±	0.1	8	ns	3	±	0.3	4	ns	**
P272A	2.2	±	0.3	6	ns	2.4	±	0.3	5	ns	ns
P320A	2.5	±	0.3	5	ns	2.4	±	0.3	4	ns	ns

NF = non-functional; n_H data = mean ± SEM. *, **, ***, **** = significantly different ($p < .05, .01, .001, .0001$, respectively)

A similar pattern is observed when analyzing changes in n_H (**Table 3.2**). Four of the fourteen functional Pro-to-Ala mutants display statistically-meaningful changes in n_H relative to wild-type ELIC in Ca^{2+}-containing buffer. However, none of the functional mutants has a n_H that is statistically different from wild-type in Ca^{2+}-free buffer. This amounts to statistically-meaningful differences in n_H in the presence versus the absence of Ca^{2+} for wild-type ELIC which are ablated in all mutants except P51A, P74A, P182A, and P253A (see rightmost column, **Table 3.2**).

Such dramatic effects of Ca^{2+} have not typically been observed for other pLGICs, although modulatory effects of Ca^{2+} that can enhance or inhibit responses are common.[23,25–30] The binding sites of Ca^{2+}, identified using structural and functional experiments, have been shown to be between subunits (**Figure 3.4**), and Ca^{2+} binding impacts gating.[29] Given the apparent loss of a modulatory effect in most of the Pro-to-Ala mutants, it is interesting to consider if there is a relationship between Ca^{2+} modulation and the role of Pros in gating. Overall, Pro-to-Ala mutations increased sensitivity of mutant receptors to GABA in the presence of Ca^{2+} while the same mutations cause no change in the absence of Ca^{2+} – ten of the fifteen Pro-to-Ala mutants fit this pattern. Intriguingly, the only mutants that do not are P120A (ß6-ß7 loop), P182A (loop C), P210A (conserved M1 Pro), P253A (M2-M3 loop), and P256A (M2-M3 loop), all of which are located in regions of the protein that have been previously identified in ELIC and other pLGICs as playing important roles in receptor gating.[1,3,31] We suggest that the Pros in ELIC that are not located in the transduction pathway help to organize the structure in such a way that it can be modulated by Ca^{2+}.

The only statistically meaningful loss of function (other than the nonfunctional P120A) we observed for a Pro-to-Ala mutation in ELIC was P182A. This Pro is located in loop C, which has been identified in numerous studies of pLGICs to play a key role

in agonist binding and channel gating.[32,33] These data therefore confirm the importance of loop C in ELIC function.

3.3.2 Non-canonical amino acid mutagenesis of Pro120

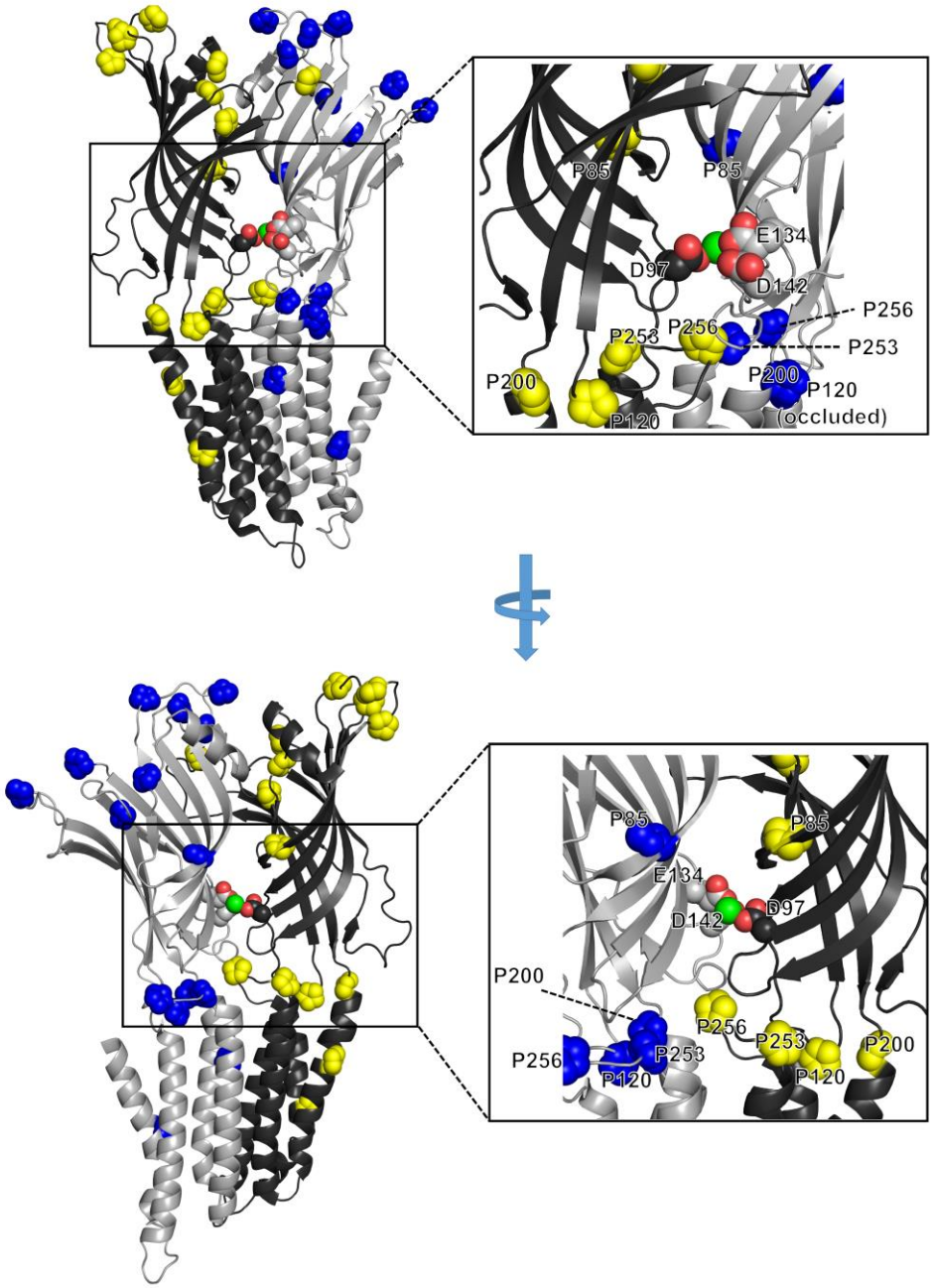

Figure 3.4. Divalent cation binding-site in ELIC, as exemplified by a crystal structure with Ba^{2+} (PDB 2YN6). Two subunits of the homopentamer are shown. The primary face is shown in light gray with Pro side chains in blue, while the complementary face is shown in black with Pros in yellow. Oxygen atoms on negatively-charged residues in the divalent cation binding site are shown in red, and the Ba^{2+} ion is shown in green. The site illustrated in this figure was shown to be responsible for the modulatory effect of Ca^{2+}.[26]

The ß6-ß7 loop in ELIC does not contain a disulfide bond as in eukaryotic pLGICs, but the equivalent region is homologous in many regards.[31,34] Most particularly it has a central Pro residue bounded by two aromatic residues. Substitution of this Pro with naturally occurring amino acids in all Cys-loop receptors tested to date results in non-functional receptors,[20,22,35] and our data in ELIC are similar. Since conventional mutagenesis of these Pros is disruptive to function, we have implemented the subtler probe of non-canonical amino acid mutagenesis. This method enables us to incorporate Pro analogues and other non-canonical amino acids of varying ring size, side chain substitution, and intrinsic preferences for the *cis* conformer (**Figure 3.5A**). A wild-type rescue experiment (*i.e.* incorporating Pro using *in vivo* non-canonical amino acid mutagenesis) revealed similar characteristics to wild-type ELIC, indicating that the non-canonical amino acid mutagenesis methodology is working appropriately. Many of the non-canonical amino acids yielded functional receptors (azetidine-2-carboxylic acid (Aze), pipecolic acid (Pip), morpholine-3-carboxylic acid (Mor), *cis*-4-fluoroproline (*cis*-F-Pro), *trans*-4-fluoroproline (*trans*-F-Pro), and N-methylalanine (N-Me-Ala), and all of these had EC_{50} and n_H values similar to wild-type (**Figure 3.5B; Table 3.3**). However, attempted incorporation of 3-methylproline (3-Me-Pro), 2-methylproline (2-Me-Pro), N-methylleucine (N-Me-Leu), and lactic acid (Aah, or α-hydroxyalanine) resulted in no measurable response.

The particular properties of Pro have resulted in its playing highly specific roles in transmembrane proteins, and we have identified 3 distinct Pro characteristics: (1) lack of a backbone hydrogen bond, (2) *cis*-bias of the prolyl peptide bond, and (3) substitution of the amine. For a given Pro, any of these could be a key characteristic required at a specific location in a pLGIC for wild type function.

To test the requirement for lack of a hydrogen bond, we introduced Aah, which generates receptors with a backbone ester in place of an amide at the site of

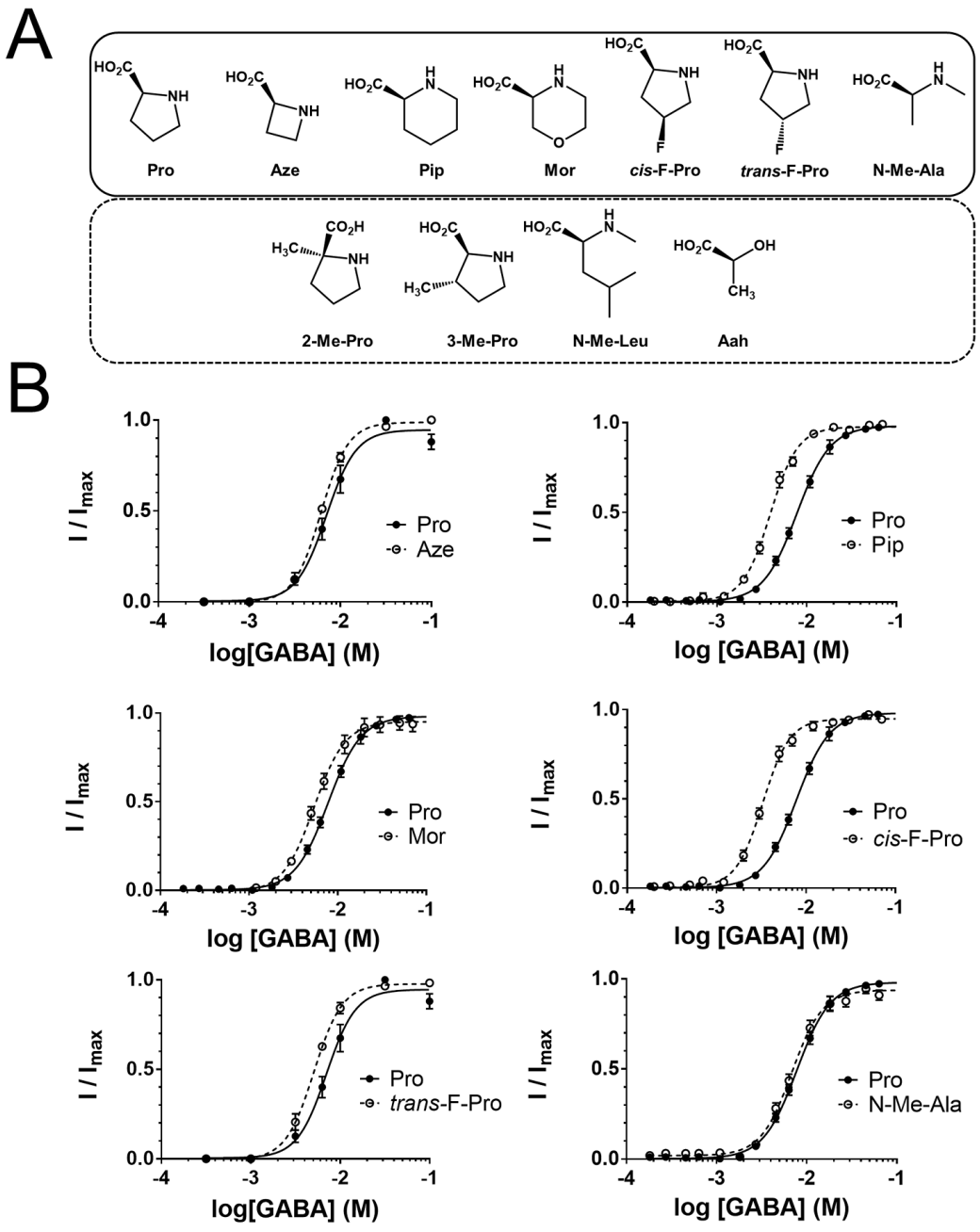

Figure 3.5. Non-canonical amino acid mutagenesis of ELIC P120. (A) Structures of non-canonical amino acids used in this study. Amino acids in the solid box were successfully incorporated whereas those in the dashed box either did not incorporate or generated non-functional receptors. (B) Dose-response curves comparing responses of ELIC to GABA for incorporation of Pro versus non-canonical amino acids. Parameters derived from these curves are shown in **Table 3.3**.

incorporation. At other Pros – for example the highly conserved Pro in the middle of M1 (P210 in ELIC) – this change leads to functional channels with near wild type behavior. However, this analog resulted in no functional response at the 120 site, suggesting that the most salient aspect of Pro at this position is not its inability to act as a hydrogen bond donor. This is also an outcome that would be expected if *cis*–bias was a factor (option 2), since this substitution would disfavor a *cis* peptide bond.

Support for option 2 comes from our data showing functional responses upon incorporation of analogs with increased *cis*-bias relative to Pro, i.e. Aze, Pip, Mor, and *cis*-F-Pro. The %*cis* of these residues when adjacent to a phenylalanine is 30%, 39%, 48%, and 32%, respectively, compared to 17% for Pro.[22] Incorporation of two Pro analogues with a lower %*cis*, 3-Me-Pro (12%) and 2-Me-Pro (0%), resulted in non-functional receptors, consistent with a requirement for a *cis* peptide bond at this position. An inconsistency is seen, however, with *trans*-F-Pro. Despite having a lower intrinsic

Table 3.3
Functional parameters for non-canonical amino acid incorporation at P120 in ELIC[a]

Pro analogue	%*cis*	pEC_{50}	EC_{50} (mM)	n_H	Max current (nA)	n
Pro	17	2.11 ± 0.01	7.7	2.3 ± 0.1	860	9
Aze	30	2.21 ± 0.03	6.2	2.9 ± 0.3	600	7
Pip	39	2.40 ± 0.01	3.9	2.8 ± 0.2	600	12
Mor	48	2.27 ± 0.02	5.4	2.5 ± 0.3	720	7
cis-F-Pro	32	2.48 ± 0.01	3.3	2.9 ± 0.2	140	9
trans-F-Pro	12	2.29 ± 0.03	5.1	2.7 ± 0.2	190	6
N-Me-Ala	ND	2.17 ± 0.02	6.8	2.5 ± 0.2	330	13
2-Me-Pro	0	NF				6
3-Me-Pro	12	NF				8
N-Me-Leu	ND	NF				7
Aah	ND	NF				4

[a]NF= non-functional; ND = not determined. *p*EC50 data = mean ± SEM. No values were statistically different to WT. %*cis* values for Pro, Pip, Aze, *cis*-F-Pro, 3-Me-Pro, 2-Me-Pro, and Mor were determined from NMR analysis of GFXG tetrapeptides[22] while that for *trans*-F-Pro was determined using a different approach.[18]

cis preference than Pro (12% versus 17%),[18] *trans*-F-Pro yields no meaningful functional differences from wild-type ELIC when incorporated in place of P120. It is perhaps salient that this %*cis* value was not determined from *trans*-F-Pro with an adjacent aromatic residue, which affects *cis*/*trans* ratios of Pro amide bonds, and thus the value of 12% may be an underestimate in this situation.[36,37] Still, *trans*-F-Pro has a higher intrinsic *cis* bias than any naturally-occurring amino acid other than Pro.

The N-substituted amino acids N-Me-Ala and N-Me-Leu were incorporated in place of P120 in order to probe option 3, amine substitution. N-Me-Ala incorporation yielded functional receptors with pharmacological properties very similar to wild-type ELIC. Note that an N-substituted peptide bond is also expected to exist more in the *cis* conformation than a conventional amino acid.[38,39] However, incorporation of N-Me-Leu in place of P120 yielded no measurable response. This, together with the observation that 3-Me-Pro also failed to generate functional receptors, can perhaps be rationalized by considering branching of the side chain. N-Me-Leu and 3-Me-Pro failed

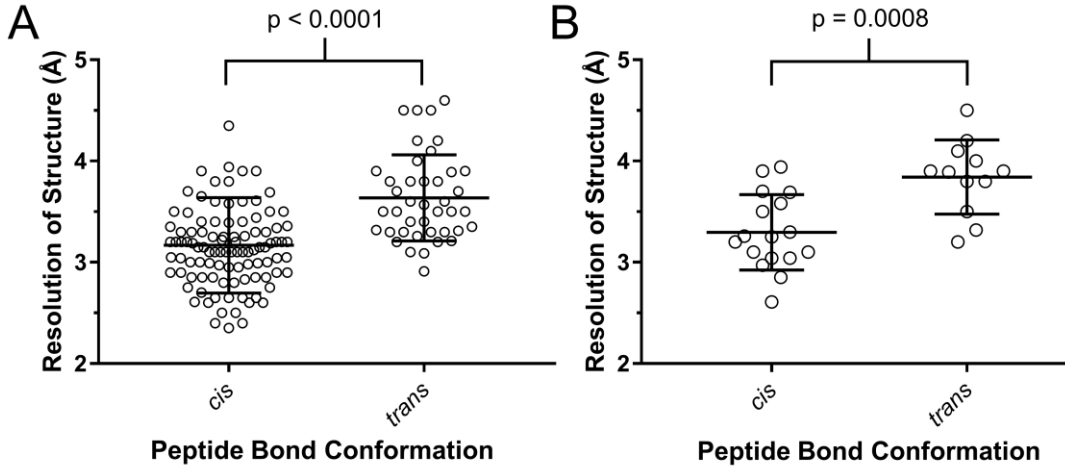

Figure 3.6. Analysis of the conformations about the completely-conserved ß6-ß7 loop prolyl peptide bond in pLGIC structures. (A) Correlation between higher structural resolution and assignment of a *cis* peptide bond. 142 X-ray crystal structures and cryo-EM structures of full-length pLGICs were included in this analysis. (B) Correlation between higher structural resolution and assignment of a *cis* peptide bond is still present when considering only full-length mammalian pLGIC structures.

to give functional receptors, and these are also the only two amino acids studied herein with tertiary carbon centers on their side chains. This sensitivity to side chain branching at P120 in ELIC would distinguish it from other pLGICs, where functional incorporation of 3-Me-Pro at the equivalent position has been seen.[20,22]

Together, the data using non-canonical amino acid mutagenesis of P120 suggest a requirement for substitution of the amine, as well as a preference for a *cis* peptide bond at this position. Further support for the presence of a *cis* peptide bond comes from an analysis of pLGIC structures in the RCSB Protein Data Bank. Of the 142 pLGIC structures we examined, 101 were found to have the ß6-ß7 loop Pro in the *cis* conformation. Moreover, we observe a statistically significant correlation between the resolution of the structure and the presence of a *cis* peptide bond at this Pro; higher-resolution structures tend to assign the *cis* conformation while those of lower resolution tend to assign a *trans* peptide bond ($p < 0.0001$, **Figure 3.6A**). While there are still 41 pLGIC structures with *trans* peptide bonds to this Pro, it seems that the peptide bond is more likely to be simply assigned a *trans* conformation when the resolution is too low to observe the peptide bond conformation definitively. The correlation is still present when the analysis is limited to structures of mammalian Cys-loop receptors ($p = 0.0008$, **Figure 3.6B**).

3.4 Conclusions

In conclusion, our data show that ELIC is largely tolerant of Pro-to-Ala substitutions, although we note key differences between functional changes in media with Ca^{2+} versus media without Ca^{2+}; this tolerance differs from previously-observed results in other pLGICs, perhaps indicating a departure from a canonical mechanism of action of these proteins.

The absolutely-conserved P120 in the ß6-ß7 loop, however, is critical for receptor function. Investigations using non-canonical amino acids demonstrate that substitution of the amide nitrogen is key at this position, and also highlight a potential role for a *cis* peptide bond. Comparisons with other pLGICs show that the role of this Pro in ELIC may contribute in a similar manner to that in other pLGIC.

3.5 Experimental Procedures

3.5.1 Molecular biology

The cDNA for ELIC was in the pGEMhe plasmid. Site-directed mutagenesis was performed using the Stratagene QuikChange protocol to generate the appropriate codon. For non-canonical amino acid mutants and conventional mutants generated by non-canonical amino acid mutagenesis, the site of interest was mutated to the TAG stop codon. Plasmids were linearized with the SbfI restriction enzyme, and receptor mRNA was then prepared by *in vitro* runoff transcription using the Ambion T7 mMessage mMachine kit.

Hydroxy or 4,5-dimethoxy-2-nitrobenzyloxycarbonyl (NVOC) protected amino acid-dCA couples were enzymatically ligated to truncated 74mer THG73 tRNA as previously described.[40,41] The 74mer tRNA was prepared using the Ambion T7MEGAshortscript kit by transcription from a modified DNA oligonucleotide template as described in the literature to enhance RNA transcript homogeneity.[42] Crude tRNA-amino acid or tRNA-hydroxy acid product was used without desalting, and the product was confirmed by matrix-assisted laser desorption ionization time-of-flight mass spectrometry on a 3-hydroxypicolinic acid matrix. Deprotection of the NVOC group on the tRNA-amino acids was carried out by 5-min photolysis on a 1 kW xenon lamp with WG-335 and UG-11 filters or for 2.5-min using

a 1150mW 365nm LED (Thorlabs) immediately prior to injection. Either deprotection strategy yielded fully deprotected aminoacyl tRNAs as assayed by MALDI-TOF mass spectrometry.

3.5.2 Oocyte preparation and RNA injection

Stage V-VI oocytes of *Xenopus laevis* were harvested and injected with RNAs as described previously.[41] For non-canonical amino acid mutagenesis experiments, each cell was injected with 50-100 ng each of receptor mRNA and appropriate tRNA approximately 48h before recording. Mutants yielding small responses required 72h of incubation, with a second injection of mRNA and tRNA 48h before recording.

For wild type experiments and conventional mutants, each cell received a single injection of 1-25 ng of receptor mRNA approximately 24 h before recording. Injection volumes for each injection session were 50-100 nL per cell.

As a negative control for suppression experiments at each site, unacylated full-length tRNA was co-injected with mRNA in the same manner as charged tRNA. These experiments yielded negligible responses for all sites. Wild-type recovery conditions (injecting tRNA charged with the appropriate amino acid to regenerate a wild type channel *via* non-canonical amino acid mutagenesis at a TAG stop codon) were injected alongside mutant non-canonical amino acid mutagenesis conditions as a positive control.

3.5.3 Electrophysiology

Oocyte recordings were made in two-electrode voltage clamp mode using the OpusXpress 6000A (Axon Instruments). Oocyte equilibration and washes were performed with ND96 (96 mM NaCl, 2 mM KCl, 1.8m $CaCl_2$, 1 mM $MgCl_2$, 5 mM HEPES, pH 7.4). Initial holding potential was -60 mV. Data were sampled at 125 Hz

and filtered at 50 Hz. Micro-electrodes were fabricated from borosilicate glass (GC120TF-10, Harvard Apparatus, Kent, UK) using a one stage horizontal pull (P-87, Sutter Instrument Company, Novato, CA) and filled with 3M KCl. Pipette resistances ranged from 0.3 – 3.0 MΩ. Analysis and curve fitting was performed using the 4 parameter equation in Prism (GraphPad Software, La Jolla, CA). Concentration-response data for each oocyte was normalized to the maximum current for that oocyte. Parameters were compared using ANOVA with a Dunnetts multiple comparisons test. Values of $p < 0.05$ were taken as significant.

3.5.4 Analysis of ß6-ß7 loop proline peptide bond conformation

Only X-ray crystal structures and cryo-EM structures of full-length receptors were considered for analysis. The PDB IDs of the structures used for this analysis are as follows: **Mammalian Cys-loop receptors:** 5-HT_3Rs: 4PIR, 6HIS, 6HIN, 6HIQ, 6HIO, 6DG7, 6DG8. nAChRs: 2BG9, 6CNJ, 6CNK, 5KXI. GlyR α-subunit homopentamers: 5CFB, 3JAF, 3JAE, 3JAD, 5VDH, 5TIO, 5TIN, 5VDI. $GABA_AR$ ß3 homopentamer: 4COF. $GABA_AR$ ß3-α5 chimeras: 5O8F, 5OJM. $GABA_AR$ heteropentamers: 6HUG, 6HUJ, 6HUK, 6HUO, 6HUP, 6DW0. **Protostome Cys-loop receptors:** GluCl: 4TNW, 4TNV, 3RHW, 3RIF, 3RI5, 3RIA. **Prokaryotic pLGICs:** GLIC & GLIC variants: 4HFI, 4IL4, 4HFH, 4HFE, 3EAM, 5HCJ, 4F8H, 4ILC, 4QH5, 4HFD, 4ZZC, 5HCM, 3P4W, 4QH4, 5J0Z, 3P50, 5L47, 5L4H, 4QH1, 4ZZB, 4ILA, 5L4E, 4NPQ, 3EHZ, 2XQ7, 2XQ3, 2XQ5, 2XQ4, 2XQ8, 2XQ6, 2XQA, 5MUO, 6F7A, 3TLW, 3TLU, 3TLV, 3UU5, 3UUB, 3UU6, 3UU4, 3UU3, 3UU8, 4IL9, 4ILB, 5V6N, 6F11, 6F0Z, 6F10, 6F12, 3TLS, 2XQ9, 3EI0, 6F0I, 6F0J, 6F0U, 6F0M, 6F13, 6F0N, 6F0R, 6F0V, 4HFB, 4HFC, 5MUR, 5MVM, 5V6O, 3TLT, 6F15, 5MZR, 5MZT, 6F16, 4LML, 5MZQ, 5MVN, 5HEG, 5HEH, 4LMJ, 5IUX, 4IRE, 4LMK, 5OSA, 5OSC, 5OSB, 4NPP. ELIC & ELIC variants: 4Z90, 5SXU, 4TWD, 4A97, 4Z91, 5SXV, 4A98,

3ZKR, 2YOE, 4TWF, 3RQW, 3RQU, 2VL0, 2YN6, 5LG3, 5LID, 5HEJ, 4TWH, 2YKS, 3UQ7, 3UQ5, 5HEO, 5HEW. ELIC/GLIC chimera: 4YEU. **Mammalian/Prokaryotic chimera:** GlyR/GLIC chimera: 4X5T.

Each structure was manually examined in Pymol 2.3 in regard to the conformation about the peptide bond to the conserved ß6-ß7 loop proline. Two structures (PDB ID 3RQW and 3UQ4) had an ambiguous, bent conformation about the prolyl peptide bond, and were excluded from this analysis. GraphPad Prism 7 was used to plot the data and analysis of statistical significance was performed using a nonparametric Mann-Whitney test.

3.6 References

1. Miller, P. S. & Smart, T. G. Binding, activation and modulation of Cys-loop receptors. Trends Pharmacol. Sci. 31, 161–174 (2010).
2. Lynagh, T. & Pless, S. A. Principles of agonist recognition in Cys-loop receptors. Front. Physiol. 5, (2014).
3. Andrew J Thompson, H. A. L. The structural basis of function in Cys-loop receptors. Q. Rev. Biophys. 43, 449–99 (2010).
4. Hassaine, G. et al. X-ray structure of the mouse serotonin 5-HT3 receptor. Nature 512, 276–281 (2014).
5. Miller, P. S. & Aricescu, A. R. Crystal structure of a human GABAA receptor. Nature 512, 270–275 (2014).
6. Du, J., Lü, W., Wu, S., Cheng, Y. & Gouaux, E. Glycine receptor mechanism elucidated by electron cryo-microscopy. Nature 526, 224–229 (2015).
7. Huang, X., Chen, H., Michelsen, K., Schneider, S. & Shaffer, P. L. Crystal structure of human glycine receptor-α3 bound to antagonist strychnine. Nature 526, 277–280 (2015).
8. Morales-Perez, C. L., Noviello, C. M. & Hibbs, R. E. X-ray structure of the human α4β2 nicotinic receptor. Nature 538, 411–415 (2016).
9. Tasneem, A., Iyer, L. M., Jakobsson, E. & Aravind, L. Identification of the prokaryotic ligand-gated ion channels and their implications for the mechanisms and origins of animal Cys-loop ion channels. Genome Biol. 6, R4 (2004).
10. Thompson, A. J., Alqazzaz, M., Ulens, C. & Lummis, S. C. R. The pharmacological profile of ELIC, a prokaryotic GABA-gated receptor. Neuropharmacology 63, 761–767 (2012).
11. Bocquet, N. et al. A prokaryotic proton-gated ion channel from the nicotinic acetylcholine receptor family. Nature 445, 116–119 (2007).
12. Hilf, R. J. C. & Dutzler, R. X-ray structure of a prokaryotic pentameric ligand-gated ion channel. Nature 452, 375–379 (2008).
13. Hilf, R. J. C. & Dutzler, R. Structure of a potentially open state of a proton-activated pentameric ligand-gated ion channel. Nature 457, 115–118 (2009).

14. Zimmermann, I. & Dutzler, R. Ligand Activation of the Prokaryotic Pentameric Ligand-Gated Ion Channel ELIC. PLoS Biol 9, e1001101 (2011).
15. Rienzo, M., Lummis, S. C. R. & Dougherty, D. A. Structural Requirements in the Transmembrane Domain of GLIC Revealed by Incorporation of Noncanonical Histidine Analogs. Chem. Biol. 21, 1700–1706 (2014).
16. Nemecz, Á. et al. Full mutational mapping of titratable residues helps to identify proton-sensors involved in the control of channel gating in the Gloeobacter violaceus pentameric ligand-gated ion channel. PLOS Biol. 15, e2004470 (2017).
17. Gonzalez-Gutierrez, G. & Grosman, C. The atypical cation-conduction and gating properties of ELIC underscore the marked functional versatility of the pentameric ligand-gated ion-channel fold. J. Gen. Physiol. 146, 15–36 (2015).
18. Dugave, C. & Demange, L. Cis−Trans Isomerization of Organic Molecules and Biomolecules: Implications and Applications. Chem. Rev. 103, 2475–2532 (2003).
19. MacArthur, M. W. & Thornton, J. M. Influence of proline residues on protein conformation. J. Mol. Biol. 218, 397–412 (1991).
20. Rienzo, M., Rocchi, A. R., Threatt, S. D., Dougherty, D. A. & Lummis, S. C. R. Perturbation of Critical Prolines in Gloeobacter violaceus Ligand-gated Ion Channel (GLIC) Supports Conserved Gating Motions among Cys-loop Receptors. J. Biol. Chem. 291, 6272–6280 (2016).
21. Lummis, S. C. R. et al. Cis–trans isomerization at a proline opens the pore of a neurotransmitter-gated ion channel. Nature 438, 248–252 (2005).
22. Limapichat, W., Lester, H. A. & Dougherty, D. A. Chemical Scale Studies of the Phe-Pro Conserved Motif in the Cys Loop of Cys Loop Receptors. J. Biol. Chem. 285, 8976–8984 (2010).
23. Zimmermann, I., Marabelli, A., Bertozzi, C., Sivilotti, L. G. & Dutzler, R. Inhibition of the Prokaryotic Pentameric Ligand-Gated Ion Channel ELIC by Divalent Cations. PLOS Biol. 10, e1001429 (2012).
24. Spurny, R. et al. Pentameric ligand-gated ion channel ELIC is activated by GABA and modulated by benzodiazepines. Proc. Natl. Acad. Sci. U. S. A. 109, E3028–E3034 (2012).
25. Vernino, S., Amador, M., Luetje, C. W., Patrick, J. & Dani, J. A. Calcium modulation and high calcium permeability of neuronal nicotinic acetylcholine receptors. Neuron 8, 127–134 (1992).
26. Galzi, J. L., Bertrand, S., Corringer, P. J., Changeux, J. P. & Bertrand, D. Identification of calcium binding sites that regulate potentiation of a neuronal nicotinic acetylcholine receptor. EMBO J. 15, 5824–5832 (1996).
27. Le Novère, N., Grutter, T. & Changeux, J.-P. Models of the extracellular domain of the nicotinic receptors and of agonist- and Ca2+-binding sites. Proc. Natl. Acad. Sci. U. S. A. 99, 3210–3215 (2002).
28. Thompson, A. J. & Lummis, S. C. R. Calcium modulation of 5-HT3 receptor binding and function. Neuropharmacology 56, 285–291 (2009).
29. Buldakova, S., Real, E., Jacob, Y. & Bregestovski, P. Calcium-dependent modulation of human glycine receptors expressed in cultivated cell lines. Cell Tissue Biol. 1, 30–33 (2007).
30. Majewska, M. D. & Chuang, D. M. Modulation by calcium of gamma-aminobutyric acid (GABA) binding to GABAA and GABAB recognition sites in rat brain. Involvement of different mechanisms. Mol. Pharmacol. 25, 352–359 (1984).

31. daCosta, C. J. B. & Baenziger, J. E. Gating of Pentameric Ligand-Gated Ion Channels: Structural Insights and Ambiguities. Structure 21, 1271–1283 (2013).
32. Nys, M., Kesters, D. & Ulens, C. Structural insights into Cys-loop receptor function and ligand recognition. Biochem. Pharmacol. 86, 1042–1053 (2013).
33. Chang, Y., Wu, W., Zhang, J. & Huang, Y. Allosteric activation mechanism of the cys-loop receptors. Acta Pharmacol. Sin. 30, 663–672 (2009).
34. Jaiteh, M., Taly, A. & Hénin, J. Evolution of Pentameric Ligand-Gated Ion Channels: Pro-Loop Receptors. PLOS ONE 11, e0151934 (2016).
35. Deane, C. M. & Lummis, S. C. The role and predicted propensity of conserved proline residues in the 5-HT3 receptor. J. Biol. Chem. 276, 37962–37966 (2001).
36. Thomas, K. M., Naduthambi, D. & Zondlo, N. J. Electronic Control of Amide cis−trans Isomerism via the Aromatic−Prolyl Interaction. J. Am. Chem. Soc. 128, 2216–2217 (2006).
37. Zondlo, N. J. Aromatic-Proline Interactions: Electronically Tunable CH/π Interactions. Acc. Chem. Res. 46, 1039–1049 (2013).
38. LaPlanche, L. A. & Rogers, M. T. cis and trans Configurations of the Peptide Bond in N-Monosubstituted Amides by Nuclear Magnetic Resonance. J. Am. Chem. Soc. 86, 337–341 (1964).
39. Portnova, S. L., Bystrov, V. F., Balashova, T. A., Ivanov, V. T. & Ovchinnikov, Y. A. cis-trans-isomerism of the peptide bond in N-methylated alanine dipeptides. Bull. Acad. Sci. USSR Div. Chem. Sci. 19, 776–780 (1970).
40. England, P. M., Lester, H. A. & Dougherty, D. A. Incorporation of esters into proteins: Improved synthesis of hydroxyacyl tRNAs. Tetrahedron Lett. 40, 6189–6192 (1999).
41. Nowak, M. W. et al. [28] In vivo incorporation of unnatural amino acids into ion channels in Xenopus oocyte expression system. in (ed. Enzymology, B.-M. in) 293, 504–529 (Academic Press, 1998).
42. Kao, C., Zheng, M. & Rüdisser, S. A simple and efficient method to reduce nontemplated nucleotide addition at the 3 terminus of RNAs transcribed by T7 RNA polymerase. RNA 5, 1268–1272 (1999).

Chapter 4: Molecular Details of 5-HT_{3A}R Gating

4.1 Abstract

Cys-loop receptors are ligand-gated ion channels that facilitate communication between cells of the nervous system and are implicated in a wide range of afflictions. Much is known about the binding of endogenous agonists and other ligands, however the process of allosteric communication of the ligand binding event into receptor activation, a process known generally as "gating," is not as well-characterized. Herein we have used a combination of canonical and non-canonical amino acid mutagenesis and mutant cycle analysis in order to elucidate details of the gating mechanism of one Cys-loop receptor, the type 3 serotonin receptor (5-HT_3R). The results reported in this study contribute to our understanding of 5-HT_3R and may provide valuable insights into the gating mechanisms of Cys-loop receptors as a whole.

4.2 Introduction

Communication between cells of the nervous system happens in part by the process of synaptic transmission, wherein neurotransmitters are released from a presynaptic cell to convey a signal to a postsynaptic cell.[1–3] The sensing of neurotransmitters by the postsynaptic cell is achieved by the action of receptors on its surface, including pentameric ligand-gated ion channels (pLGICs) that convert a chemical signal in the form of ligand binding into an electrochemical signal in the form of ion flux across the membrane.[1–3]

Many pLGICs have been studied extensively to date, but a significant amount of research has been done on vertebrate pLGICs, the so-called Cys-loop receptor superfamily, comprised of nicotinic acetylcholine receptors (nAChRs), type A γ-aminobutyric acid receptors ($GABA_A$Rs), glycine receptors (GlyRs), and type 3 serotonin receptors (5-

HT_3Rs).[4–7] Within the Cys-loop receptor superfamily, 5-HT_3Rs have garnered much interest.[7–10] These receptors carry out fast excitatory neurotransmission by responding to their native agonist serotonin, also known as 5-hydroxytryptamine or 5-HT. 5-HT_3Rs are abundant in the gastrointestinal tract, where they regulate physiological functions such as gut motility, peristalsis, and emesis.[7,9] Currently-marketed pharmaceuticals targeting 5-HT_3Rs competitively antagonize the serotonin binding site, and are prescribed for the treatment of radiotherapy- or chemotherapy-induced nausea and vomiting, post-operative emesis, and irritable bowel syndrome.[9,10] Additionally, 5-HT_3Rs have been implicated in a range of other treatment areas including cognition, emotion, learning, anxiety, and bipolar disorder.[10]

A single 5-HT_3R is composed of five identical or homologous subunits assembled about a five-fold axis to form a central pore.[7,8] In humans there are five distinct subunits of 5-HT_3Rs, assigned letters A through E. The A subunit can form homopentameric receptors, and is obligate for the formation of heteromeric receptors.[7,8] Given that all 5-HT_3Rs must contain the A subunit, all drugs on the market which target 5-HT_3Rs have been characterized based on their action at homomeric 5-$HT_{3A}Rs$.[7] We too have focused our research on the homopentameric 5-$HT_{3A}R$.

In 5-$HT_{3A}Rs$, as with other Cys-loop receptors, the N-terminal domain folds into ten β strands, which assemble into a β sandwich to form the extracellular domain (ECD; **Figure 4.1**).[1–3] The transmembrane domain (TMD) is comprised of four α-helices, numbered M1-M4; loops connecting the transmembrane helices extend into the intracellular and extracellular space.[1–3] During receptor activation, the ligand binds at the interface between two subunits in the ECD, causing conformational changes collectively

known as “gating” that ultimately result in an expansion of the channel pore formed by the M2 helices, allowing the selective passage of ions across the cell membrane.[1–3]

While structural studies of pLGICS have provided great insight into the global structural changes underlying activation of the 5-HT$_{3A}$R and other pLGICs, the exact molecular details of the gating processes for different receptors have remained elusive.[1,2,11] Nonetheless, numerous studies across the pLGIC superfamily have highlighted the importance of a region at the interface between the ECD and TMD in channel gating.[1,2,11] Key secondary structures in this “interfacial region” include the ß1-ß2 loop, the Cys-loop (or ß6-ß7 loop in prokaryotic receptors, which lack the signature disulfide bond of eukaryotic receptors), the ß8-ß9 loop, the pre-M1 region, and the M2-M3 loop (**Figure 4.1**).[1,2,11] Herein we have performed mutagenesis experiments on the 5-HT$_{3A}$R to define key chemical features of and functionally-relevant interactions between residues in the

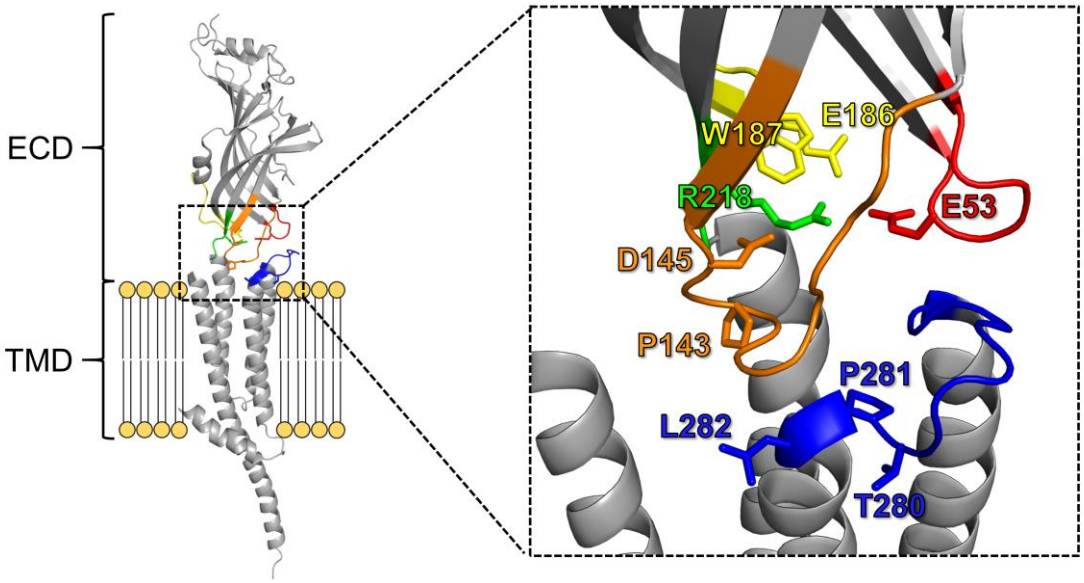

Figure 4.1. Overall topology of a single 5-HT$_{3A}$R subunit (left) and interfacial region (right). Key structural elements of the interfacial region are highlighted and side chains of amino acid residues under investigation are shown as sticks. Red, ß1-ß2 loop; orange, Cys-loop; yellow, ß8-ß9 loop; green, pre-M1 region; blue, M2-M3 loop. For simplicity, carbon atoms and heteroatoms are the same color. PDB ID 6HIS.[25]

interfacial region of this receptor. In doing so, we aim to reconcile previous results regarding the roles of these residues and nearby residues in gating of the 5-HT_{3A}R and other pLGICs.

4.3 Results and Discussion

4.3.1 Non-canonical amino acid mutagenesis of the 5-HT_{3A}R Cys-loop proline[*]

In the namesake Cys-loop (the ß6-ß7 loop of prokaryotic pLGICs) of Cys-loop receptors, there is an absolutely-conserved proline that was shown to be critical for surface expression of 5-HT_{3A}Rs in a very early study.[12] Since then, the precise chemical features of the aligning proline have been examined in GLIC, ELIC, and the muscle-type nAChR by means of non-canonical amino acid mutagenesis.[13–15] Herein we sought to perform the same type of analysis of the Cys-loop proline in the 5-HT_{3A}R in order to compare results with those of other pLGICs.

In all pLGICs, this proline is adjacent to at least one if not two aromatic amino acids (either phenylalanine or tyrosine).[13–16] In addition to there being an increased prevalence of *cis* peptide bonds to proline residues relative to all other amino acids,[17] it is well-established that the presence of an aromatic residue immediately preceding a proline residue in the primary sequence increases the intrinsic *cis* bias of the prolyl peptide bond via polar-π interactions between the π system of the aromatic ring and hydrogens on the proline pyrrolidinyl ring.[18–20]

We therefore sought to elucidate the salient chemical features of the Cys-loop proline residue in the 5-HT_{3A}R, especially in regard to the conformation about the P143 peptide bond. Employing both natural and non-canonical amino acids, we substituted P143

[*]Part of this section was written in collaboration with Prof. Sarah C.R. Lummis.

with an array of amino acids and amino acid analogs and characterized receptor function in response to 5-HT. The results are summarized in **Table 4.1**. Consistent with previous results, there was no measurable response up to 800μM 5-HT of 5-HT_{3A}Rs bearing Ala or Val substitutions for this proline. This could be due either to a lack of surface expression (presumably resulting from misfolding) or surface expression of nonfunctional receptors. We did not assay for surface expression, so either possibility is open.

Given the results from the two natural mutants, we next attempted incorporation of non-canonical amino acid analogues at the proline site of interest. All told, we attempted incorporation of azetidine-2-carboxylic acid (Aze), pipecolic acid (Pip), morpholine-3-carboxylic acid (Mor), *cis*-4-fluoroproline (*cis*-F-Pro), *trans*-4-fluoroproline (*trans*-F-Pro),

Table 4.1
Mutations to the 5-HT_{3A}R Cys-loop proline, P143.

Mutation	%cis[a]	EC_{50} (μM)	n_H	$\lvert I_{max}\rvert$(μA)	Fold	N
-	17	1.3 ± 0.03	2.4 ± 0.11	1.0 - 78	1.0	21
Pro*	17	1.3 ± 0.03	2.7 ± 0.19	0.04 - 3.6	1.0	20
3-Me-Pro	12	0.27 ± 0.01	2.6 ± 0.18	0.09 - 1.5	0.21	19
Pip	39	0.53 ± 0.01	4.2 ± 0.34	0.37 - 6.2	0.41	23
cis-F-Pro	ND	0.58 ± 0.03	5.2 ± 1.3	1.1 - 8.8	0.45	8
Aze	30	1.2 ± 0.14	1.1 ± 0.11	0.05 - 0.69	1.0	15
trans-F-Pro	32	1.5 ± 0.05	2.1 ± 0.13	0.12 - 4.9	1.1	19
N-Me-Ala	ND	2.3 ± 0.10	2.4 ± 0.25	0.10 - 1.5	1.7	23
dhP	ND	4.0 ± 0.14	2.6 ± 0.19	0.50 - 1.5	3.1	10
Mor	48	5.5 ± 0.14	2.1 ± 0.08	0.24 - 6.1	4.3	32
2-Me-Pro	ND	NR				12
DMP	ND	NR				10
N-Me-Leu	ND	NR				8
Aah	ND	NR				8
Ala[†]	ND	NR				8
Gly[†]	ND	NR				11

[a]From Ref. 15 *Wild-type recovery experiment incorporating Pro using non-canonical amino acid mutagenesis. [†]Conventional mutants. NR, no response. ± SEM

3-methylproline (3-Me-Pro), 3,4-dehydroproline (dhP), N-methylalanine (N-Me-Ala), 2-methylproline (2-Me-Pro), 5,5-dimethylproline (DMP), lactic acid (α-hydroxyalanine, or

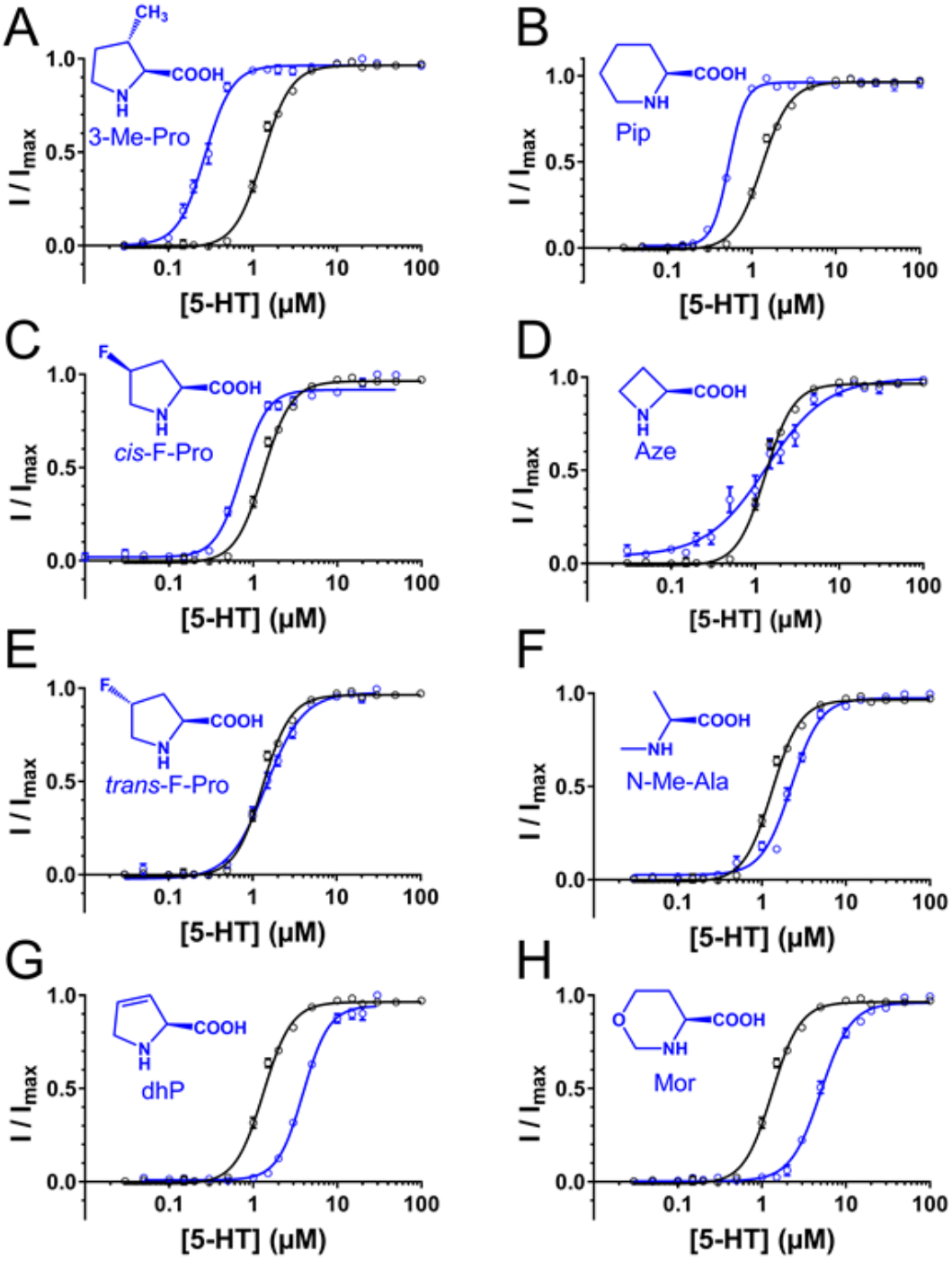

Figure 4.2. Dose-response curves for non-canonical amino acids incorporated at P143 in the 5-HT$_{3A}$R. Each is compared to the wild-type recovery experiment, P143Pro. ± SEM

Aah), and N-methylleucine (N-Me-Leu). The dose-response relationships for the amino acids successfully incorporated are provided in **Figure 4.2**. Each is compared to the positive control "P143Pro," for which responses were very nearly identical to those observed from expression of wild-type 5-HT_{3A}Rs. All but the latter four non-canonicals (**Figure 4.3**) gave robust responses upon expression in *Xenopus laevis* ooctyes. A range effects was observed for the different non-canonical amino acids, spanning a ~5-fold decrease in EC_{50} for 3-Me-Pro to a ~4-fold increase in EC_{50} for Mor.

When considering the different chemical features of these amino acids in relation to receptor function (or lack thereof), no clear pattern is immediately obvious. There are, however, some general inferences that can be made. In the case of the non-functional amino acids 2-Me-Pro, DMP, and N-Me-Leu, we note the common feature of branched side chains, which we speculate may result in improper folding/trafficking due to steric constraints in this region of the protein. Nevertheless, the branched 3-Me-Pro yielded functional receptors, so the exact placement of the methyl groups in these amino acids may be important. The α-hydroxy analogue of alanine, Aah, also did not yield functional surface expression of 5-HT_{3A}Rs, which implies that simply removing the ability of Ala to H-bond donate via its backbone amide is insufficient to recapitulate the required properties of proline at this position (recall that P143A was also nonfunctional).

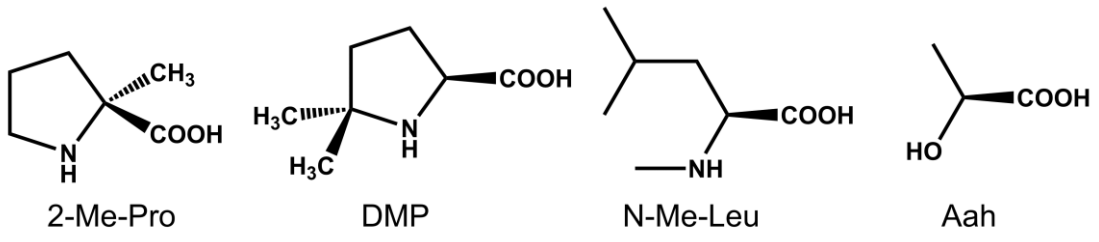

Figure 4.3. Non-canonical amino acids that did not yield functional receptors upon attempted incorporation in place of 5-HT_{3A}R P143.

A possible explanation of the data from the functional mutants is that a *cis* peptide bond may be a structural requirement at this position in the 5-HT_{3A}R. As mentioned previously, prolyl peptide bonds have a greater intrinsic propensity to exist in the *cis* conformation than the other naturally-occurring amino acids.[17] Likewise, all of the non-canonical analogues successfully incorporated have higher intrinsic *cis* biases than natural amino acids other than proline.[15,19,21–23] Many pLGIC structures depict the peptide bond to this proline in this *cis* conformation, and indeed there is an undeniable correlation between high structural resolution and assignment of a *cis* peptide bond across all pLGIC structures currently in the Protein Data Bank (see *section 3.3.2*, **Figure 3.6** for a full discussion of the structural data regarding this proline in pLGICs).

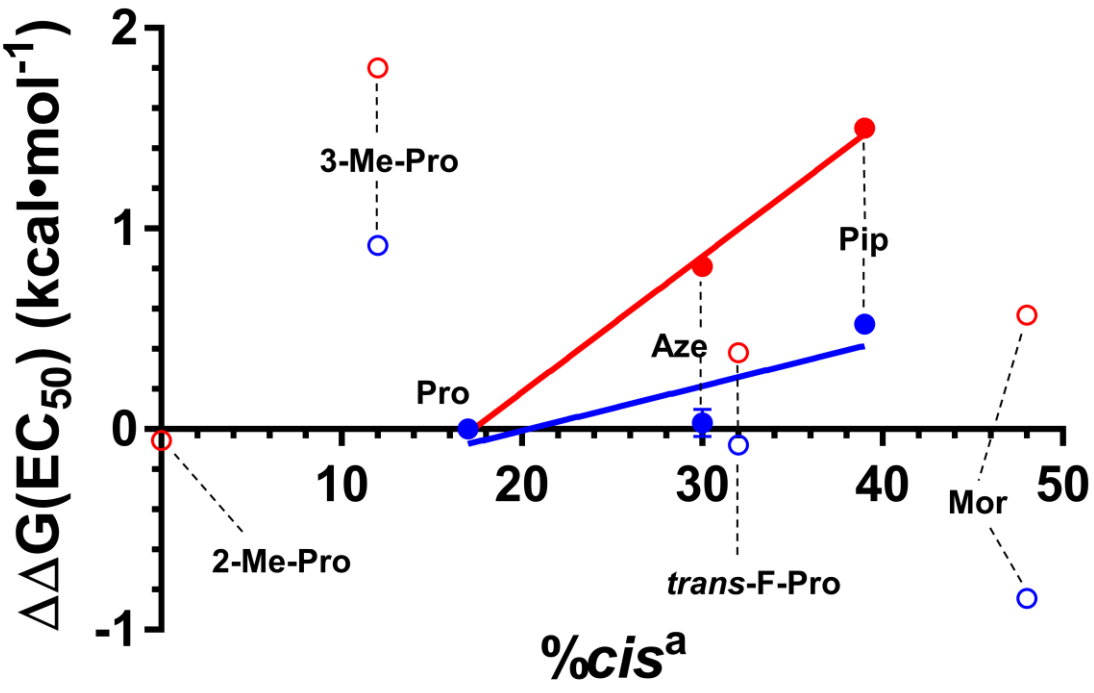

Figure 4.4. Relationship between *cis* bias and change in EC_{50} for non-canonical amino acids incorporated in place of the Cys-loop proline. The data for the 5-HT_{3A}R is shown in blue and that of the muscle-type nAChR (previously-reported[15]) is shown in red. Increased *cis* bias does not correlate closely with decreased EC_{50} for substitutions in the 5-HT_{3A}R, even for the simple series of Pro, Pip, and Aze (R^2 = 0.65).

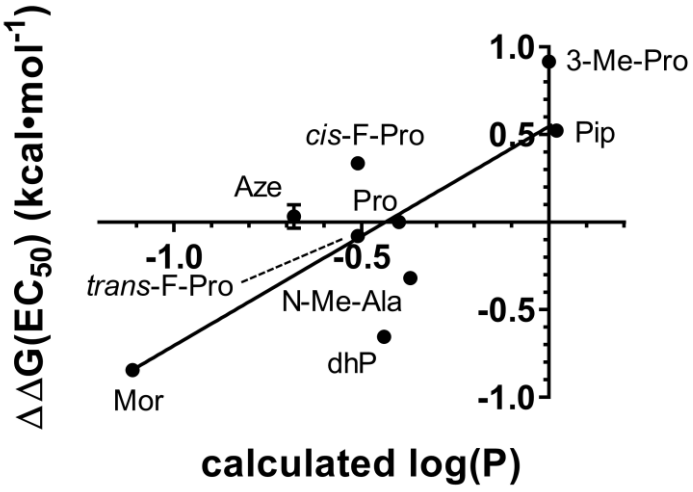

Figure 4.5. Lack of correlation between changes in EC_{50} and log(P) of non-canonical substitutions of P143 in the 5-HT_{3A}R. Data ± SEM

A plot of *cis* preference versus relative EC_{50}, however, does not correlate especially well (R^2 = 0.65 for the simplest series Pro, Aze, Pip, which differ only in ring size; **Figure 4.4**) and P143 is in the *trans* conformation in all 5-HT_{3A}R structures currently available.[24–27] However, it is possible that the lower resolution of the 5-HT_{3A}R structures may have resulted in an inaccurate representation.

These data differ from those previously obtained from experiments in the muscle-type nAChR where the *cis* preference strongly correlated (R^2 = 0.99; **Figure 4.4**).[15] Other proline analogous did not fit the trend in this analysis, but these could be largely explained if hydrophobicity was also considered. For the 5-HT_{3A}R, hydrophobicity does not seem a likely explanation, as a plot comparing EC_{50} versus the side chain log(P) (calculated in SPARTAN14) did not indicate a significant correlation (**Figure 4.5**). Nevertheless, given that functional surface expression of 5-HT_{3A}Rs occurred only when P143 was replaced by non-canonical amino acids having higher intrinsic *cis* biases than naturally-occurring amino acids other than Pro, it is possible that, despite the relatively poor correlation, a *cis* peptide bond is required at this position, but that it is not the only important aspect of proline at this position.

4.3.2 Investigation of the electrostatic network within the interfacial region of the 5-HT$_{3A}$R

Another highly-conserved feature of the interfacial region of pLGICs is an extensive electrostatic network of amino acid residues side chains that bridge interactions between secondary structures closely implicated in receptor gating.[1,2] Interactions between residues within this electrostatic network have been studied extensively across different members of the pLGIC superfamily, with differing and sometimes contradictory results.[28–36]

In the 5-HT$_{3A}$R, several interactions between the pre-M1 arginine (R218) and nearby electron-rich residues are apparent (**Figure 4.6**).[25] Specifically, it appears from this structure[25] and other 5-HT$_{3A}$R structures[24,26,27] that interactions exist between the R218 side chain and the side chains of E53 (ß1-ß2 loop), D145 (Cys-loop), and E186 and W187 (ß8-ß9 loop). We have built off of a limited amount of previous experimental work on this region of the 5-HT$_{3A}$R[29] to define the contributions of interactions within this electrostatic network to receptor gating in the 5-HT$_{3A}$R.

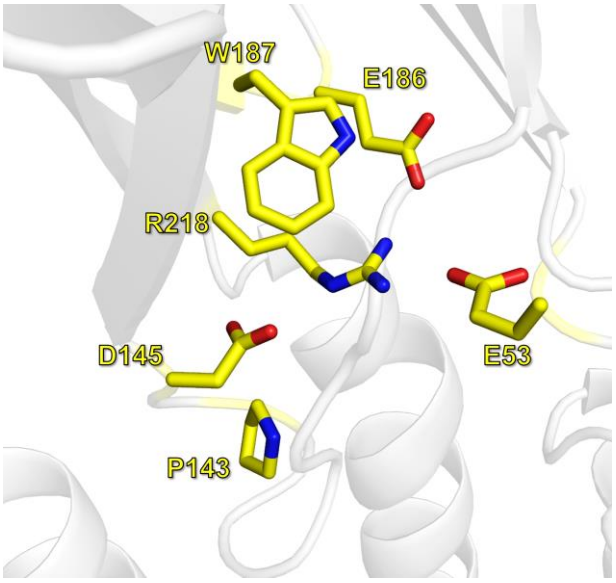

Figure 4.6. Electrostatic network of residues at the ECD-TMD interface of the 5-HT$_{3A}$R. P143 is also shown for context. Atoms are colored by element: yellow, carbon; red, oxygen; blue, nitrogen. (PDB ID 6HIS)[25]

The results from this line of investigation are tabulated in **Table 4.2** and dose-response curves for functional mutants are provided in **Figure 4.7**. Unfortunately, mutations to R218 and D145 did not yield measurable responses, consistent

with previous results.[29] We were nonetheless able to investigate the electrostatics of this region by mutating E53, E186, and W187.

It was previously observed that mutating E53 to Ala, Cys, or Arg resulted in no interpretable response.[29] We instead tried subtler mutations to probe the relevant steric and electrostatic contributions of this residue, although we also were able to express functional 5-HT_{3A}Rs with a dramatic mutation, E53L (**Table 4.2**). Much to our surprise, all mutations to E53 intended to impair the interaction between this residue and R218 led to decreases in 5-HT EC_{50} values of the mutant 5-HT_{3A}Rs. This is reflected in leftward shifts in the dose-response relationships of E53 mutants relative to wild-type (**Figure 4.7A**). Thus it appears that, in a general sense, weakening the interaction between E53 and R218 enhances receptor gating. This enhanced gating may result from increased motional freedom of the ß1-ß2 loop, which has been shown to undergo rearrangements during the gating process.[1,2,25]

Table 4.2.
Functional consequences of mutations to the interfacial region of the 5-HT_{3A}R.

Mutation(s)	EC_{50} (μM)	n_H	$\lvert I_{max}\rvert$(μA)	Fold	N	$\lvert\Delta\Delta G\rvert^{\dagger}$
-	1.3 ± 0.03	2.4 ± 0.11	1.0 - 78	1.0	21	
E53D	0.16 ± 0.01	2.8 ± 0.26	0.26 - 11	0.13	11	
E53Q	0.21 ± 0.01	2.9 ± 0.28	2.8 - 19	0.17	13	
E53L	0.05 ± 0.01	1.6 ± 0.24	0.07 - 1.1	0.041	9	
E53Nha	0.23 ± 0.005	3.7 ± 0.25	0.29 - 2.2	0.19	6	
E186D	3.6 ± 0.07	2.4 ± 0.08	0.54 - 69	2.9	14	
E186Nha	1.4 ± 0.10	2.7 ± 0.50	0.10 - 0.47	1.2	5	
W187F_4Trp	1.1 ± 0.07	1.4 ± 0.09	0.11 - 0.79	0.87	6	
E53D E186D	0.15 ± 0.01	1.7 ± 0.24	0.69 - 1.4	0.12	6	0.67
E53D P143Pip	0.13 ± 0.001	3.1 ± 0.11	2.7 - 6.5	0.10	8	0.39
D145N	NR				15	
R218A	NR				3	
R218K	NR				7	

†kcal•mol^{-1}. NR, no response. ± SEM

The gain of function observed for the variant E53L was particularly pronounced: this receptor had a ~25-fold lower 5-HT EC_{50} than the wild-type 5-HT_{3A}R. Mutating the native glutamate to leucine is expected not only to abrogate salt-bridging/hydrogen bonding to this residue, but also to introduce a substantial amount of steric bulk not present in the planar carboxyl side-chain. Thus, this is the most-perturbing mutation we employed at this site, consistent with perturbations of interactions with this residue resulting generally in enhanced receptor gating. We also note that the E53L mutation resulted in a dramatic reduction in the macroscopic deactivation rate of the mutant 5-HT_{3A}Rs, evident in a slowing of the return to baseline cell potential upon washout of 5-HT (**Figure 4.8**). This would be consistent with a substantial stabilization of the open state, resulting in an increased energetic barrier between the open state and resting state of the receptor.

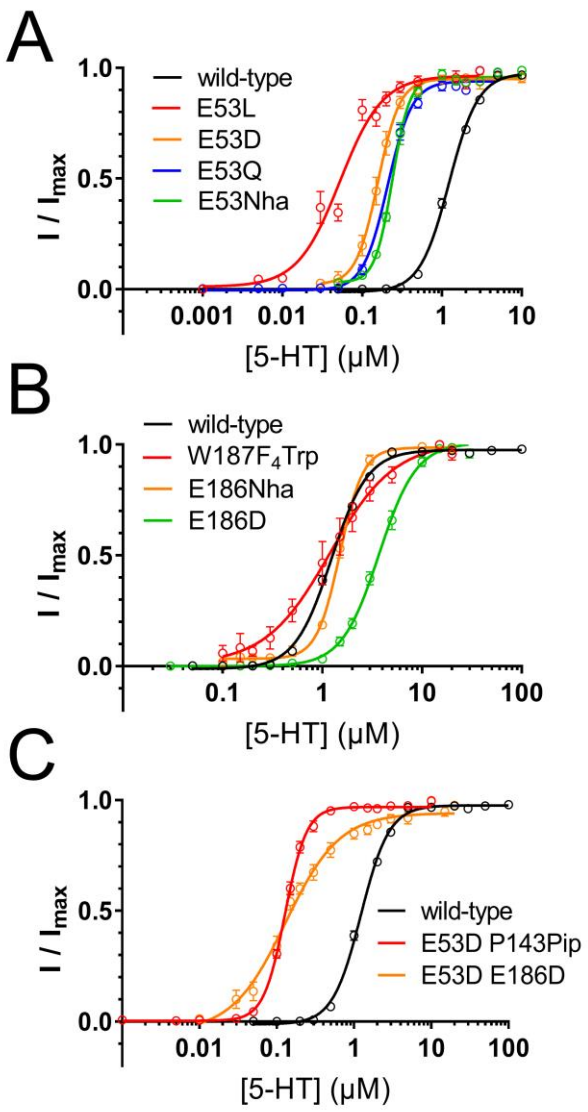

Figure 4.7. Dose-response curves for *A*, E53 single-mutants, *B*, E186 and W187 single-mutants, and *C*, double-mutants in the interfacial region of the 5-HT_{3A}R. ± SEM

We sought to further assess the role of E53 in 5-HT_{3A}R gating by using non-canonical amino acid mutagenesis to incorporate the amino acid γ-nitrohomoalanine (Nha). This non-canonical amino acid has been used previously to probe interactions with glutamate residues.[30,37,38] As illustrated by the electrostatic potential map in **Figure 4.9A**, Nha is a nonpolar isostere of glutamate, having a nitro group in place of the glutamate carboxyl. Thus, Nha removes the polar carboxyl group of glutamate while otherwise not altering the sterics of the amino acid. Akin to the results for natural amino acids, the E53Nha mutation resulted in a ~5-fold decrease in 5-HT EC_{50} relative to wild-type. Unfortunately, we were unable to run the appropriate positive control (incorporating glutamate using the non-canonical strategy) due to poor tRNA quality, which led to low signals.

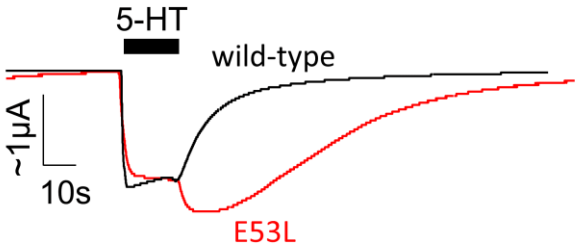

Figure 4.8. Comparison of electrophysiological trace shapes for wild-type and E53L 5-HT_{3A}Rs at 5-HT concentrations eliciting a maximal response.

To further investigate the electrostatics in this region, we introduced mutations to perturb interactions to E186 (**Figure 4.7B**). It had been previously observed that substituting this residue with glutamine (E186Q) caused no meaningful change in 5-HT_{3A}R function.[39] We tried two other substitutions: E186D and E186Nha. The mutation E186D resulted in a modest ~3-fold loss-of-function, contrasting with the gains of function seen for E53 mutations. Employing the nonpolar glutamate isostere Nha in place of E186, we observed near wild-type responses to 5-HT. Thus, it appears that the exact positioning of the E186 side chain is more important for proper receptor gating than the electron-rich

carboxyl group. But even in the case of E186D, the loss of function is meaningful but not particularly substantial.

Further, we probed the functional relevance of the electron-rich indole ring of W187 via non-canonical amino acid mutagenesis to the fluorinated tryptophan analog, F_4Trp. Substitution of the indole ring with electron-withdrawing fluorine atoms reduce the electron density of the aromatic ring to the point that it has nearly-neutral electrostatic potential in the tetrasubstituted F_4Trp (**Figure 4.9B**). Thus, substituting W187 with F_4Trp should attenuate the cation-π interaction with R218 suggested by 5-HT_{3A}R structures. Upon mutating W187 to F_4Trp, we observed a 5-HT EC_{50} very close to that of wild-type 5-HT_{3A}Rs (**Table 4.2**; **Figure 4.7B**). This result suggests either that a cation-π interaction does not exist between these residues, or perhaps that there is a cation-π interaction but it is not functionally relevant. Recent 5-HT_{3A}R structures have suggested that the important feature of W187 is its steric bulk, contributing to a hydrophobic "sandwich" around the Cys-loop, especially P143.[25]

Finally, we sought to examine functionally-relevant interactions between residues by means of mutant cycle analysis. Given that the most dramatic EC_{50} shifts were seen for the E53 mutants, we performed mutant cycles between E53D and mutations

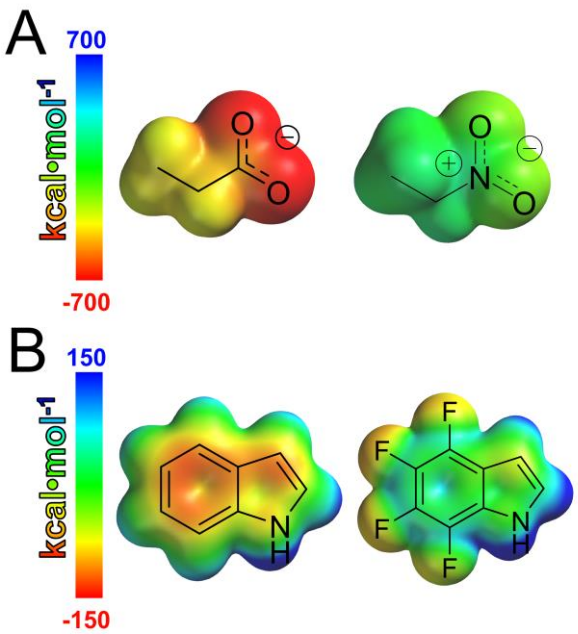

Figure 4.9. Electrostatic potential maps comparing side chain groups of *A*, glutamate to Nha, and *B*, tryptophan to F_4Trp.

to E186 and P143. The results are summarized in **Table 4.2** and dose-response relationships are provided in **Figure 4.7C**. The coupling energies observed were 0.67kcal•mol^{-1} for the E53D E186D double mutant and 0.39kcal•mol^{-1} for the E53D P143Pip double mutant. As mentioned in Chapter 1, our criterion for a "meaningful" coupling energy is 0.40kcal•mol^{-1}, representing a two-fold deviation from purely additive effects. Thus, it appears that E53D and E186D cooperate meaningfully in 5-HT$_{3A}$R gating, but the coupling energy for the E53D P143Pip mutant pair is just short of what we would consider to be meaningfully coupled. There is substantial room for interpretation here, but it would appear in both mutant cycles that the effects of the mutations are somewhat dependent, but not tightly cooperative in the gating mechanism. This is surprising given the close proximity between these residue pairs and the observation in 5-HT$_{3A}$R structures that E53 and E186 both interact directly with R218.[24–27] One could speculate that there are compensatory effects at play, especially considering the opposite effects of E53 and E186 mutations on receptor function.

4.3.3 Contribution of the M2-M3 loop residue T280 to 5-HT$_{3A}$R gating

The M2-M3 loop is another secondary structure in the interfacial region of pLGICs closely involved in the gating mechanisms of pLGICs.[1,2] While there have been many insights into functional roles of residues in the M2-M3 loop, the 5-HT$_{3A}$R is the only pLGIC for which it has been explicitly shown that a proline residue in the M2-M3 loop (P281) undergoes *cis/trans* isomerization about the peptide bond during activation.[21] Upon incorporation of non-canonical proline analogues with varying intrinsic propensities for *cis/trans* peptide bonds, a linear correlation was observed between changes in EC$_{50}$ and the *cis/trans* biases of the amino acids incorporated at P281.[21]

Herein we sought to identify other features of the M2-M3 loop as they relate to *cis/trans* isomerization of P281, and 5-HT_{3A}R gating as a whole. It was previously discussed that part of the motivation behind examining *cis/trans* bias as it relates to the conserved Cys-loop proline, P143, was that the residues immediately flanking P143 are both phenylalanine residues in the 5-HT_{3A}R, and that the presence of aromatic amino acids next to proline residues in the primary sequence greatly increases the propensity for those prolyl peptide bonds to exist in the *cis* conformation.[18–20] The residues on either side of P281 in the 5-HT_{3A}R are T280 and L282, which is perhaps surprising given that P281 has been shown to *cis/trans* isomerize but lacks adjacent aromatics whereas P143 does not clearly *cis/trans* isomerize (see *section 4.3.1*) but has aromatics on both sides. We therefore attempted to modulate the *cis/trans* bias of P281 via aromatic substitutions to the adjacent residues.

Table 4.3
Effects of single mutations to T280 in the M2-M3 loop of the 5-HT_{3A}R.

Mutation	EC_{50} (μM)	n_H	$\lvert I_{max}\rvert$(μA)	Fold	N
-	1.3 ± 0.03	2.4 ± 0.11	1.0 - 78	1.0	21
T280Y	0.064 ± 0.003	2.2 ± 0.19	0.46 - 50	0.051	17
T280MeOThr	0.21 ± 0.01	4.3 ± 0.41	0.09 - 5.9	0.17	24
T280A	0.26 ± 0.01	2.9 ± 0.23	2.8 - 65	0.21	12
T280F	0.29 ± 0.01	2.8 ± 0.17	0.28 - 3.2	0.23	12
T280V	0.32 ± 0.01	3.5 ± 0.26	1.0 - 39	0.26	11
T280S	0.48 ± 0.01	4.0 ± 0.18	8.5 - 27	0.38	10
T280Thr	1.2 ± 0.04	1.9 ± 0.12	0.06 - 1.2	1.0	15
T280-4-CH_3Phe	NR				14
T280-4-FPhe	NR				12
T280-4-OMePhe	NR				12
T280-4-BrPhe	NR				5
T280-4-CNPhe	NR				7
T280Cha	NR				10

NR, no response. ± SEM

The results from the T280 mutations are the most noteworthy (**Table 4.3**; **Figure 4.10**). Initial results seemed to suggest that the strategy had worked as planned: substituting T280 with phenylalanine (T280F) or tyrosine (T280Y) caused ~4-fold and ~20-fold decreases in 5-HT EC_{50}, respectively, consistent with there being an isomerization from the *trans* conformation to the *cis* conformation upon receptor activation. It is also worth noting that tyrosine is expected to increase the *cis* preference of adjacent prolyl peptide

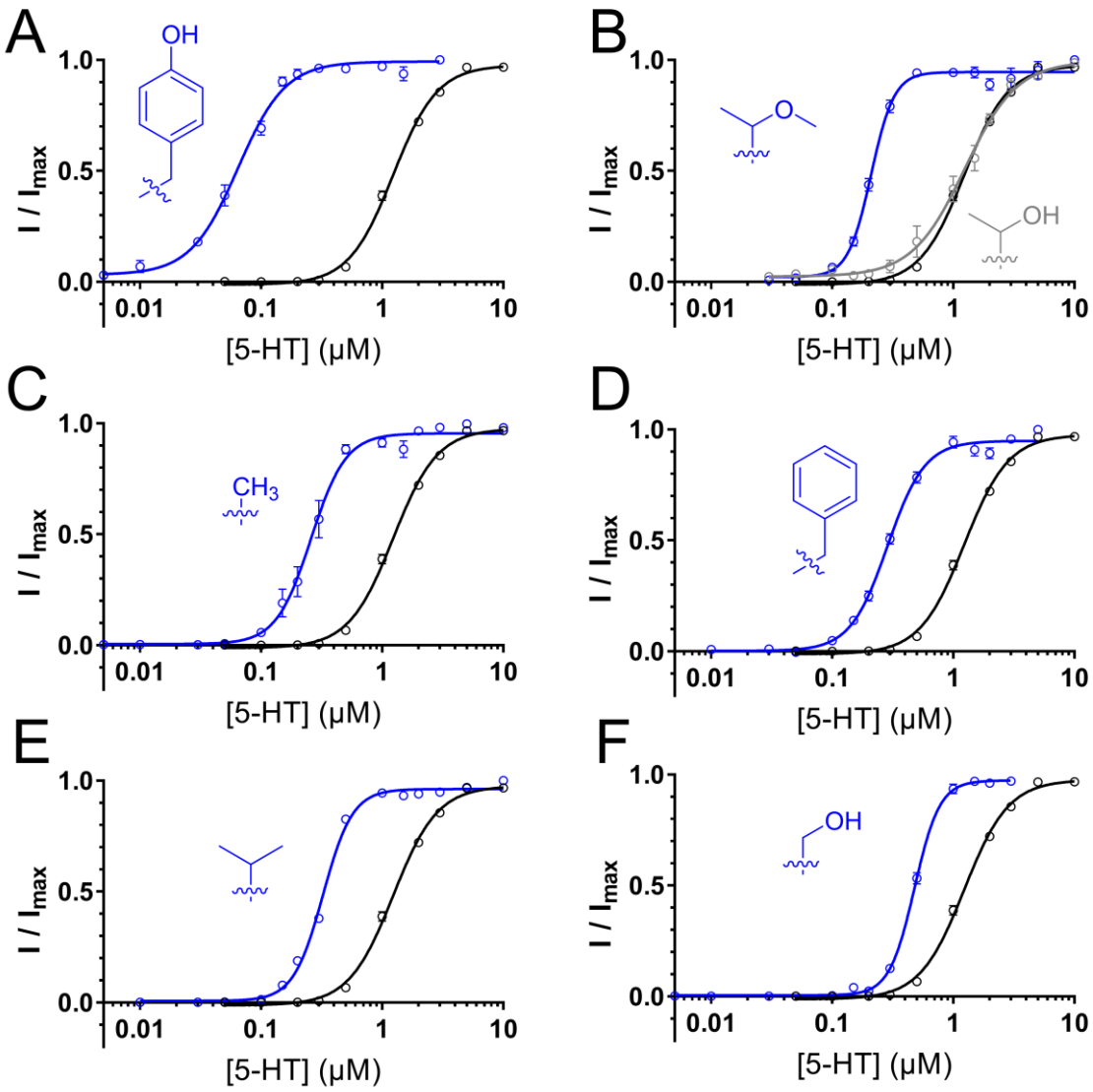

Figure 4.10. Dose-response curves of 5-HT_{3A}Rs with the indicated side-chain substitutions at T280. ± SEM

bonds to a greater extent than phenylalanine, which would be consistent with the greater gain-of-function we observed for T280Y versus T280F.[18–20] Interestingly, there was a marked change in the macroscopic activation/deactivation rates for T280Y receptors (**Figure 4.11**), similar to what was observed previously for the mutant E53L which had a similarly large gain-of-function. Comparing the T280Y electrophysiological traces to those of wild-type 5-HT_{3A}Rs, the rates of activation and deactivation are both reduced, suggesting perhaps a stabilization of the open state as well as either a stabilization of the resting state or a destabilization of the transition state. In the absence of single-channel electrophysiological data, it is impossible to tell exactly how the energetics of different receptor states have been affected.

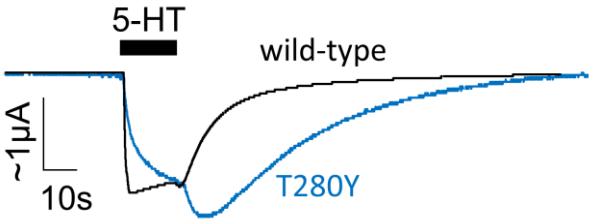

Figure 4.11. Comparison of electrophysiological trace shapes for wild-type and T280Y 5-HT_{3A}Rs at 5-HT concentrations eliciting a maximal response.

As negative controls, we characterized the function of the mutants T280A, T280V, and T280S. All of these amino acids lack the aromaticity of Phe and Tyr but resemble Thr in other ways. Val is sterically similar to Thr but lacks the ability to hydrogen bond; Ser preserves hydrogen bonding but has reduced steric volume; Ala both reduces sterics and lacks the ability to hydrogen bond. These negative controls were expected to give functional responses that were loss of function or near wild-type, however all three mutations gave gains of function comparable to that observed for T280F (**Table 4.3; Figure 4.10**). Thus. it appears in a general sense that perturbing interactions to the T280

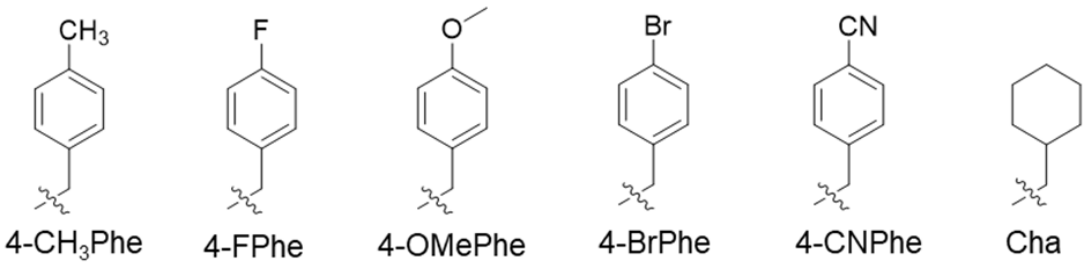

Figure 4.12. Side chains of non-canonical amino acids residues that yielded no measurable response upon attempted incorporation in place of T280.

side chain – either by way of removing the hydroxyl group or reducing steric bulk – result in enhanced receptor gating.

The large reduction in EC_{50} for T280Y was intriguing, and the possibility that this mutation was having multiple effects including increasing the *cis* bias of the P281 peptide bond was not patently excluded by the above analysis, so we attempted substitution of T280 with a variety of non-canonical amino acids to gain more insight into the role of this residue. It has been shown that the electron density of the aromatic ring adjacent to a proline correlates with increased proportions of the *cis* prolyl peptide bond,[20] so we attempted incorporation of a variety of 4-substituted phenylalanine analogs via non-canonical amino acid mutagenesis. The amino acids we attempted to incorporate are shown in **Figure 4.12**. Unfortunately, none of these non-canonicals incorporated well-enough in place of T280 in order for us to measure electrophysiological responses. We did, however, successfully incorporate O-methylthreonine (MeOThr) and the positive control, threonine, via the non-canonical amino acid mutagenesis strategy. The resultant dose-response curves are shown in **Figure 4.10B**. Incorporation of the wild-type threonine gave responses very close to those of unmutated wild-type receptors, and incorporation of MeOThr led to a ~6-fold decrease in the EC_{50} of 5-HT. Thu,s methylating the T280 side-chain hydroxyl group, both removing the ability to hydrogen-bond donate and increasing steric bulk, led to a gain-of-

function, in line with every other substitution of T280 for which we could measure responses.

Given the lack of conclusive results regarding the effects of the above-described T280 mutations on *cis/trans* isomerization of P281, we next turned to a different strategy involving mutant cycle analysis between T280 mutations and P281 mutations. We reasoned that if a mutation to T280 results in a gain-of-function by means of increasing the *cis* bias of P281, then a P281 mutation that increases the intrinsic *cis* bias of the peptide bond should have non-additive effects in combination with the T280 mutation, reflect in a large $|\Delta\Delta G|$ (at least >0.40kcal•mol^{-1}). The most obvious candidate T280 mutation for the mutant cycle analyses was T280Y, since this mutation caused a large gain-of-function that could result in part from increasing the *cis* bias of P281. When considering the mutation to introduce at P281, the best candidates would be 5,5-dimethylproline (DMP) or 5-tertbutylproline (Tbp), as these proline analogs were previously reported to have strong *cis* biases and accordingly cause large decreases in 5-HT EC_{50} when incorporated at P281 in the 5-HT_{3A}R.[21] Unfortunately, however, Tbp tRNA was not readily available to us and attempted incorporation of DMP led to no measurable response in our hands. We did,

Table 4.4
Substitutions of P281 and mutant cycles between T280Y and P281 mutations.

Mutation(s)	EC_{50} (μM)	n_H	$\|I_{max}\|$(μA)	Fold	N	$\|\Delta\Delta G\|^{\dagger}$
P281Pro	1.4 ± 0.007	4.0 ± 0.08	1.8 - 9.0	1.0	17	
P281Mor	0.57 ± 0.04	1.7 ± 0.17	0.10 - 0.15	0.46	5	
P281*trans*-F-Pro	1.1 ± 0.03	3.3 ± 0.31	0.14 - 11	0.84	11	
P281*cis*-F-Pro	0.83 ± 0.06	3.1 ± 0.53	0.49 - 9.0	0.67	13	
T280Y P281Pro	0.067 ± 0.004	1.6 ± 0.10	0.03 - 4.2	0.05	23	0.057
T280Y P281Mor	0.052 ± 0.005	1.9 ± 0.32	0.14 - 0.71	0.037	6	0.29
T280Y P281*trans*-F-Pro	0.040 ± 0.002	2.1 ± 0.23	0.08 - 6.1	0.029	13	0.17
T280Y P281*cis*-F-Pro	0.031 ± 0.004	1.5 ± 0.26	1.1 - 3.0	0.51	10	0.11

†kcal•mol^{-1}. ± SEM

however, have ready access to amber-suppressing tRNA aminoacylated with Mor. This proline analog, while not included in the initial investigation of *cis/trans* isomerization at P281 in the 5-HT_{3A}R, has been shown to have increased *cis* bias relative to proline in a model peptide system.[15]

The overall pharmacological parameters for P281Mor and the positive control P281Pro are provided in **Table 4.4** and dose-response curves are illustrated in **Figure 4.13**. Substitution of P281 with Mor led to a ~2-fold gain-of-function relative to the wild-type recovery experiment, the dose-response relationship of which was in line with the wild-type 5-HT_{3A}R. Plotting the ΔΔG(*cis-trans*) value for Mor versus the ΔΔG(EC_{50}) for the change in receptor function reveals a very close match with the previously-reported results for non-canonical proline analogs at P281 (**Figure 4.14**).[21] Although the ΔΔG(*cis-trans*) value for Mor was determined using a different method than those reported in the initial investigation,[15,21] ΔΔG(*cis-trans*) values for non-canonical proline analogs in both studies were indexed to that of proline itself, which was set to 0 kcal•mol^{-1}. Thus, while not a perfect representation, this analysis supports the conclusion that the gain-of-function of P281Mor results primarily from an increased *cis* bias of the peptide bond at that position.

We next combined T280Y and P281Mor in a mutant cycle analysis. The results again are tabulated in **Table 4.4** and dose-response curves

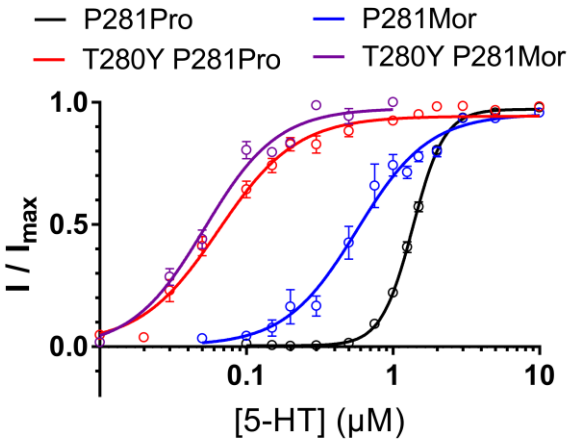

Figure 4.13. Dose-response curves for a mutant cycle between T280Y and P281Mor in the 5-HT_{3A}R. ± SEM

are illustrated in **Figure 4.12**. Combining the mutations yielded receptors with a 5-HT EC_{50} value of 0.052 ± 0.005μM, a slight gain-of-function relative to the positive control T280Y P281Pro, the dose-response relationship of which was closely in line with T280Y 5-HT_{3A}R. Thus the effects were mostly additive, with a |ΔΔG| of 0.29kcal•mol^{-1}, falling short of our criterion for meaningful coupling.

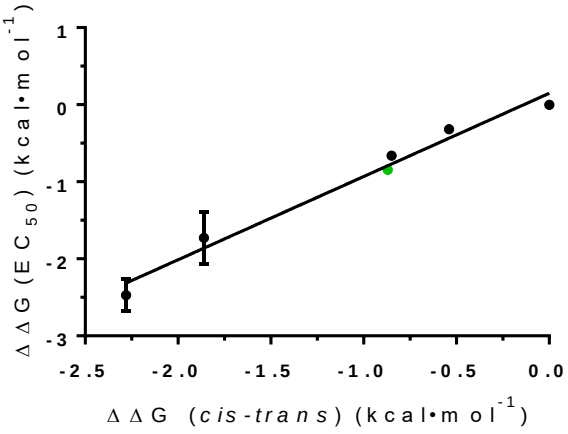

Figure 4.14. The 5-HT_{3A}R mutation P281Mor. The newly-reported datum (green) aligns closely with previously-reported data regarding *cis/trans* bias at P281 in the 5-HT_{3A}R.[21] ± SEM

To take one last look at the potential role of the T280Y mutation in modulating the *cis/trans* bias of the P281 peptide bond, we performed mutant cycles between T280Y and the non-canonical proline analogs *cis*-F-Pro and *trans*-F-Pro at P281. The rationale behind this line of experimentation is illustrated in **Figure 4.15**: *cis*-F-Pro and *trans*-F-Pro are known to affect the ring "pucker" of the pyrrolidinyl group of these non-canonicals, with *cis*-F-Pro favoring the Cγ-*endo* pucker and *trans*-F-Pro biasing toward the Cγ-*exo* pucker.[20] In the case of an adjacent tyrosine residue, as in T280Y 5-HT_{3A}Rs, one would expect *cis*-F-Pro to promote a conformation conducive to polar-π interactions between hydrogen atoms of the pyrrolidinyl group and the pi-face of the tyrosine phenol in the presence of a *cis* peptide bond at the 281 position, while the pucker of *trans*-F-Pro would both reorient the pyrrolidinyl hydrogens away from the tyrosine phenol and cause repulsive interactions between the fluorine atom and the negative electrostatic potential of the aromatic. Thus we

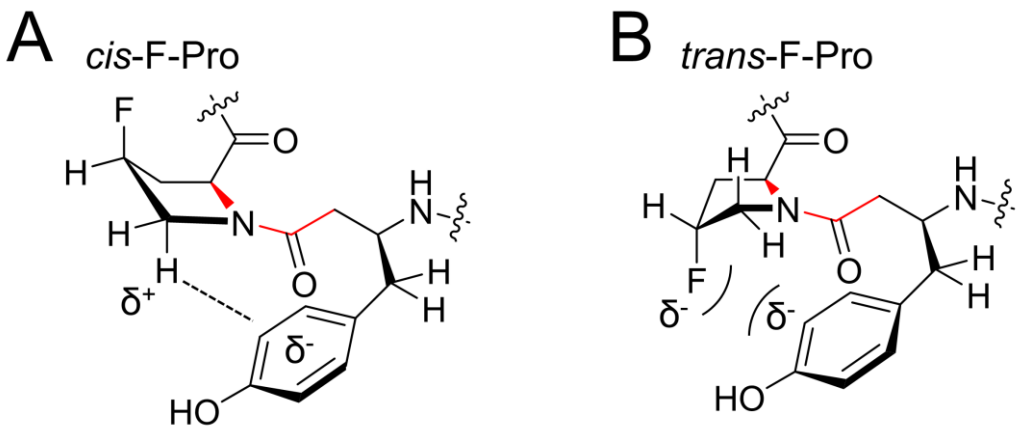

Figure 4.15. Rationale behind mutant cycle analyses between T280Y and *cis/trans*-F-Pro substitutions at P281. The *cis* peptide bond is highlighted in red. *A*, *cis*-F-Pro favors the Cγ-*endo* pucker, which should enable favorable interactions between the pyrrolidinyl hydrogens and the π-face of T280Y in the *cis* conformation of the peptide bond at the 281 position. *B*, *trans*-F-Pro favors the Cγ-*exo* pucker, which should disfavor a *cis* conformation of the 281 peptide bond.

would expect the effects of T280Y and P281*cis*-F-Pro to be superadditive, while the P281*trans*-F-Pro mutation should mitigate the gain-of-function of T280Y.

The observed results were not consistent with our predictions. Tabulated results are given in **Table 4.4** and dose-response data are shown in **Figure 4.16**. In either mutant cycle, the values for $|\Delta\Delta G|$ are well below our criterion for meaningful; thus it does not appear that introducing a fluorine on the proline pyrrolidinyl ring has any effect on the gain-of-function caused by T280Y.

In our last attempt to understand the effects of the T280 mutations examined herein, we made substitutions to L282, the next residue in the primary sequence after P281. In the 5-HT_{3A}R crystal structure (PDB ID 4PIR) and one 5-HT_{3A}R cryo-EM structure (PDB ID 6HIS), the T280 side-chain hydroxyl hydrogen-bonds to either the backbone amide NH of L282 or the backbone amide carbonyl contributed by P281 (**Figure 4.17**). While the state of the receptor in the crystal structure is unclear, the cryo-EM structure has been assigned

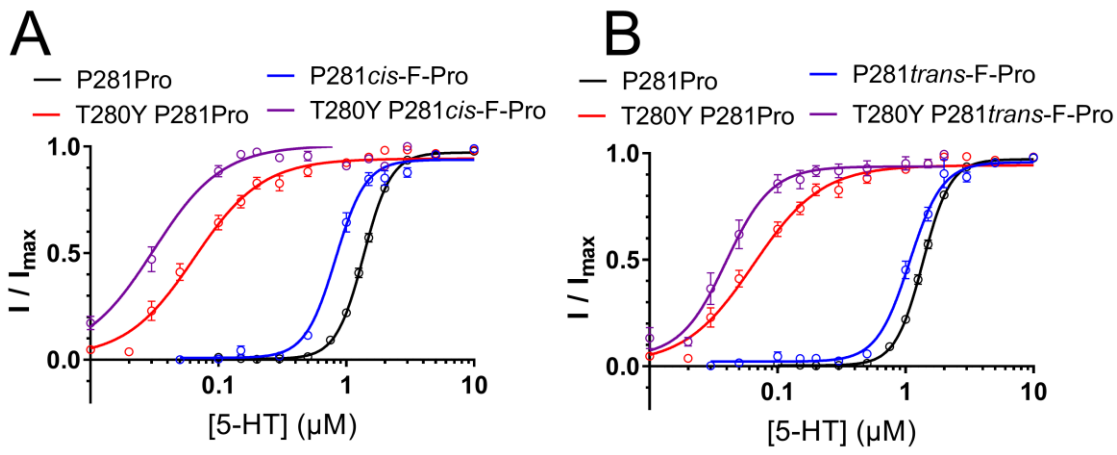

Figure 4.16. Dose-response curves for mutant cycles between T280Y and *A*, P281*cis*-F-Pro and *B*, P281*trans*-F-Pro. ± SEM

to the closed state of the 5-HT_{3A}R.[24,25] Notably, the gains of function associated with disrupting the ability of T280 to hydrogen bond we report herein would be consistent with the existence of this hydrogen bond to the backbone stabilizing a closed state of the receptor.

To examine the potential role of this hydrogen bond in receptor gating, we intended to attempt a mutant cycle between mutations that ablate the ability of T280 to hydrogen bond and abolish/weaken the hydrogen bonding capacity of the L282/P281 backbone amide bond. The latter can be accomplished via non-canonical amino acid mutagenesis employing 2-hydroxy-4-methylpentanoic acid (α-hydroxyleucine, or Lah), the α-hydroxy acid analog of leucine. This substitution would abolish hydrogen bonding between the T280 side-chain hydroxyl and the L282 backbone NH (**Figure 4.17A**) or would greatly weaken the hydrogen bond to the P281 backbone carbonyl (**Figure 4.17B**), as ester carbonyls are much poorer H-bond acceptors than amide carbonyls. This is an established means of probing main-chain hydrogen bonding interactions.[40]

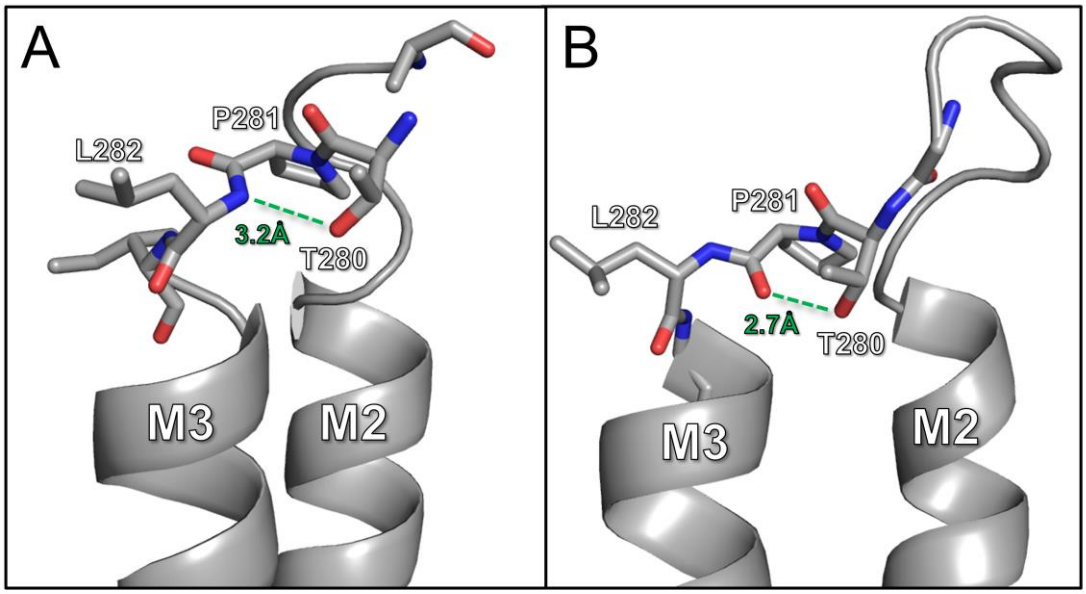

Figure 4.17. Hydrogen bonding between the T280 side-chain hydroxyl and the peptide backbone suggested by *A*, the 5-HT_{3A}R crystal structure (PDB ID 4PIR)[24] and *B*, a 5-HT_{3A}R cryo-EM structure (PDB ID 6HIS).[25]

Thus we introduced the mutations L282Lah and the positive control L282Leu using the non-canonical amino acid mutagenesis strategy. The results are provided in **Table 4.5** and dose-response curves are given in **Figure 4.18**. The L282Lah mutation did not result in a meaningful change in receptor function, so it appears that there is no functionally-relevant interaction to the peptide backbone at this position. Therefore, we did not proceed with a mutant cycle with any T280 mutations.

Lastly, with a plasmid encoding m5-HT_{3A} L282TAG and amber-suppressing tRNAs aminoacylated with aromatic amino acids at our ready disposal, we sought to assess

Table 4.5
Mutations to L282 in the 5-HT_{3A}R.

Mutation	EC_{50} (μM)	n_H	$\|I_{max}\|$(μA)	Fold	N
L282Leu	1.3 ± 0.02	3.4 ± 0.16	5.5 - 36	1.0	19
L282Lah	1.7 ± 0.03	3.4 ± 0.19	0.44 - 31	1.3	24
L282Phe	0.78 ± 0.02	3.7 ± 0.21	3.2 - 12	0.62	8
L282Trp	1.4 ± 0.03	3.9 ± 0.30	0.32 - 7.3	1.1	8

± SEM

the generality of the results observed from aromatic substitutions at T280 by using the non-canonical amino acid mutagenesis method to conveniently introduce different aromatic amino acids in place of L282. In this way, we introduced the mutations L282F and L282W (**Table 4.5**; **Figure 4.18**). There was a small gain-of-function for the L282F mutation that nonetheless fell short of our "meaningful" criterion of a two-fold change in function, and function of the L282W receptors was very nearly identical to wild-type. Thus it does not appear that the results from aromatic substitutions to T280 extend to the other residue neighboring P281, providing further evidence that we have not successfully modulated *cis/trans* bias at P281 via aromatic substitutions to T280.

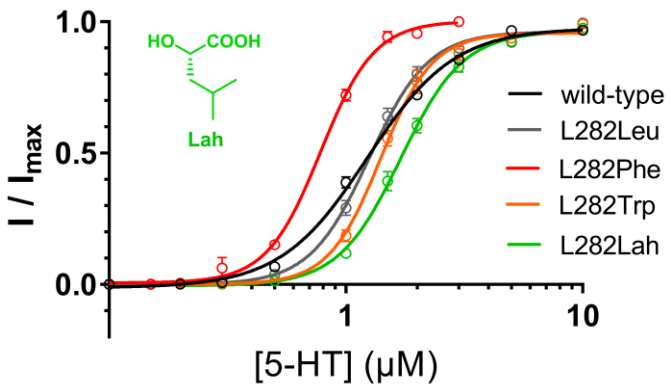

Figure 4.18. Dose-response curves for L282 mutations in the 5-HT$_{3A}$R. ± SEM

4.3.4 Long-range interactions between T280 and other 5-HT$_{3A}$R residues

The gating process of the 5-HT$_{3A}$R and pLGICs at large involves allosteric communication of a ligand binding event in the extracellular domain to the membrane-spanning channel pore, around 60Å away.[1,2] Thus there must be cooperation across this entire distance to bring about the requisite structural rearrangements that lead to channel opening. We therefore sought to use mutant cycle analysis to evaluate the energetic coupling of T280 mutations to mutations of other residues studied herein that are not in direct contact with T280.

Figures 4.19A-F compare the dose-response curves of receptor variants with a mutation at T280 and another mutation in the interfacial region to those of wild-type receptors and those of the cognate single-mutants. The pharmacological parameters of the

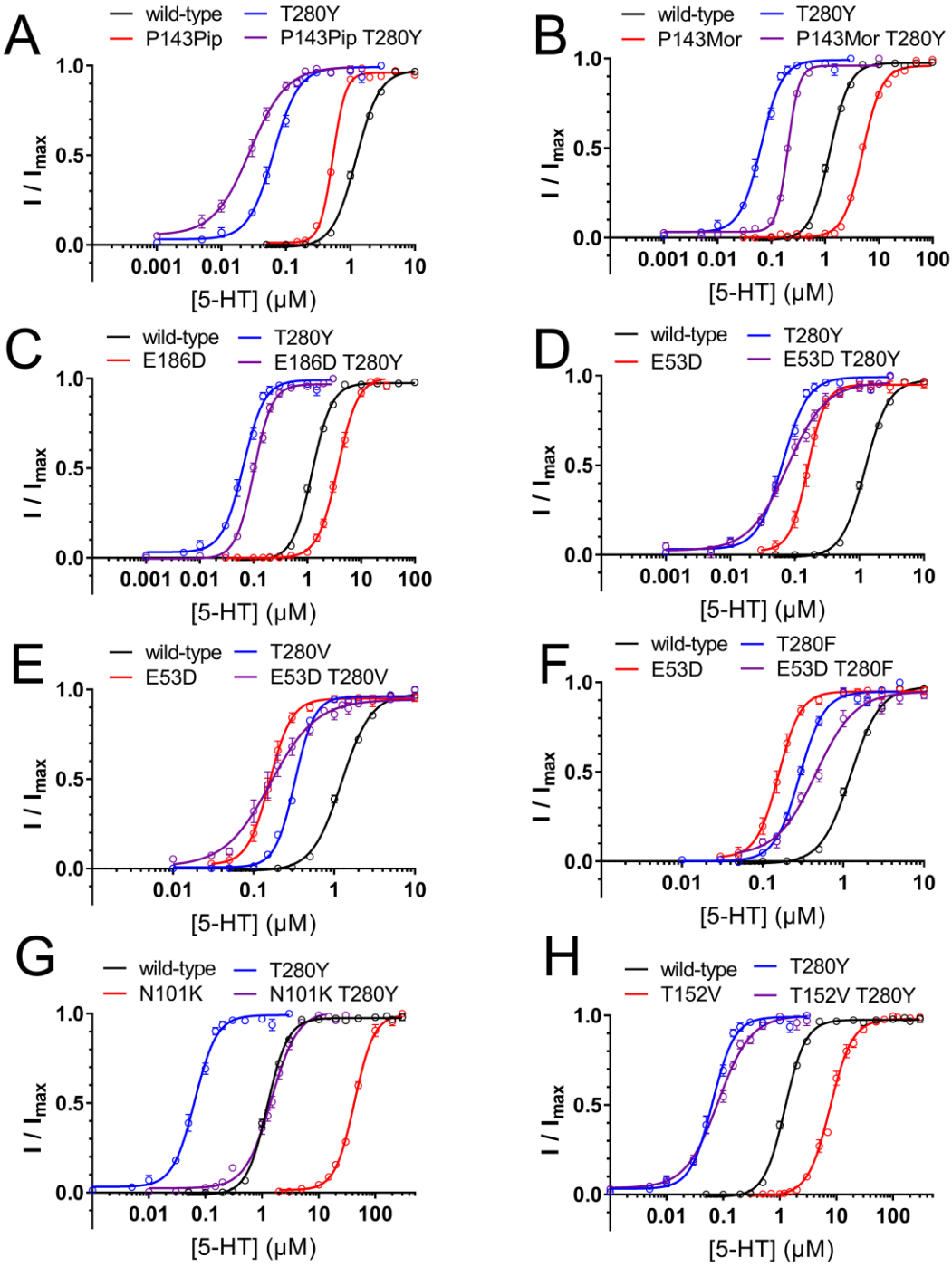

Figure 4.19. Dose-response curves for mutant cycles between T280Y and other residues involved in 5-HT$_{3A}$R gating. ± SEM

double-mutants, including |ΔΔG| values, are tabulated in **Table 4.6**. T280Y does not couple appreciably to P143Pip or P143Mor. T280Y does couple weakly to E186D (|ΔΔG| = 0.43 kcal•mol^{-1}), but couples much more strongly to E53D (|ΔΔG| = 1.2 kcal•mol^{-1}).

Given the observed coupling between E53D and T280Y, we wanted to test the generality of this coupling by combining E53D with other T280 mutations. While we do not consider small (<0.40 kcal•mol^{-1}) differences in |ΔΔG| values to be worth discussing, it is of note that E53D is more energetically coupled to aromatic substitutions at T280 than to T280V (**Table 4.6**). In particular, the single-mutants T280V and T280F result in very comparable gains-of-function relative to wild-type, yet T280V couples to E53D with a |ΔΔG| of only 0.81 kcal•mol^{-1} while T280F couples to E53D with a |ΔΔG| of 1.5 kcal•mol^{-1}.

To probe for long-range allosteric cooperation between T280 and residues that may be involved in early steps in receptor gating, we performed mutant cycle analyses between T280Y and the mutations T152V and N101K. In Chapter 2, we demonstrated allosteric communication between these two mutations and the channel pore mutation T6'S, establishing a role for these residues in receptor gating. Here, we report energetic coupling

Table 4.6
Mutant cycles between T280Y and other residues involved in 5-HT$_{3A}$R gating.

Mutation(s)	EC_{50} (μM)	n_H	$\|I_{max}\|$(μA)	Fold	N	$\|\Delta\Delta G\|^{\dagger}$
P143Pip T280Y	0.025 ± 0.001	1.3 ± 0.09	0.06 - 0.44	0.02	11	0.13
P143Mor T280Y	0.19 ± 0.01	4.0 ± 0.41	0.06 - 0.94	0.15	12	0.30
E186D T280Y	0.10 ± 0.004	2.6 ± 0.23	10 - 30.	0.08	12	0.43
E53D T280V	0.16 ± 0.01	1.5 ± 0.10	0.05 - 0.20	0.13	11	0.81
E53D T280Y	0.074 ± 0.004	1.4 ± 0.09	0.15 - 1.3	0.06	12	1.2
E53D T280F	0.51 ± 0.05	1.4 ± 0.16	0.08 - 0.61	0.41	10	1.5
N101K T280Y	1.3 ± 0.08	1.5 ± 0.11	1.1 - 37	1.1	9	0.36
T152V T280Y	0.087 ± 0.01	1.6 ± 0.16	0.05 - 0.48	0.069	9	0.95

†kcal•mol^{-1}. ± SEM

between T152V and T280Y and a lack of meaningful energetic coupling between N101K and T280Y (**Table 4.6**). Full dose-response curves are shown in **Figure 4.19G-H**. It appears from these results that T152V affects gating via a pathway that is affected by T280Y, whereas the effects of N101K and T280Y are more independent.

4.4 Conclusions

Herein we have used mutagenesis to conduct an investigation of 5-HT_{3A}R gating in regard to amino acid residues in the interfacial region between the extracellular domain and transmembrane domain of this receptor. Using mutant cycle analysis, we have quantified energetic couplings between pairs of mutations that affect the gating process in dependent ways.

Mutating the conserved Cys-loop proline, P143, to a series of non-canonical amino acids, we report a lack of evidence for *cis/trans* isomerization of the P143 peptide bond during activation of the 5-HT_{3A}R, although our results suggest that a *cis* peptide bond or at least a substituted amide nitrogen may be critical features of this residue for receptor function. These results are somewhat in line with those observed in other pLGICs, namely GLIC,[13] ELIC,[14] and the muscle-type nAChR,[15] however there do seem to be differences in regard to the exact features of this proline residue that influence function in these different receptors.

We have further investigated interactions between residues comprising the electrostatic network within the interfacial region of the 5-HT_{3A}R, which is largely conserved across the pLGIC superfamily.[1,2] Of particular note is the ß1-ß2 loop residue, E53, the mutation of which leads to receptor variants with up to 25-fold increased sensitivity to 5-HT. Via mutant cycle analysis, we establish a functionally-relevant

interaction between E53 and the nearby E186, the mutation of which impairs receptor function. Other residues in this network include W187, D145, and R218. Being the apparent linchpin of the electrostatic network (as evident in 5-HT_{3A}R structures), we have identified no functional mutants of R218, in line with previous results.[29] Likewise, D145 appears to be critical for receptor function. Via non-canonical amino acid mutagenesis of W187 to F_4Trp, we identify no functionally-relevant cation-pi interaction between this residue and R218.

Lastly, we have conducted a thorough investigation into the role of the 5-HT_{3A}R residue T280 in receptor gating. Initially trying to modulate *cis/trans* isomerization of P281 by mutating T280 to aromatic residues, we identified a number of mutations that lead to gain-of-function phenotypes, of which that for T280Y was particularly pronounced. We employed mutant cycles to assess whether this gain-of-function resulted from effects on the *cis/trans* bias of P281 or from ablation of a nearby hydrogen bond, but ultimately have not identified the exact means by which T280Y and other mutations lead to gains of function. Mutant cycles between T280 mutations and more-distant residues have revealed that E53 and T152 are energetically coupled to T280 in the 5-HT_{3A}R activation mechanism.

4.5 Experimental Procedures

4.5.1 Molecular biology

The cDNA for the mouse 5-HT_3R A subunit was in the pGEMhe vector. Site-directed mutagenesis was performed using a QuikChange mutagenesis kit (Stratagene). For non-canonical amino acid mutants and conventional mutants generated by non-canonical amino acid mutagenesis, the site of interest was mutated to the TAG stop codon. cDNA was linearized using XhoI (New England Biolabs). Linearized DNA was purified using a

Qiaquick PCR Purification Kit (Qiagen) before performing an *in vitro* runoff transcription using a T7 mMessage mMachine kit (Ambion). The mRNA was purified using an RNEasy Mini Kit (Qiagen) and concentrations were quantified via UV-Vis spectroscopy (Nanodrop 2000, ThermoFisher Scientific). cDNA was stored at -20ºC and mRNA was stored at -80ºC.

Hydroxy or 4,5-dimethoxy-2-nitrobenzyloxycarbonyl (NVOC) protected amino acid-dCA couples were enzymatically ligated to truncated 74mer THG73 tRNA as previously described.[41,42] The 74mer tRNA was prepared using the Ambion T7MEGAshortscript kit by transcription from a modified DNA oligonucleotide template as described in the literature to enhance RNA transcript homogeneity.[43] Crude tRNA-amino acid or tRNA-hydroxy acid product was used without desalting, and the product was confirmed by matrix-assisted laser desorption ionization time-of-flight mass spectrometry on a 3-hydroxypicolinic acid matrix. Deprotection of the NVOC group on the tRNA-amino acids was carried out by 5-min photolysis on a 1 kW xenon lamp with WG-335 and UG-11 filters or for 2.5-min using a 1150mW 365nm LED (Thorlabs) immediately prior to injection. Either deprotection strategy yielded fully deprotected aminoacyl tRNAs as assayed by MALDI-TOF mass spectrometry.

4.5.2 Protein expression in Xenopus laevis oocytes

Stage V-VI oocytes of *Xenopus laevis* were harvested and injected with RNAs as described previously.[42] For non-canonical amino acid mutagenesis experiments, each cell was injected with 25-100ng each of receptor mRNA and appropriate tRNA in 50nL of nuclease-free water approximately 48h before recording. Mutants yielding small responses

required 72h of incubation, with a second injection of mRNA and tRNA 48h before recording.

As a negative control for non-canonical mutagenesis experiments at each site, unacylated full-length tRNA was co-injected with mRNA in the same manner as charged tRNA. These experiments yielded no measurable responses, or negligible responses for all sites. Wild-type recovery conditions (injecting tRNA charged with the appropriate amino acid to regenerate a wild type channel *via* non-canonical amino acid mutagenesis at a TAG stop codon) were injected alongside mutant non-canonical amino acid mutagenesis conditions as a positive control.

For wild-type experiments and conventional mutants, the procedure varied depending on expression levels. For higher-expressing variants, each cell received a single injection of 1-25 ng of receptor mRNA dissolved in 50nL of nuclease-free water approximately 24 h before recording. For lower-expressing variants, oocytes were injected up to twice – once at t = 0h and once more at t ≈ 24h – and incubated for a total of up to 72h from the first injection.

In all experiments, cells were incubated at 18ºC in ND96 (96mM NaCl, 2mM KCl, 1mM $MgCl_2$, 1.8mM $CaCl_2$, and 5mM HEPES at pH 7.5) with 0.05mg/mL gentamycin (Sigma Aldrich), 2.5mM sodium pyruvate (Acros Organics), and 0.67mM theophylline (Sigma Aldrich).

4.5.3 Whole-cell electrophysiological recording

Electrophysiology and drug perfusion were performed at ambient temperature (20-25ºC) using the OpusXpress 6000A (Axon Instruments) in two-electrode voltage clamp

(TEVC) mode. Oocytes were impaled with borosilicate glass pipettes filled with 3M KCl (R = 0.3 – 3.0MΩ) and clamped at a holding potential of -60mV. Data were sampled at 125Hz. The running buffer was Ca^{2+}-free ND96 (96mM NaCl, 2mM KCl, 1mM $MgCl_2$, and 5mM HEPES at pH 7.5). Solutions of serotonin hydrochloride (Sigma Aldrich) were prepared 0-24h before recording from stock solutions stored at -80ºC.

For dose-response experiments, cells underwent a 30s pre-wash in Ca^{2+}-free ND96 before 1mL of each concentration of drug (dissolved in Ca^{2+}-free ND96) was applied for 15s. Cells were then washed for 116s using Ca^{2+}-free ND96 before subsequent doses. For slow-activating variants, 1mL of drug solution was applied for 15s and cells were incubated in the drug solution for an additional 15s before washout. For slow-deactivating variants, washout times were increased to 176s in between doses. The different procedure for slow activating/deactivating variants did not meaningfully change the overall dose-response relationships recorded versus the standard 15s application / 116s wash procedure.

4.5.4 Data analysis

Raw TEVC traces were prepared and analyzed in Clampfit 10.3 (Axon Instruments). Raw data were first filtered using a lowpass Gaussian filter at 1Hz. A 30s baseline was established prior to each drug application during which cells were continuously perfused with Ca^{2+}-free ND96. The averaged current of the baseline was subtracted from the peak amplitude following each drug application in order to generate dose-response data.

Dose-response data for individual concentrations were averaged, plotted, and fitted to the Hill equation $I / I_{max} = 1 / (1 + (EC_{50} / [agonist]^{nH})$ in Prism 7 (GraphPad), where

EC_{50} is the concentration for a half-maximal response, n_H is the Hill coefficient, and I / I_{max} is the normalized response at a given drug concentration. For dose-response experiments, data were normalized to the maximum current observed.

Coupling energies for double-mutant cycles were calculated using the formula $\Delta\Delta G = -R*T*\ln((EC_{50wt}*EC_{50AB}) / (EC_{50A}*EC_{50B}))$, where R is the gas constant, T is temperature, A and B denote individual mutations, and AB denotes double mutant receptors. The value used for T was 293.15K.

4.6 References

1. daCosta, C. J. B. & Baenziger, J. E. Gating of Pentameric Ligand-Gated Ion Channels: Structural Insights and Ambiguities. *Structure* **21**, 1271–1283 (2013).
2. Jennie M E Cederholm, P. R. S. Gating mechanisms in Cys-loop receptors. *Eur. Biophys. J. EBJ* **39**, 37–49 (2009).
3. Andrew J Thompson, H. A. L. The structural basis of function in Cys-loop receptors. *Q. Rev. Biophys.* **43**, 449–99 (2010).
4. Albuquerque, E. X., Pereira, E. F. R., Alkondon, M. & Rogers, S. W. Mammalian Nicotinic Acetylcholine Receptors: From Structure to Function. *Physiol. Rev.* **89**, 73–120 (2009).
5. Sigel, E. & Steinmann, M. E. Structure, Function, and Modulation of GABAA Receptors. *J. Biol. Chem.* **287**, 40224–40231 (2012).
6. Betz, H. & Laube, B. Glycine receptors: recent insights into their structural organization and functional diversity. *J. Neurochem.* **97**, 1600–1610 (2006).
7. Lummis, S. C. R. 5-HT3 Receptors. *J. Biol. Chem.* **287**, 40239–40245 (2012).
8. Kesters, D. *et al.* Structural basis of ligand recognition in 5-HT3 receptors. *EMBO Rep.* **14**, 49–56 (2013).
9. Thompson, A. J. & Lummis, S. C. The 5-HT3 receptor as a therapeutic target. *Expert Opin. Ther. Targets* **11**, 527–540 (2007).
10. Niesler, B. 5-HT3 receptors: potential of individual isoforms for personalised therapy. *Curr. Opin. Pharmacol.* **11**, 81–86 (2011).
11. Nys, M., Kesters, D. & Ulens, C. Structural insights into Cys-loop receptor function and ligand recognition. *Biochem. Pharmacol.* **86**, 1042–1053 (2013).
12. Deane, C. M. & Lummis, S. C. The role and predicted propensity of conserved proline residues in the 5-HT3 receptor. *J. Biol. Chem.* **276**, 37962–37966 (2001).
13. Rienzo, M., Rocchi, A. R., Threatt, S. D., Dougherty, D. A. & Lummis, S. C. R. Perturbation of Critical Prolines in Gloeobacter violaceus Ligand-Gated Ion Channel (GLIC) Supports Conserved Gating Motions Among Cys-Loop Receptors. *J. Biol. Chem.* jbc.M115.694372 (2015). doi:10.1074/jbc.M115.694372

14. Mosesso, R., Dougherty, D. A. & Lummis, S. C. R. Probing Proline Residues in the Prokaryotic Ligand-Gated Ion Channel, ELIC. *Biochemistry* **57**, 4036–4043 (2018).
15. Limapichat, W., Lester, H. A. & Dougherty, D. A. Chemical Scale Studies of the Phe-Pro Conserved Motif in the Cys Loop of Cys Loop Receptors. *J. Biol. Chem.* **285**, 8976–8984 (2010).
16. Jaiteh, M., Taly, A. & Hénin, J. Evolution of Pentameric Ligand-Gated Ion Channels: Pro-Loop Receptors. *PLOS ONE* **11**, e0151934 (2016).
17. Stewart, D. E., Sarkar, A. & Wampler, J. E. Occurrence and role ofcis peptide bonds in protein structures. *J. Mol. Biol.* **214**, 253–260 (1990).
18. Thomas, K. M., Naduthambi, D. & Zondlo, N. J. Electronic Control of Amide cis−trans Isomerism via the Aromatic−Prolyl Interaction. *J. Am. Chem. Soc.* **128**, 2216–2217 (2006).
19. Dugave, C. & Demange, L. Cis−Trans Isomerization of Organic Molecules and Biomolecules: Implications and Applications. *Chem. Rev.* **103**, 2475–2532 (2003).
20. Zondlo, N. J. Aromatic-Proline Interactions: Electronically Tunable CH/π Interactions. *Acc. Chem. Res.* **46**, 1039–1049 (2013).
21. Lummis, S. C. R. *et al.* Cis–trans isomerization at a proline opens the pore of a neurotransmitter-gated ion channel. *Nature* **438**, 248–252 (2005).
22. Kubyshkin, V. & Budisa, N. cis–trans-Amide isomerism of the 3,4-dehydroproline residue, the 'unpuckered' proline. *Beilstein J. Org. Chem.* **12**, 589–593 (2016).
23. Laufer, B., Chatterjee, J., Frank, A. O. & Kessler, H. Can N-methylated amino acids serve as substitutes for prolines in conformational design of cyclic pentapeptides? *J. Pept. Sci. Off. Publ. Eur. Pept. Soc.* **15**, 141–146 (2009).
24. Hassaine, G. *et al.* X-ray structure of the mouse serotonin 5-HT3 receptor. *Nature* **512**, 276–281 (2014).
25. Polovinkin, L. *et al.* Conformational transitions of the serotonin 5-HT 3 receptor. *Nature* 1 (2018). doi:10.1038/s41586-018-0672-3
26. Basak, S., Gicheru, Y., Rao, S., Sansom, M. S. P. & Chakrapani, S. Cryo-EM reveals two distinct serotonin-bound conformations of full-length 5-HT 3A receptor. *Nature* **563**, 270 (2018).
27. Basak, S. *et al.* Cryo-EM structure of 5-HT3A receptor in its resting conformation. *Nat. Commun.* **9**, (2018).
28. Xiu, X., Hanek, A. P., Wang, J., Lester, H. A. & Dougherty, D. A. A Unified View of the Role of Electrostatic Interactions in Modulating the Gating of Cys Loop Receptors. *J. Biol. Chem.* **280**, 41655–41666 (2005).
29. Price, K. L., Millen, K. S. & Lummis, S. C. R. Transducing Agonist Binding to Channel Gating Involves Different Interactions in 5-HT3 and GABAC Receptors. *J. Biol. Chem.* **282**, 25623–25630 (2007).
30. Wang, J., Lester, H. A. & Dougherty, D. A. Establishing an Ion Pair Interaction in the Homomeric ρ1 γ-Aminobutyric Acid Type A Receptor That Contributes to the Gating Pathway. *J. Biol. Chem.* **282**, 26210–26216 (2007).
31. Absalom, N. L., Lewis, T. M., Kaplan, W., Pierce, K. D. & Schofield, P. R. Role of Charged Residues in Coupling Ligand Binding and Channel Activation in the Extracellular Domain of the Glycine Receptor. *J. Biol. Chem.* **278**, 50151–50157 (2003).

32. Lee, W. Y. & Sine, S. M. Principal pathway coupling agonist binding to channel gating in nicotinic receptors. *Nature* **438**, 243–247 (2005).
33. Purohit, P. & Auerbach, A. Acetylcholine Receptor Gating at Extracellular Transmembrane Domain Interface: the "Pre-M1" Linker. *J. Gen. Physiol.* **130**, 559–568 (2007).
34. Kash, T. L., Dizon, M.-J. F., Trudell, J. R. & Harrison, N. L. Charged Residues in the β2 Subunit Involved in GABAA Receptor Activation. *J. Biol. Chem.* **279**, 4887–4893 (2004).
35. Duret, G. *et al.* Functional prokaryotic–eukaryotic chimera from the pentameric ligand-gated ion channel family. *Proc. Natl. Acad. Sci.* **108**, 12143–12148 (2011).
36. Mukhtasimova, N. & Sine, S. M. Nicotinic Receptor Transduction Zone: Invariant Arginine Couples to Multiple Electron-Rich Residues. *Biophys. J.* **104**, 355–367 (2013).
37. Pless, S. A. *et al.* Asymmetric functional contributions of acidic and aromatic side chains in sodium channel voltage-sensor domains. *J. Gen. Physiol.* **143**, 645–656 (2014).
38. Gleitsman, K. R., Kedrowski, S. M. A., Lester, H. A. & Dougherty, D. A. An Intersubunit Hydrogen Bond in the Nicotinic Acetylcholine Receptor That Contributes to Channel Gating. *J. Biol. Chem.* **283**, 35638–35643 (2008).
39. Thompson, A. J. & Lummis, S. C. R. Calcium modulation of 5-HT3 receptor binding and function. *Neuropharmacology* **56**, 285–291 (2009).
40. Dougherty, D. A. & Van Arnam, E. B. In Vivo Incorporation of Unnatural Amino Acids Using the Chemical Aminoacylation Strategy. A Broadly Applicable Mechanistic Tool. *Chembiochem Eur. J. Chem. Biol.* **15**, 1710–1720 (2014).
41. England, P. M., Lester, H. A. & Dougherty, D. A. Incorporation of esters into proteins: Improved synthesis of hydroxyacyl tRNAs. *Tetrahedron Lett.* **40**, 6189–6192 (1999).
42. Nowak, M. W. *et al.* [28] In vivo incorporation of unnatural amino acids into ion channels in Xenopus oocyte expression system. in *Methods in Enzymology* **293**, 504–529 (Academic Press, 1998).
43. Kao, C., Zheng, M. & Rüdisser, S. A simple and efficient method to reduce nontemplated nucleotide addition at the 3 terminus of RNAs transcribed by T7 RNA polymerase. *RNA* **5**, 1268–1272 (1999).

Chapter 5: Investigations of Signaling via Estrogen Receptor α Using a Photocrosslinking Non-canonical Amino Acid*

5.1 Abstract

The estrogen receptor α (ERα) is a transcription factor in the nuclear receptor superfamily, and is an important drug target for the treatment of various cancers. Much research into the activation mechanism of ERα has been done, but some inconsistencies have been reported between different systems. Moreover, the molecular details of how the intrinsically disordered N-terminal domain (NTD) of ERα contributes to receptor function are not well-characterized. Herein we have used photocrosslinking of non-canonical amino acids (NCAAs) incorporated site-specifically into ERα to study dimerization of the receptor (a critical step in transcriptional activation), and to scan for interactions between ERα and coregulatory proteins in a region of the NTD that is known to contribute to receptor function. The results of this study may inform future research using photoactivatable NCAAs for the study of ERα and other receptors.

5.2 Introduction

Proteins in the nuclear receptor family of transcription factors play important roles in regulating the expression of genes.[1] The estrogen receptor α (ERα) is a member of the nuclear receptor family and is involved in oncogenic signaling pathways that contribute to several different cancers, most notably breast cancer.[2,3] ERα is a validated drug target, with antiestrogens like tamoxifen (TMX) being widely prescribed in the treatment and prevention of breast cancer.[4,5]

---

* *This work was done in close collaboration with Stephen Grant, and was based on previous work by Dr. Matthew Rienzo.*

The overall mechanism of action of ERα was discussed generally in *section 1.2*, but we will reiterate key points and highlight more specific details here. ERα is a multidomain protein, with an intrinsically-disordered N-terminal domain (NTD), a DNA-binding domain (DBD), a ligand-binding domain (LBD), and a "hinge domain" between the latter two.[6–8] ERα natively responds to endogenous estrogens such as ß-estradiol (E2), which are agonists of this receptor. Binding of estrogen agonists in the LBD causes ERα to dissociate from a chaperone complex in the cytosol and to next dimerize and translocate to the nucleus, where it assembles along with coregulatory proteins and RNA polymerase into a transcriptionally-active complex. Recognition of estrogen response elements (EREs) via the ERα DBD guides the complex to regulate expression of the appropriate genes.

While the mechanism of action of ERα is straightforward in principle, there are a myriad of factors that can contribute to the differential activity of ERα in different cellular environments. The archetypal example of this comes from the observation that TMX, the widely-prescribed antiestrogen, has different effects in different tissue types: while TMX is antiproliferative in breast cancer cells, it has a proliferative effect in bone and uterus tissues.[9,10] The action of ERα has been described as an "Ensemble Allosteric Model" in which the activity of the receptor can be modulated by variables such as type and accessibility of EREs, relative expression levels of coregulatory proteins, expression of different ERα splice variants, post-translational modifications of ERα, and intracellular conditions including pH and osmolyte levels.[10,11]

Given the complexity of signaling through ERα, it would be useful to have a precise technique to investigate aspects of ERα activation and regulation involving protein-protein interactions, such as homodimerization and cofactor binding. Previous work in our lab by

Dr. Matthew Rienzo addressed this need, establishing the use of photocrosslinking non-canonical amino acids (NCAAs) to study ERα homodimerization (DOI 10.7907/Z9G44N8W). Using a modified procedure from the Krogsgaard group (New York University), Dr. Rienzo optimized expression via nonsense suppression (*section 1.3*; the "synthetase method") of N-terminally eGFP-tagged human ERα containing single mutations to photoactivatable NCAAs in the LBD at the dimerization interface and demonstrated dose-dependent covalent crosslinking of ERα dimers in response to E2.

Herein we have expanded on that work to demonstrate the dose-dependent dimerization of N-terminally eGFP-tagged ERα in response to (Z)-4-hydroxytamoxifen (4-OHT), the active metabolite of TMX, and the selective estrogen receptor downregulator (SERD) ICI-182780, also known as fulvestrant.[12,13] We have also applied the photocrosslinking strategy to probe for cofactor interactions in the ERα NTD and have identified several potential hits. This research adds to our collective understanding of ERα function, and may inspire future investigations of protein-protein interactions in nuclear receptors and other proteins.

5.3 Results & Discussion

5.3.1 Studying dimerization of ERα using photocrosslinking

It is well-known that dimerization of ERα is essential for transcriptional activity, and that E2 induces dimerization of the receptor.[6,14,15] Many studies have studied dimerization of purified ERα *in vitro*, however relatively few *in vivo* methodologies exist and all come with their own limitations.[16–20] Considering the ability of ERα to behave differently in response to its cellular environment, it is especially important to be able to study ERα dimerization *in vivo* using methods that are minimally perturbing, such as

photocrosslinking of NCAAs.[21] This strategy allows us not only to study protein-protein interactions in a more nearly native environment, but also to probe interactions site-specifically at the resolution of individual residues.

Previous efforts in our lab by Dr. Matthew Rienzo laid the groundwork for using photocrosslinking of NCAAs to study ERα dimerization. The NCAAs 4-benzoylphenylalanine (Bpa) and 4-azidophenylalanine (N_3Phe) (**Figure 5.1**) were used to probe several sites at the ERα dimerization interface contributed by the LBD. When irradiated with UV light, both of these NCAAs generate a radical species that will react to form a covalent crosslink with a broad range of functional groups, even including aliphatic C-H bonds. It was found that the substitutions T460Bpa and H516N_3Phe gave robust crosslinking of the ERα dimer, and that dimerization increased with increasing concentrations of E2 in the cell culture medium. For the experiments described herein, we proceeded with the H516N_3Phe substitution for studying dimerization, as the crosslinking reaction is more general for N_3Phe than Bpa, and N_3Phe is less sterically bulky than Bpa.[22] The H516 site is depicted in **Figure 5.2**; this residue resides at the dimerization interface in the LBD of ERα.

In collaboration with Stephen Grant, we first replicated the dose-dependent dimerization of eGFP-ERα H516N_3Phe in response to E2. We expressed the mutant

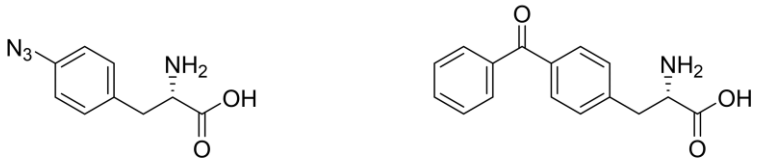

4-azidophenylalanine (N_3Phe) 4-benzoylphenylalanine (Bpa)

Figure 5.1. Photocrosslinking NCAAs used previously by our lab to study ERα dimerization. Only N_3Phe was used in this study.

receptors in HEK293T cells, incubated with varying concentrations of E2, and subsequently irradiated whole cells for 20min with a 1150mW 365nm LED to generate our crosslinked species. Cells were then lysed in PBS containing 1% SDS, subjected to SDS-PAGE, and gels were imaged for eGFP. Band intensities were analyzed and percent dimerization values were determined as described in *section 5.5.5*. **Figure 5.3** presents averaged dimerization data for multiple trials. There is clear dose-dependent dimerization in response to E2, however we do not yet consider these data to be quantitative.

We wanted to analyze the effects of other drugs on dimerization of ERα. Broadly speaking, antiestrogens tend to fall into two classes of compounds: selective estrogen receptor modulators (SERMs), which can behave as agonists or antagonists under different sets of conditions, and selective estrogen receptor degraders (SERDs), which cause conformational changes in ERα that lead to its degradation via the ubiquitin proteasome system.[5,12,13] The active metabolite of TMX, 4-OHT, acts as a SERM; thus we chose to assay for dimerization in response to 4-OHT. We additionally chose to assay for dimerization in response to the marketed drug fulvestrant (ICI 182,780) as a prototypical SERD.

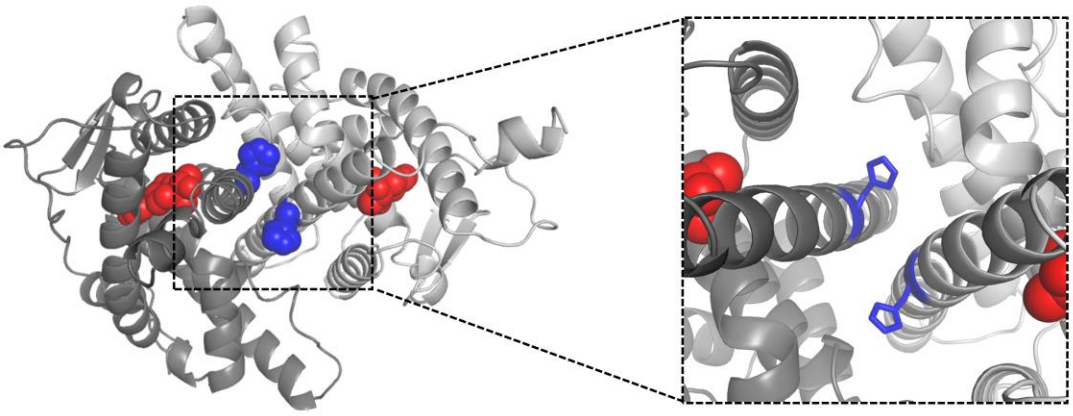

Figure 5.2. Dimerization interface in the LBD of ERα. H516 is shown as blue spheres/sticks, and E2 is shown as red spheres. PDB ID 1A52

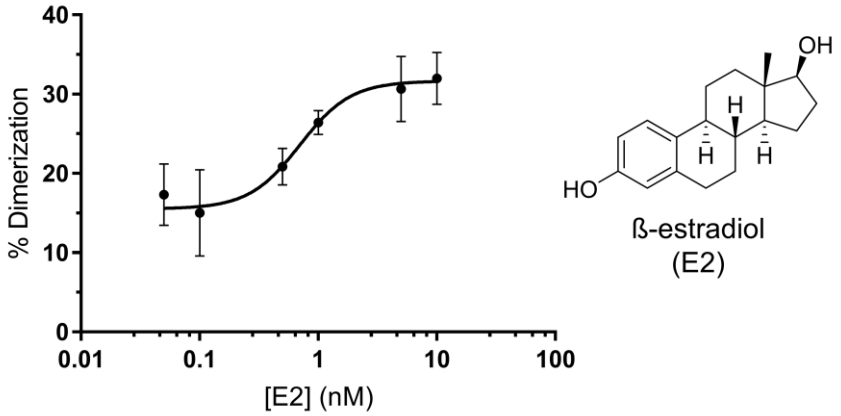

Figure 5.3. Dimerization of eGFP-ERα in response to E2, as measured using our photocrosslinking assay.

The results from photolysis of cells expressing ERα H516N_3Phe that were treated with 4-OHT are shown in **Figure 5.4**. Note the appearance of two bands of comparable molecular weight in the region of the dimer. We believe the lower molecular-weight band is due to crosslinking of full-length ERα to truncated monomer, given the similar difference in mass observed for the non-crosslinked full-length ERα versus truncated protein. This second band was observed in all gels. For our determinations of percent dimerization, we only analyzed the higher-mass band. As with E2, we observed dose-dependent dimerization in response to 4-OHT. However, it appears that the greatest [4-OHT] we tested did not induce a maximal percent dimerization, as the fit does not level off. Future experiments will be needed to construct a full dose-response curve for dimerization induced by 4-OHT. The results from photolysis of cells expressing ERα H516N_3Phe that were treated with fulvestrant are shown in **Figure 5.5**. Fulvestrant likewise caused dose-dependent dimerization, although there was substantial scatter at higher concentrations of fulvestrant.

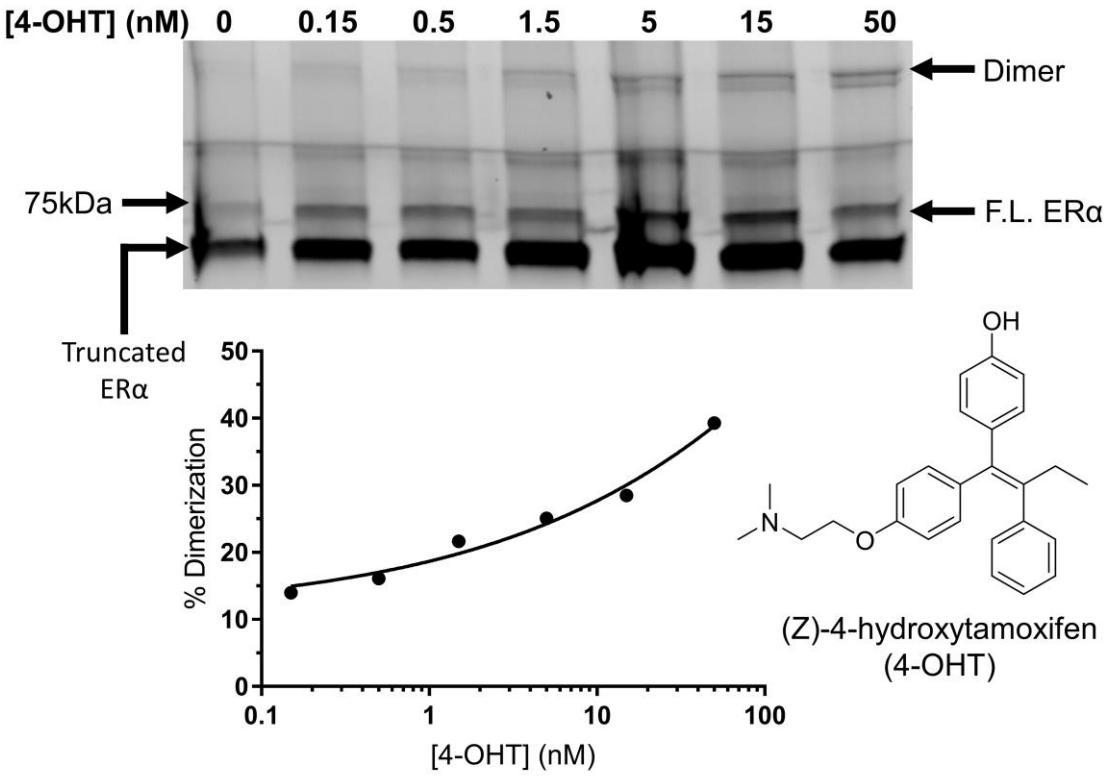

Figure 5.4. Dimerization of eGFP-ERα in response to 4-OHT, as measured using our photocrosslinking assay. "F.L." = Full-length

At this point, we do not consider a quantitative comparison of the data to be appropriate; the assay needs to be optimized and data need to be replicated and should be considered preliminary. In all cases, we do observe some amount of baseline dimerization of ERα as well that cannot be ascribed to the action of the drugs. This will have to be reconciled in future experiments. Also, in the above-described experiments we use an eGFP-tagged ERα construct, which to some extent defeats the purpose of our minimally-perturbing method of photocrosslinking. Future studies could use immunoblotting of untagged ERα with anti-ERα antibodies to circumvent this issue, but for now we wanted to test the method in the simplest way possible.

We further note that dimerization in response to 4-OHT and fulvestrant has been previously observed using other methodologies.[19,20] What the above-described research represents, however, is an alternative approach for studying ERα function that offers great chemical precision. It is well-appreciated that the function of ERα is a complex problem; there have even been conflicting results regarding ERα dimerization in response to fulvestrant that have been reported in the literature – in some systems it blocks dimerization while in others it promotes dimerization.[19,20,23,24] Considering the minimal amount of manipulation that needs to be introduced to study ERα dimerization using our approach, we hope that future research using this strategy may provide more clarity into the dimerization of ERα in response to different stimuli.

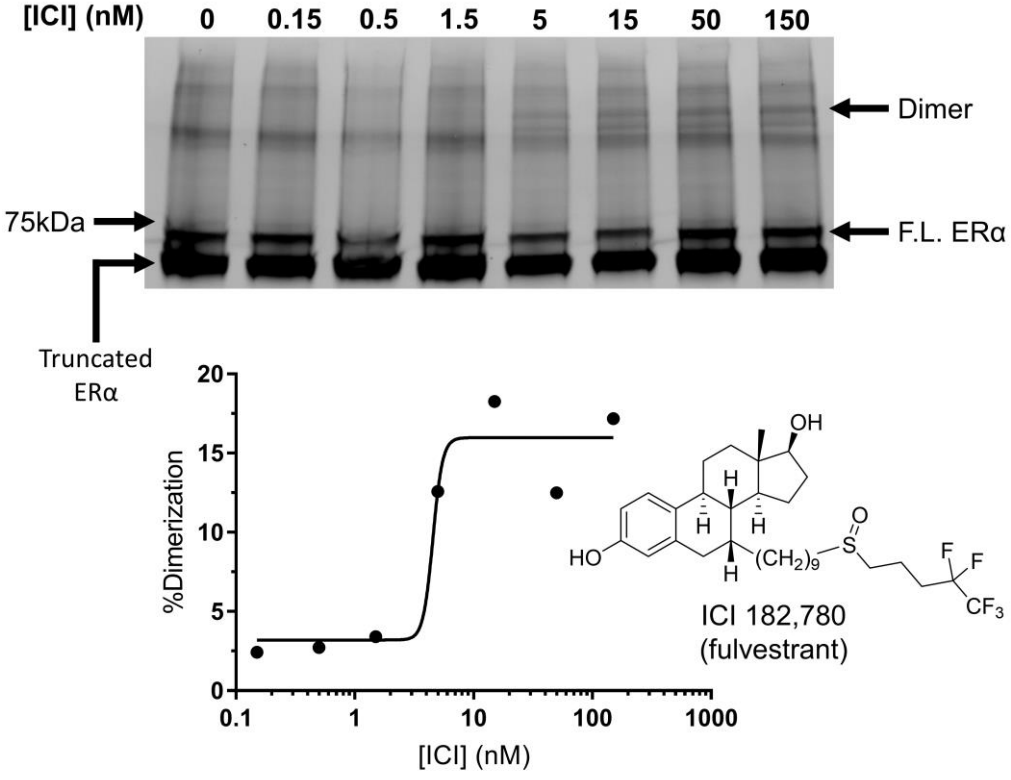

Figure 5.5. Dimerization of eGFP-ERα in response to fulvestrant, as measured using our photocrosslinking assay. "F.L." = Full-length; "ICI" = ICI 182,1780

5.3.2 Probing for cofactor interactions with the ERα NTD using photocrosslinking

Interactions between ERα and coregulatory proteins are key determinants of receptor function.[6,25] Hundreds of proteins have been identified that interact with ERα, many of which affect transcriptional activity of the receptor.[6,26] Recall from *section 1.2* that ERα contains two transcriptional "activation functions," AF-1 in the NTD and AF-2 in the LBD. AF-2 is chiefly responsible for the increase in transcriptional activity of ERα in response to activating estrogens, however AF-1 often contributes more to transcriptional activity than AF-2.[27] Moreover, there is growing evidence that AF-1 is the predominant contributor to differential actions of ERα (and other steroid hormone receptors) in different tissues.[27–29]

The ERα LBD is able to fold independently of the rest of the protein and is amenable to crystallization; thus interactions between this region of ERα and coregulatory proteins are relatively well-characterized.[27,30–32] Information regarding interactions between coregulatory proteins and the ERα NTD, however, is sparser.[27] The ERα NTD is largely intrinsically disordered and as such has never been crystallized with or without coregulatory proteins. This very intrinsic disorder, however, is likely an important aspect of regulation of AF-1: intrinsically disordered regions are known to promote highly specific yet low-affinity binding interactions via induced fit, which is ideal for transient regulation of signaling via transcription factors like ERα.[9,11,27,33–35]

Photocrosslinking using site-specific incorporation of NCAAs is especially well-suited for studying weak interactions such as those that would exist between coregulatory proteins and the ERα NTD.[36] Methods like co-immunoprecipitation that rely on noncovalent interactions between proteins would likely miss the weak interactions between

proteins and the intrinsically disordered NTD. Bifunctional chemical crosslinkers could be used to form a covalent complex, however these rely on the presence of reactive groups and surface-accessibility of the protein-protein interface of interest and are not site-specific.[21,37] Feeding cells photoactivatable NCAAs that can be incorporated using endogenous translational machinery offers yet another alternative, but also lacks precise site-specificity, which could complicate analysis.[38] We therefore set out to apply site-specific incorporation of the NCAA N_3Phe in the ERα NTD in order to probe for interactions with coregulatory proteins.

Our approach is depicted in **Figure 5.6**. We aimed to first incorporate N_3Phe site-specifically using the synthetase method (*section 1.3*) into all of the positions in the ERα AF-1 that exist as aromatic amino acids in the wild-type receptor. All-told, we identified 16 sites for modification: Y52, Y54, Y60, F62, Y73, Y80, F89, F97, H112, F120, H124, Y130, Y131, Y139, F149, and Y150. These residues were chosen based on previous work

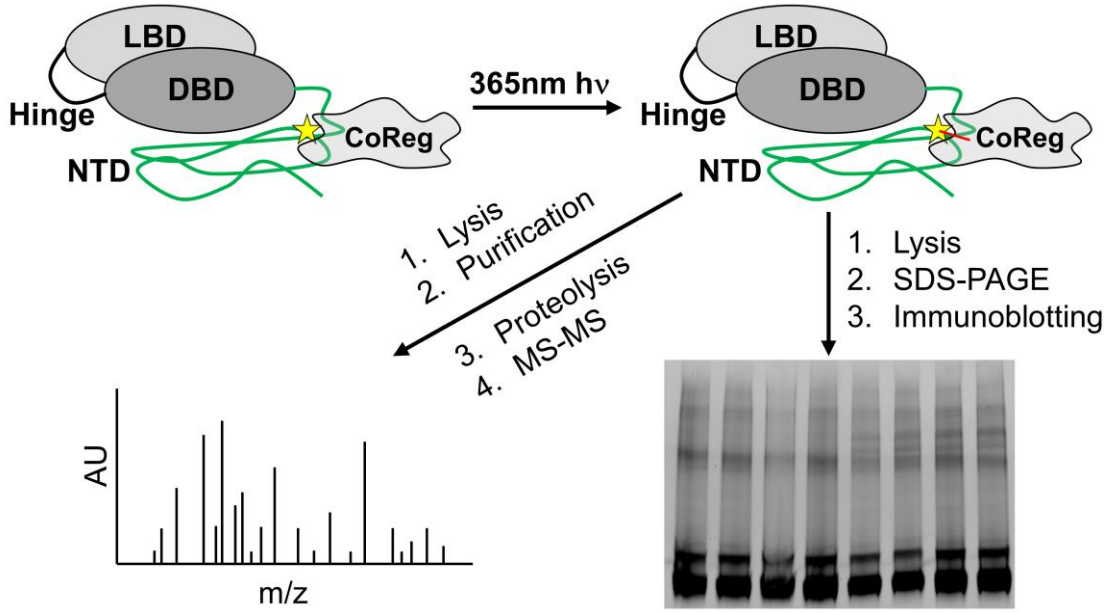

Figure 5.6. Envisioned strategy for using photocrosslinking to study interactions between coregulatory proteins (CoReg) and the ERα NTD. N_3Phe is depicted as a yellow star.

identifying residues 50 to 150 of the NTD as containing the ERα AF-1.[39] The ultimate goal was to then irradiate these receptors, analyze initially for hits by SDS-PAGE and immunoblotting, and identify the crosslinked species by mass spectrometry. This would require purification of the crosslinked complexes, so we used a C-terminally His_6-tagged ERα. This way, with the affinity tag on the C-terminus, only full-length products would contain the His_6 tag for visualization and purification.

The results from our scan of aromatic residues in AF-1 of ERα are shown in **Figure 5.7**. N_3Phe was incorporated into ERα-His_6 in HEK293T cells at the indicated positions, cells were irradiated with UV light for each experimental condition alongside a negative control dish that was not irradiated, and cells were lysed, subjected to SDS-PAGE, and immunoblotted as described in *section 5.5.4.*

Looking just at the results from the negative control (-hν) lysates, many bands are typically present; this is something that we have observed previously with wild-type ERα-His_6. We presume these heavier bands are ubiquitinated ERα; their presence is fairly consistent across experiments and we also observe lower molecular weight bands that may be proteolysis products. Thus the important thing to look for is not merely the presence of bands other than the ERα monomer band, but bands that appear only upon UV irradiation.

Comparing -hν lysates to +hν lysates, we believe that we have identified several sites in the ERα NTD that have been crosslinked to some other species. In the absence of further verification of these hits, we hesitate to make any absolute claims, but it appears that there was an appreciable amount of crosslinking at least for F149N_3Phe and Y150N_3Phe, and perhaps weaker crosslinking of Y60N_3Phe, F62N_3Phe, F89N_3Phe, F120N_3Phe, and Y139N_3Phe. We believe in these cases that we have observed crosslinking

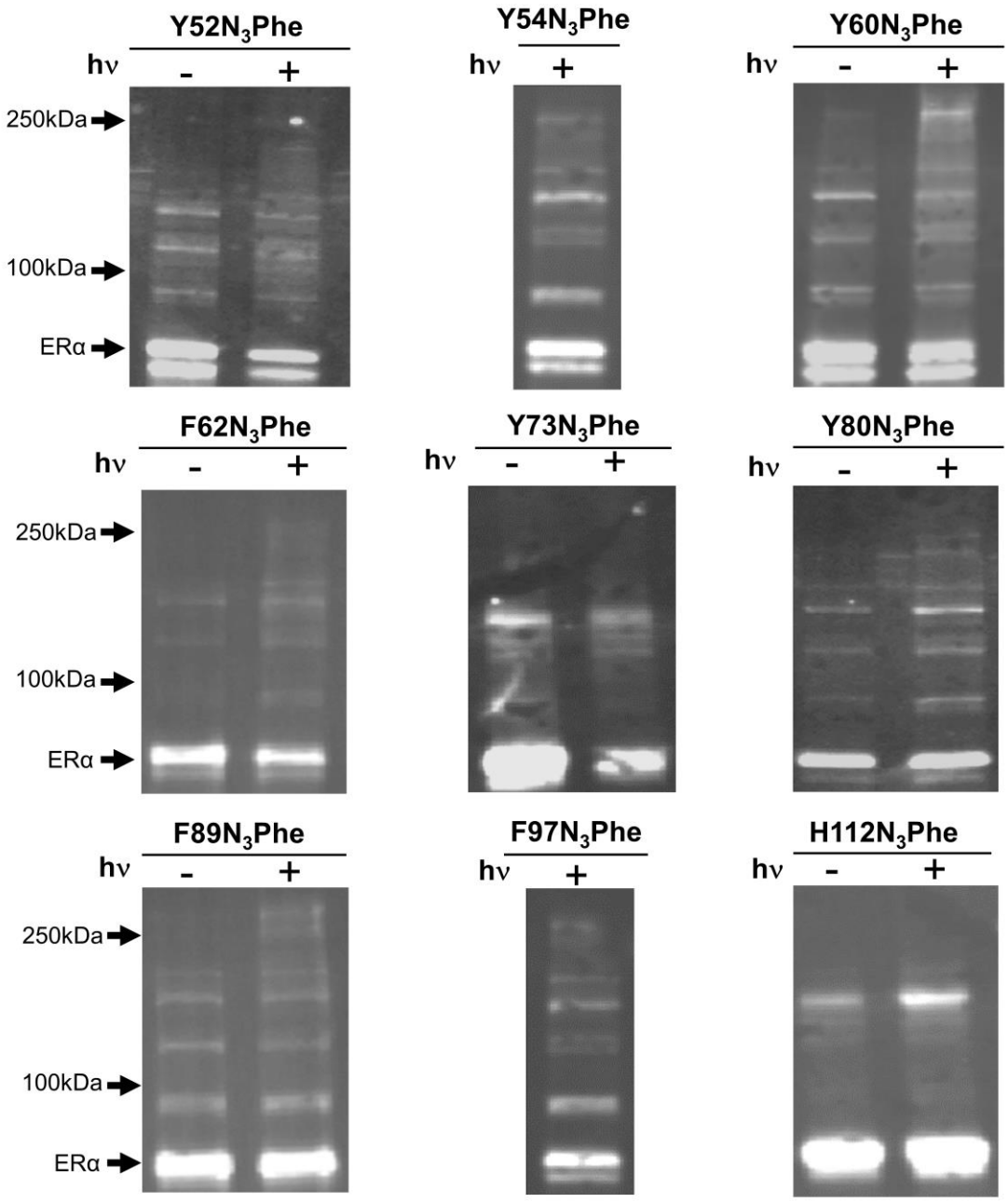

Figure 5.7. Western blots using photocrosslinking of N_3Phe to probe for interactions between coregulatory proteins and the AF-1 of the ERα NTD. Results continue on the next page…

due to two key observations: 1) the appearance of new bands in the +hν lysates compared to the -hν lysates, indicating the formation of some new species that is recognized by an anti-His_6 antibody only if the samples are irradiated with UV light, and 2) the site-

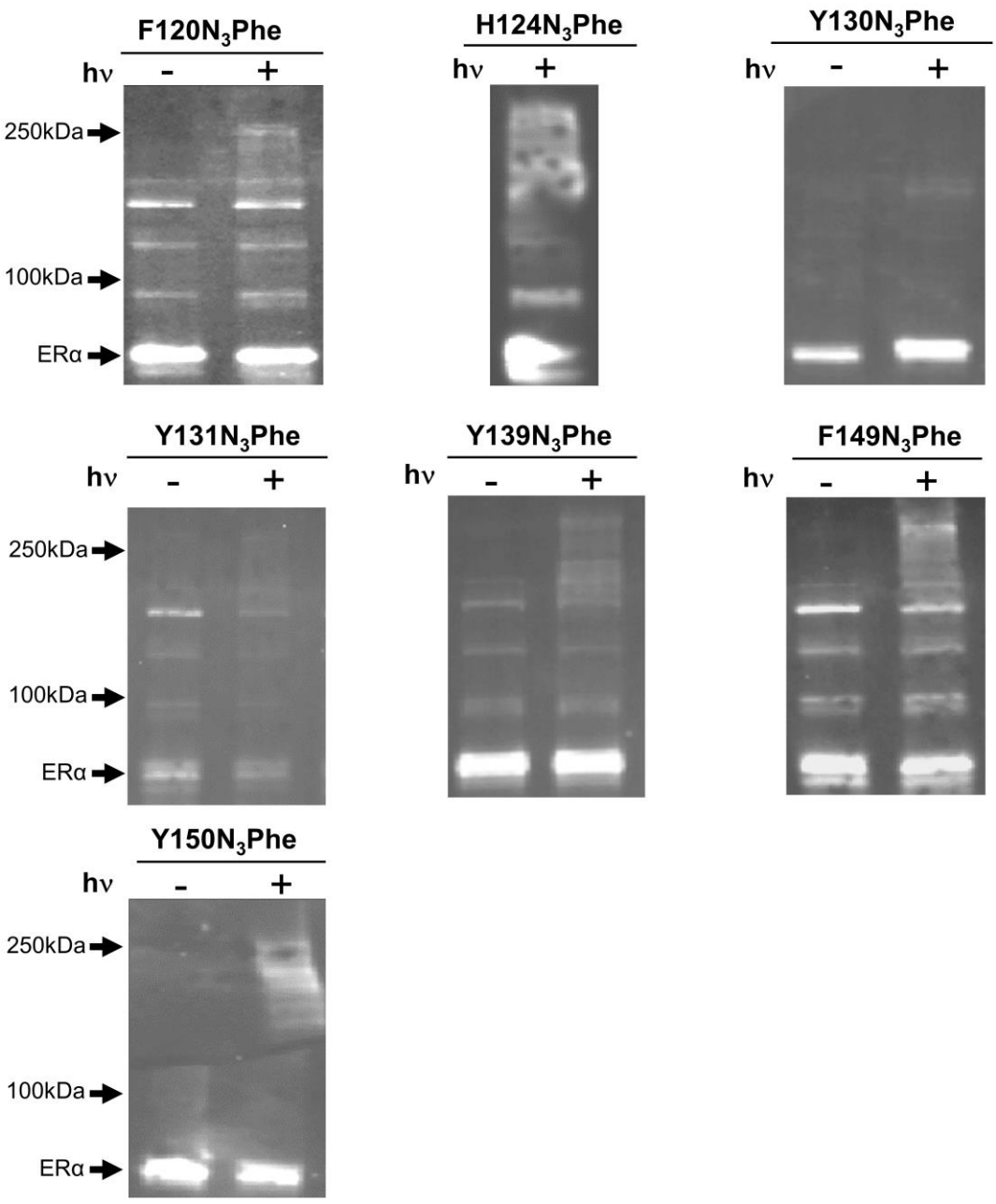

Figure 5.7. …continued from previous page.

specificity of the appearance of these new bands, given that some sites did not yield apparent crosslinking, which would imply that the appearance of the purportedly crosslinked species is not a mere fluke of the system. Unfortunately, in the experiments involving Y54, F97, and H124, lysates from the unirradiated dishes in these experiments

did not have good expression of ERα, so we do not have a negative control for these, but it does appear that ERα H124N_3Phe was successfully crosslinked in the +hν experiment.

The end goal of the above-described work is to use the photocrosslinking strategy to identify new coregulatory partners of the ERα AF-1 and/or quantify changes in the interactome of AF-1 in response to different stimuli. Either of these goals would benefit from the ability to purify the crosslinked complexes and analyze them by mass spectrometry. Initial efforts in our lab to purify crosslinked ERα complexes via FPLC using a Ni-NTA column have not been successful, likely owing to the abundance of other nickel-binding species natively expressed in HEK293T cells. Future efforts to purify crosslinked ERα complexes may involve a forward/reverse immobilized metal affinity chromatography (IMAC) strategy, in which nickel-binding species are first purified by affinity chromatography with a Ni-NTA column, the His_6 tag is removed from the ERα complex with a protease, and IMAC is again performed but the flowthrough is collected instead of the species that bind the column.[40] We have introduced a cut site for TEV protease into our ERα-His_6 plasmid (see *section 5.5.1*) just upstream of the C-terminal His_6 tag in order to pursue this forward/reverse IMAC strategy.

5.4 Conclusions & Future Directions

The work described herein has sought to use site-specific incorporation of the photocrosslinking NCAA, N_3Phe, to gain insights into ERα function. We have built upon previous work in our lab to demonstrate dimerization of eGFP-ERα in response to the clinically-relevant drugs 4-OHT and fulvestrant using a novel strategy that may find future applications as a minimally-perturbing means of probing receptor dimerization of ERα and other receptors. We have also demonstrated the potential utility of site-specific

incorporation of N_3Phe for studying interactions with the intrinsically disordered NTD of ERα.

There are many potential future directions for this research. The work on ERα dimerization could be expanded upon to create a more robust system for studying dimerization of ERα and other receptors *in vivo* in response to different stimuli. Contingent upon successful purification of crosslinked ERα complexes and identification of binding partners by mass spectrometry, the approach we've used herein could be used to study how regulatory proteins interact with the ERα NTD and similar disordered regions of other proteins. Variables within the system, of which there are many that influence ERα function, could then be changed systematically to ultimately gain a better understanding of the roles coregulatory proteins play in modulating the response of ERα (and other steroid hormone receptors).

5.5 Experimental Procedures

5.5.1 Molecular biology

The gene ESR1 for human ERα was in the pcDNA3.1(+) expression vector with a C-terminal His_6 tag. The N-terminal eGFP ERα fusion protein was also in the pcDNA3.1(+) vector, with a 15-residue linker, SGRSRAASNSAVDGT, between the C-terminus of eGFP and the N-terminus of ERα. Mutations were introduced using a QuikChange mutagenesis kit (Stratagene). Introduction of a TEV protease restriction site immediately N-terminal to the His_6 tag of the ERα-His_6 construct was accomplished using an established two-stage PCR protocol with the QuikChange kit.[41]

A PU6 plasmid encoding the tRNA/synthetase pair for N_3Phe was a kind gift from the lab of Professor Michelle Krogsgaard (New York University).[22]

5.5.2 Mammalian cell culture and protein expression

HEK293T cells (ATCC) were aliquoted from a low passage number monolayer culture, stored in large liquid nitrogen dewar, and thawed and recovered for use as per standard procedure.[42] Cells were grown in DMEM/F12 (Gibco) supplemented with 10% heat-inactivated FBS (Gibco) and 100 U/mL penicillin and 100µg/mL streptomycin at 37ºC under 5% CO_2 and passaged every 2-4 days once they reached 80-90% confluence. All routine manipulations of HEK293T cells were performed in a class II biosafety cabinet.

For expressing proteins of interest, cells were subcultured in 35-mm petri dishes from a parent monolayer culture and incubated until 50-75% confluent prior to transfection. Transfection was carried out using the Xfect reagent (Clontech) by premixing plasmid DNA and Xfect buffer before adding Xfect polymer (0.3µL polymer / 1µg DNA). For expression of wild-type ERα, 5µg of plasmid DNA was transfected. For nonsense suppression experiments, 5-7.5µg of ERα plasmid DNA was transfected alongside 2.5µg of the PU6 plasmid encoding the tRNA/synthetase pair for N_3Phe.

Following preparation of the appropriately-diluted transfection mixture, the cell culture medium for each dish was replaced with 900µL of fresh medium and 100µL of transfection mixture was added. Transfections were incubated at 37ºC under 5% CO_2 for 3-4h, at which point the medium was discarded and replaced with 3mL of fresh medium containing 0.5mM N_3Phe in the case of nonsense suppression experiments.

Cells were grown for ~24h to allow for expression of protein before addition of drugs of interest. ß-estradiol (E2; Sigma-Aldrich), (Z)-4-hydroxytamoxifen (4-OHT; Sigma-Aldrich), and ICI 182,780 (Sigma-Aldrich) were prepared as stock solutions in

DMSO and stored at -20ºC. Drugs were added in 30µL DMSO to dishes containing 3mL of medium and incubated 16-24h prior to irradiation for photocrosslinking and/or lysis.

5.5.3 Photocrosslinking

Following ~48h total incubation time post-transfection, photocrosslinking was performed on cells expressing ERα incorporating N_3Phe. 0-60min prior to irradiation, cell culture medium was discarded and replaced with 1mL of fresh medium not containing N_3Phe or drug. Dishes were then irradiated from below at a distance of 1-2cm with a 1150mW 365nm LED (Thorlabs) for 20min. Cells were immediately lysed and put on ice following photocrosslinking. Photocrosslinking was carried out separately for each cell culture dish / condition.

5.5.4 Lysis, SDS-PAGE, and immunoblotting

Following protein expression and, in most experiments, photocrosslinking, cells were lysed in 200-500µL of lysis buffer and immediately put on ice prior to storage at -80ºC. For most experiments, cells were lysed in 1% SDS in PBS with protease inhibitors, followed by a 10s sonication with an immersion sonicator.

For separation by SDS-PAGE, 12µL of lysate were mixed with 3µL of a 5X stock solution containing 5% SDS, 25% glycerol, 250mM Tris, and 0.5mg/mL bromophenol blue, and loaded into precast Biorad Mini-Protean TGX 15-well gels with an AnykD gradient. 1µL of Precision Plus Protein Dual Color Standard (Bio-Rad) was used for molecular weight calibrations. Gels were run at 150V for 45-60min prior to imaging and/or transfer for immunoblotting.

For immunoblotting, LF-PVDF membranes (Bio-Rad) were soaked for 10min in neat methanol immediately prior to transfer at 4ºC in Towbin's Buffer (prepared in-house)

at 30mV for 30min, followed by 100V for 90min. The membranes were then incubated at 4ºC in 5% milk in TPBS (PBS containing 0.1% Tween-20) for ~1h, and subsequently incubated at 4ºC with 1µg/mL of mouse anti-His_6 primary antibody (AD1.1.10; Novus Biologicals) in 5% milk TPBS for ~24h. Blots were then washed four times for five minutes per wash with TPBS, prior to incubation for ~2h with AzureSpectra 700 goat anti-mouse secondary antibody (Azure Biosystems) in 5% milk TPBS. Blots were finally washed three times at five minutes per wash followed by once at 30min with TPBS prior to imaging.

5.5.5 Imaging & data analysis

For imaging of eGFP ERα, we used a Typhoon FLA 9000 with a 473nm laser excitation and a LPB (510LP) detection filter. Imaging of immunoblots was performed on a LI-COR Odyssey with a 685nm laser excitation and 700nm detection. Adjustment to brightness/contrast and quantification of band intensities were performed in ImageJ. Peak intensities were determined by integrating the area under the curve using the "wand" tool for a representative 10-pixel-wide slice including the peak maximum, and percent dimerization values were calculated from these values. Assignment of dimer bands was made by comparing to the Precision Plus Protein Dual Color Standard (Bio-Rad) molecular weight ladder, and by visual comparison with previously-observed results (DOI 10.7907/Z9G44N8W). Plots were generated in Prism 7 and fits were made via the in-suite four parameter variable slope nonlinear regression.

5.6 References

1. Sever, R. & Glass, C. K. Signaling by Nuclear Receptors. *Cold Spring Harb. Perspect. Biol.* **5**, (2013).
2. Deroo, B. J. & Korach, K. S. Estrogen receptors and human disease. *J. Clin. Invest.* **116**, 561–570 (2006).
3. Arnal, J.-F. *et al.* Membrane and Nuclear Estrogen Receptor Alpha Actions: From Tissue Specificity to Medical Implications. *Physiol. Rev.* **97**, 1045–1087 (2017).

4. Crew, K. D., Albain, K. S., Hershman, D. L., Unger, J. M. & Lo, S. S. How do we increase uptake of tamoxifen and other anti-estrogens for breast cancer prevention? *Npj Breast Cancer* **3**, 20 (2017).
5. Ali, S., Buluwela, L. & Coombes, R. C. Antiestrogens and Their Therapeutic Applications in Breast Cancer and Other Diseases. *Annu. Rev. Med.* **62**, 217–232 (2011).
6. Yaşar, P., Ayaz, G., User, S. D., Güpür, G. & Muyan, M. Molecular mechanism of estrogen–estrogen receptor signaling. *Reprod. Med. Biol.* **16**, 4–20 (2017).
7. Cheskis, B. J., Greger, J. G., Nagpal, S. & Freedman, L. P. Signaling by estrogens. *J. Cell. Physiol.* **213**, 610–617 (2007).
8. Parker, M. G. Structure and Function of Estrogen Receptors. in *Vitamins & Hormones* (ed. Litwack, G.) **51**, 267–287 (Academic Press, 1995).
9. Hilser, V. J. & Thompson, E. B. Structural Dynamics, Intrinsic Disorder, and Allostery in Nuclear Receptors as Transcription Factors. *J. Biol. Chem.* **286**, 39675–39682 (2011).
10. Motlagh, H. N. & Hilser, V. J. Agonism/antagonism switching in allosteric ensembles. *Proc. Natl. Acad. Sci.* **109**, 4134–4139 (2012).
11. White, J. T., Motlagh, H. N., Li, J., Thompson, E. B. & Hilser, V. J. Allosteric Regulation and Intrinsic Disorder in Nuclear Hormone Receptors. in *Nuclear Receptors: From Structure to the Clinic* (eds. McEwan, I. J. & Kumar, R.) 73–91 (Springer International Publishing, 2015). doi:10.1007/978-3-319-18729-7_5
12. Jordan, V. C. & O'Malley, B. W. Selective Estrogen-Receptor Modulators and Antihormonal Resistance in Breast Cancer. *J. Clin. Oncol.* **25**, 5815–5824 (2007).
13. McDonnell, D. P. & Wardell, S. E. The molecular mechanisms underlying the pharmacological actions of ER modulators: Implications for new drug discovery in breast cancer. *Curr. Opin. Pharmacol.* **10**, 620–628 (2010).
14. Tamrazi, A., Carlson, K. E., Daniels, J. R., Hurth, K. M. & Katzenellenbogen, J. A. Estrogen Receptor Dimerization: Ligand Binding Regulates Dimer Affinity and DimerDissociation Rate. *Mol. Endocrinol.* **16**, 2706–2719 (2002).
15. Lees, J. A., Fawell, S. E., White, R. & Parker, M. G. A 22-amino-acid peptide restores DNA-binding activity to dimerization-defective mutants of the estrogen receptor. *Mol. Cell. Biol.* **10**, 5529–5531 (1990).
16. Powell, E. & Xu, W. Intermolecular interactions identify ligand-selective activity of estrogen receptor α/β dimers. *Proc. Natl. Acad. Sci.* **105**, 19012–19017 (2008).
17. Iwabuchi, E. *et al.* In situ detection of estrogen receptor dimers in breast carcinoma cells in archival materials using proximity ligation assay (PLA). *J. Steroid Biochem. Mol. Biol.* **165**, 159–169 (2017).
18. Paulmurugan, R., Tamrazi, A., Massoud, T. F., Katzenellenbogen, J. A. & Gambhir, S. S. In Vitro and in Vivo Molecular Imaging of Estrogen Receptor α and β Homo- and Heterodimerization: Exploration of New Modes of Receptor Regulation. *Mol. Endocrinol.* **25**, 2029–2040 (2011).
19. Wang, H. *et al.* Yeast Two-hybrid System Demonstrates That Estrogen Receptor Dimerization Is Ligand-dependent in Vivo. *J. Biol. Chem.* **270**, 23322–23329 (1995).
20. Padron, A., Li, L., Kofoed, E. M. & Schaufele, F. Ligand-Selective Interdomain Conformations of Estrogen Receptor-α. *Mol. Endocrinol.* **21**, 49–61 (2007).

21. Coin, I. Application of non-canonical crosslinking amino acids to study protein–protein interactions in live cells. *Curr. Opin. Chem. Biol.* **46**, 156–163 (2018).
22. Wang, W. *et al.* Quantitative Analysis of T Cell Receptor Complex Interaction Sites Using Genetically Encoded Photo-Cross-Linkers. *ACS Chem. Biol.* **9**, 2165–2172 (2014).
23. Osborne, C. K., Wakeling, A. & Nicholson, R. I. Fulvestrant: an oestrogen receptor antagonist with a novel mechanism of action. *Br. J. Cancer* **90**, S2–S6 (2004).
24. Carlson, R. W. The History and Mechanism of Action of Fulvestrant. *Clin. Breast Cancer* **6**, S5–S8 (2005).
25. Hall, J. M. & McDonnell, D. P. Coregulators in nuclear estrogen receptor action: from concept to therapeutic targeting. *Mol. Interv.* **5**, 343–357 (2005).
26. Carroll, J. S. Mechanisms of oestrogen receptor (ER) gene regulation in breast cancer. *Eur. J. Endocrinol.* **175**, R41–R49 (2016).
27. Simons, S. S., Edwards, D. P. & Kumar, R. Minireview: Dynamic Structures of Nuclear Hormone Receptors: New Promises and Challenges. *Mol. Endocrinol.* **28**, 173–182 (2014).
28. Arao, Y., Coons, L. A., Zuercher, W. J. & Korach, K. S. Transactivation Function-2 of Estrogen Receptor α Contains Transactivation Function-1-regulating Element. *J. Biol. Chem.* **290**, 17611–17627 (2015).
29. Simons, S. S. & Kumar, R. Variable steroid receptor responses: Intrinsically disordered AF1 is the key. *Mol. Cell. Endocrinol.* **376**, 81–84 (2013).
30. Brzozowski, A. M. *et al.* Molecular basis of agonism and antagonism in the oestrogen receptor. *Nature* **389**, 753–758 (1997).
31. Shiau, A. K. *et al.* The Structural Basis of Estrogen Receptor/Coactivator Recognition and the Antagonism of This Interaction by Tamoxifen. *Cell* **95**, 927–937 (1998).
32. Johnson, A. B. & O'Malley, B. W. Steroid Receptor Coactivators 1, 2, and 3: Critical Regulators of Nuclear Receptor Activity and Steroid Receptor Modulator (SRM)-based Cancer Therapy. *Mol. Cell. Endocrinol.* **348**, 430–439 (2012).
33. Dunker, A. K. & Uversky, V. N. Drugs for 'protein clouds': targeting intrinsically disordered transcription factors. *Curr. Opin. Pharmacol.* **10**, 782–788 (2010).
34. Dunker, A. K. & Uversky, V. N. Signal transduction via unstructured protein conduits. *Nat. Chem. Biol.* **4**, 229–230 (2008).
35. Krasowski, M. D., Reschly, E. J. & Ekins, S. INTRINSIC DISORDER IN NUCLEAR HORMONE RECEPTORS. *J. Proteome Res.* **7**, 4359–4372 (2008).
36. Pham, N. D., Parker, R. B. & Kohler, J. J. Photocrosslinking approaches to interactome mapping. *Curr. Opin. Chem. Biol.* **17**, 90–101 (2013).
37. Chin, J. W. & Schultz, P. G. In Vivo Photocrosslinking with Unnatural Amino Acid Mutagenesis. *ChemBioChem* **3**, 1135–1137 (2002).
38. Suchanek, M., Radzikowska, A. & Thiele, C. Photo-leucine and photo-methionine allow identification of protein-protein interactions in living cells. *Nat. Methods* **2**, 261–268 (2005).
39. Metzger, D., Ali, S., Bornert, J.-M. & Chambon, P. Characterization of the Amino-terminal Transcriptional Activation Function of the Human Estrogen Receptor in Animal and Yeast Cells. *J. Biol. Chem.* **270**, 9535–9542 (1995).

40. Block, H. *et al.* Chapter 27 Immobilized-Metal Affinity Chromatography (IMAC): A Review. in *Methods in Enzymology* (eds. Burgess, R. R. & Deutscher, M. P.) **463**, 439–473 (Academic Press, 2009).
41. Wang, W. & Malcolm, B. A. Two-Stage PCR Protocol Allowing Introduction of Multiple Mutations, Deletions and Insertions Using QuikChangeTM Site-Directed Mutagenesis. *BioTechniques* **26**, 680–682 (1999).
42. Phelan, K. & May, K. M. Basic Techniques in Mammalian Cell Tissue Culture. *Curr. Protoc. Cell Biol.* **66**, 1.1.1-1.1.22 (2015).